Hindawi Publishing Corporation
International Journal of Geophysics
Volume 2016, Article ID 2410573, 50 pages
http://dx.doi.org/10.1155/2016/2410573

Research Article

Discovery of Naturally Etched Fission Tracks and Alpha-Recoil Tracks in Submarine Glasses: Reevaluation of a Putative Biosignature for Earth and Mars

Jason E. French[1] and David F. Blake[2]

[1]*Department of Earth and Atmospheric Sciences, University of Alberta, 1-26 Earth Science Building, Edmonton, Alberta, Canada T6G 2E3*
[2]*NASA Ames Research Center, Exobiology Branch, MS 239-4, Moffett Field, CA 94035-1000, USA*

Correspondence should be addressed to Jason E. French; jef@ualberta.ca

Received 3 October 2015; Accepted 8 December 2015

Academic Editor: Ghaleb H. Jarrar

Over the last two decades, conspicuously "biogenic-looking" corrosion microtextures have been found to occur globally within volcanic glass of the *in situ* oceanic crust, ophiolites, and greenstone belts dating back to ~3.5 Ga. These so-called "tubular" and "granular" microtextures are widely interpreted to represent *bona fide* microbial trace fossils; however, possible nonbiological origins for these complex alteration microtextures have yet to be explored. Here, we reevaluate the origin of these enigmatic microtextures from a strictly nonbiological standpoint, using a case study on submarine glasses from the western North Atlantic Ocean (DSDP 418A). By combining petrographic and SEM observations of corrosion microtextures at the glass-palagonite interface, considerations of the tectonic setting, measurement of U and Th concentrations of fresh basaltic glass by ICP-MS, and theoretical modelling of the present-day distribution of radiation damage in basaltic glass caused by radioactive decay of U and Th, we reinterpret these enigmatic microtextures as the end product of the preferential corrosion/dissolution of radiation damage (alpha-recoil tracks and fission tracks) in the glass by seawater, possibly combined with pressure solution etch-tunnelling. Our findings have important implications for geomicrobiology, astrobiological exploration of Mars, and understanding of the long-term breakdown of nuclear waste glass.

1. Introduction

Understanding and successfully identifying examples of preserved microbial life from extreme environments on planet Earth are pertinent to the astrobiological exploration of Mars, and this was highlighted during recent debates over Martian meteorite ALH84001 (e.g., [1–6]). Accordingly, a flurry of recent studies have focussed on understanding terrestrial examples of life-harbouring extreme environments/paleoenvironments that could have analogs on Mars, including evaporite deposits [7], thermal spring deposits [8], Antarctic paleolake deposits [9], deep sea hydrothermal vent systems and deep subsurface aquifers [5, 10], and the glassy margins of submarine pillow basalts [11, 12]. Knowledge about the geomorphology and geological setting of these environments at the macroscopic scale on Earth can help with landing site selection for Mars astrobiology missions [13]; however, even more imperative to the successful astrobiological exploration of Mars is the ability of scientists to distinguish with absolute certainty whether or not relict signs of life are present in a returned rock sample (e.g., in samples acquired and returned to Earth during future robotic rover or manned missions to Mars). Numerous lines of evidence will probably be necessary to indicate that a true biosignature is present in such a sample and, among others, may include geochemical and stable isotopic constraints [14, 15], the identification of biologically produced minerals [16, 17], detection of biomolecules [18], and paleontological arguments such as recognition of microscopic morphological biomarkers [3, 19].

Among these possible microbial biosignatures in rocks, probably the most contentious of all are the recognition of nano- to microscopic morphological biomarkers, especially because there is typically a great deal of subjectivity involved in deciding which of these tiny shapes and forms appear to look like microbial remains/traces based only on visual interpretations and comparisons to known terrestrial biotic microstructures, and, moreover, many such micro-/nanofeatures also have straightforward and readily deduced nonbiological explanations. In fact, it is quite common at this scale of observation (e.g., under petrographic microscope or in high resolution scanning electron microscope (SEM) images) that there may be multiple explanations for such tiny physical structures in rock samples, including both biogenic and nonbiogenic (e.g., mineralogical) explanations, and three well-known examples of this include (1) abiotically produced nanoscopic mineral grains (i.e., calcite) in carbonate rocks that exhibit spherical, rod, and ovoid shapes resembling bacterial remains [20]; (2) filamentous and segmented carbonaceous microstructures in the ~3.5 Ga Apex cherts of Western Australia resembling bacterial and cyanobacterial remains [21] that have also been reinterpreted as abiogenic amorphous graphite [22]; and (3) concentrically zoned carbonate globules in Martian meteorite ALH84001 originally interpreted as bacterially induced carbonate precipitates [3] that were later reinterpreted as abiotic, high temperature, hydrothermally deposited minerals associated with volcanic activity—based on the discovery of similar carbonate globules in Spitsbergen, Norway [1, 6]. These three examples clearly demonstrate the value in seeking both biological and nonbiological explanations for the origin of putative microscopic morphological biomarkers in rocks, especially when found in extreme environments on Earth that may have similar counterparts at or below the surface of Mars.

Over the last two decades, conspicuously "biogenic-looking" corrosion microtextures have been found to occur globally at the glass-alteration interface within submarine volcanic glass of the *in situ* oceanic crust, ophiolites, and greenstone belts dating back to ~3.5 Ga [11, 23–29], and more recently in terrestrial impact glasses as well [30]. These micron-scale petrographic textures, that is, the so-called *tubular texture* (Figures 1(a), 1(c), and 1(e)) and *granular* [palagonite] *texture* (Figures 2(a) and 2(c)) (see summaries in [11, 26–28, 31]), have emerged as the "prime evidence" (p. 4 in [26]) or "strongest evidence" (p. 157 in [27]) for bioalteration of basaltic glass and have been used to define what is arguably the most geographically vast and long-lived lithoautotrophic microbial ecosystem on Earth [24, 26, 27, 32], representing an important part of the deep biosphere [11, 33, 34], and they currently represent the oldest unrefuted microscopic morphological biomarkers in the geological record [35–38], as well as a key biomorphic (trace fossil) target to look for in the astrobiological search for ancient microbial life on Mars [12]. All of these claims, however, need to be scrutinized, questioned, and tested by the scientific community, but, remarkably, this is something that has not yet taken place for this vast *putative* microbial ecosystem in volcanic glass on planet Earth.

Throughout this 23-year period (i.e., since the publication of Thorseth et al. [23]—the first study to invoke microbial bioalteration of basaltic glass in the development of complex corrosion microtextures at the glass-palagonite interface), it is surprising that none of these studies characterizing putative biogenic microtextures in basaltic glass have ever seriously considered possible nonbiological explanations for these tiny etch features. Certainly, when investigating the origin of conspicuous microtextures in petrographic thin sections of volcanic rocks, a petrological (i.e., abiotic-geological or petrogenetic) origin should first be considered, especially given that these putative biogenic microtextures are typically associated with subaqueously altered (i.e., partially palagonitized) regions of *igneous* rocks (pillow rim, hyaloclastite, or tuffaceous basaltic glasses). Historically, this was actually the case for several earlier studies on partially palagonitized basaltic glasses that identified the presence of microchannels or etch-pits in fresh basaltic glass immediately adjacent to the glass-palagonite interface (e.g., [39], "mist zone" of Morgenstein and Riley [40], and [41–44]). And although their significance was not initially addressed to much extent in the literature (as highlighted by Zhou and Fyfe [44]), some of these authors suggested (in passing) that such microscopic cavities are simply the result of dissolution processes associated with the incipient stage of palagonitization during aqueous alteration of the glass [40], such as corrosion [41] or the formation of etch-pits [44], and saw that there is no need to invoke microbial activity in the formation of these tiny etch features. In contrast, however, during the more recent time period (~1992–2014), this has not been the case virtually in all studies evaluating the origin of complex microscopic rock textures at the glass-palagonite interface in volcanic glass, where only a *biogenic* origin has been sought for these micron-sized (i.e., microbe-sized) etch features, during the accumulation of at least 77 scientific papers documenting such grooved, tubular, and granular "bioalteration" microtextures in submarine glasses from geological sites spanning a large part of the globe and dating back to ~3.5 Ga [11, 12, 23–28, 31–38, 45–105]. It is quite amazing that in the face of this daunting body of scientific research purporting to have documented *bona fide* microscopic morphological biomarkers in volcanic glasses worldwide—complex microtextures supposedly resulting from microbial bioalteration, biocorrosion, or biogenic microboring of volcanic glass (i.e., *tubular, granular*, and *microgroove* textures)—to date, there have only been a handful of scientific studies that have actually proposed nonbiological origins for such complex microtextures in volcanic glass and this includes (1) linear to curvilinear *microgrooves* on glass shards attributed to preferential etching of thermal cracks (i.e., as an alternative explanation for biogenic grooving [106]); (2) complex patterns of *dendritic nanogrooves* on vesicle walls in submarine basaltic glass reminiscent of microbial trace fossils, which are attributed instead to the abiotic, fluid mechanical process of viscous fingering between magmatic vapour and hot glass surrounding vesicles upon cooling through the glass transition [107]; and (3) titanite-mineralized *tubular* textures (similar to previously reported microbial trace fossils)

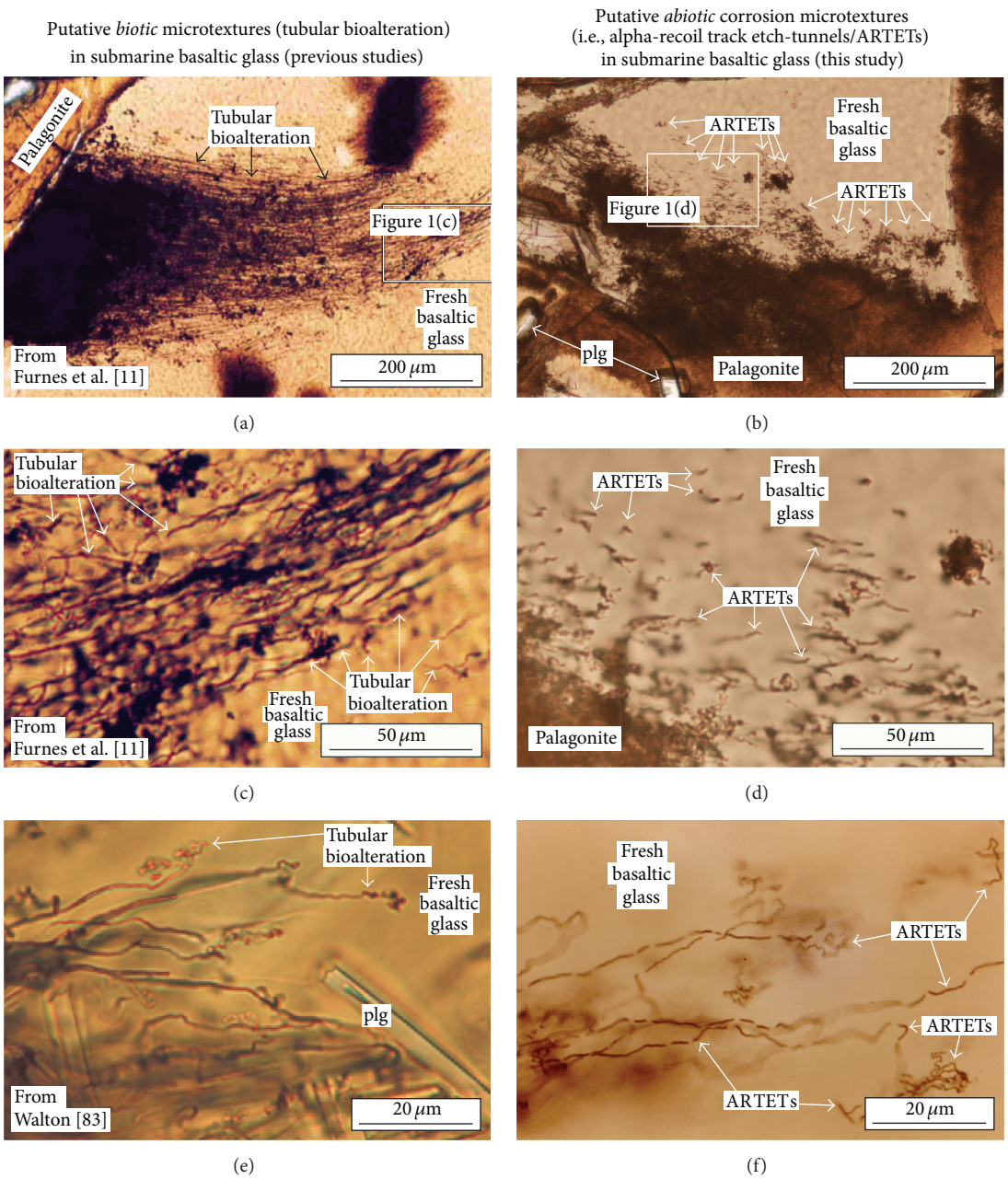

Figure 1: Scale comparisons (1 : 1) of previously reported "tubular" bioalteration microtextures in submarine basaltic glass (a, c, and e) with *abiotic* corrosion microtextures (alpha-recoil track etch-tunnels) in DSDP 418A basaltic glass (this study) (b, d, and f). All images (a–f) are photomicrographs of polished petrographic sections of submarine basaltic glasses taken in plane polarized light (uncrossed nicols). (a) and (c) are from [11] (sample *DSDP-418A-62-4-[64–70]*), and (e) is from [83] (Hawaii Scientific Drilling Project (HSDP) sample 4656.7). (b) and (d) are from sample *DSDP-418A-68-3[40–43]*, and (f) is from sample *DSDP-418A-75-3[120–123]*. Note the similarities when comparing (a), (c), and (e) to (b), (d), and (f), respectively, despite the differences in their inferred origin (biotic versus abiotic). ARTETs: alpha-recoil track etch-tunnels; plg: plagioclase phenocryst.

found in metaglassy Archean rocks attributed to nonbiological metamorphic processes [108, 109]. A few studies have touched on the topic of examining possible nonbiological origins for microscopic etch-tunnels in submarine glasses (e.g., [83, 93]), but in both cases biotic explanations were favoured in the end. One recent study [110] also noted (in passing) the occurrence of empty "tubules" at the glass-alteration interface in Hawaiian glasses, but it offered no explanation for them. Therefore, for most of these putative microbially produced "complex" etch features documented in basaltic glasses around the globe (especially tubular and granular textures), possible nonbiological explanations have

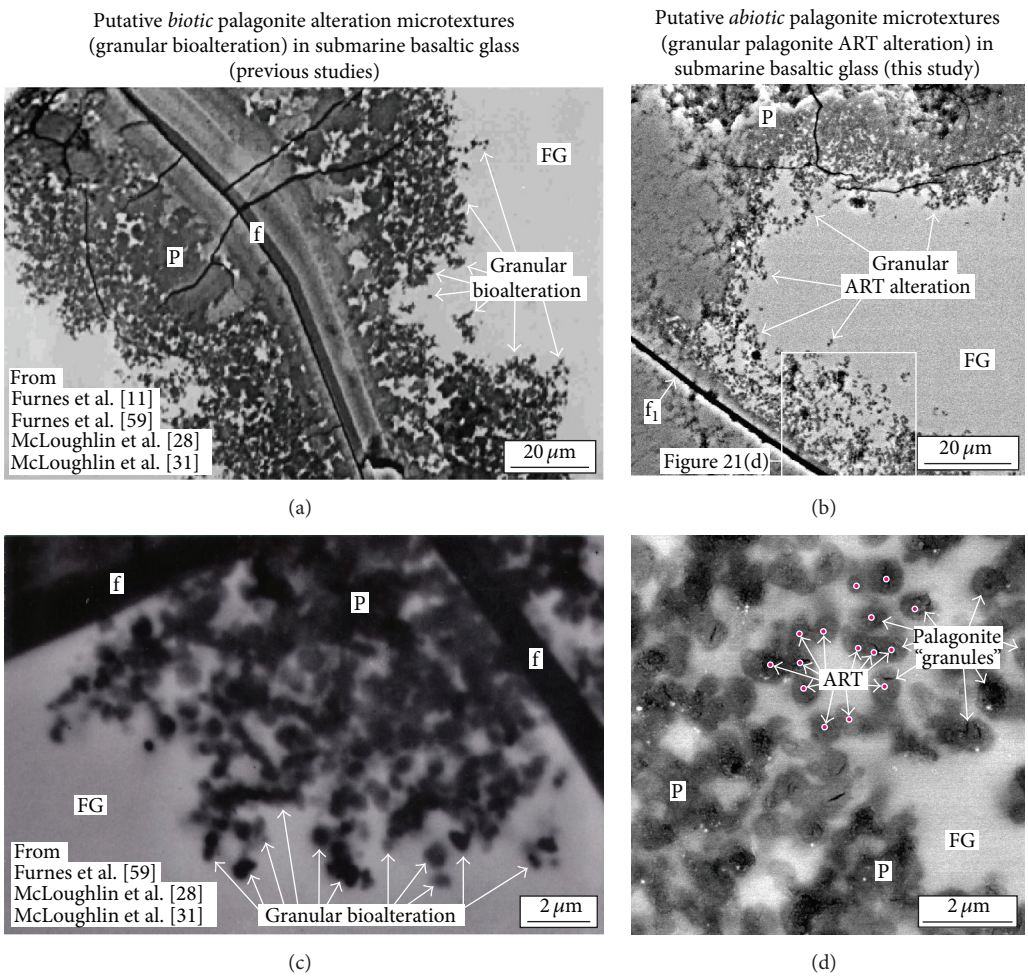

Figure 2: Approximate scale comparisons (near ~1 : 1) of previously reported "granular" bioalteration microtextures in submarine basaltic glass (a, c) with *abiotic* corrosion microtextures (granular palagonite ART alteration) in DSDP 418A basaltic glass (b, d) (this study; sample *DSDP-418A-68-3[40–43]*). All images are BSE images (acquired by SEM) of polished petrographic sections of submarine basaltic glasses. (a) is either from sample *DSDP-417D-30-6-[20–24]* (as reported in Figure 1(e) of [11]) or sample *DSDP-418A-62-4-[64–70]* (as reported in Figure 5(e) of [31] and Figure 2(c) of [28]), and (c) is from sample *DSDP-504b-4-2-[0–20]* (as reported in Figure 3(b) of [59], Figure 5(f) of [31], and Figure 2(d) of [28]). Note the similarities when comparing (a) and (c) with (b) and (d), respectively, despite the differences in their inferred origin (biotic versus abiotic). The 120 nm diameter pink circles in (d) correspond to "hypothetical" previously existing alpha-recoil tracks that have undergone selective palagonitization resulting in the formation of palagonite "granules" (or "granular" palagonite texture). ART: alpha-recoil track; f: fracture; f_1: early fracture; P: palagonite.

yet to be explored and this task is especially important in light of humanity's impending astrobiological exploration of Mars. Accordingly, after initial suggestions (by [107, 111–113]) that "abiotic" explanations can *also* be sought for the origin of corrosion microtextures in submarine glasses (especially "tubular" and "granular" microtextures), some more recent studies have begun to follow suit (e.g., [114]).

Searching for possible nonbiological origins for microscopic tunnels in volcanic glass is quite logical, especially because *abiotic* natural and experimental chemical etching of minerals has long been known to produce elongate microscopic etch-tunnels that exhibit a wide diversity of morphological forms, ranging from straight to curvilinear tubes, branched tubes, and those exhibiting spiral-/helical-, ribbon-, zigzag-, and worm-like shapes [115–123] that collectively are somewhat similar to the morphological diversity of naturally formed microscopic channels found in basaltic glass (i.e., straight to curvilinear microscopic tubular channels exhibiting spiral/helical, vermicular (worm-like), branched, and annulated tubular textures attributed to microbial activity [11, 26–28, 31]). In addition, morphologically similar (i.e., having straight to curvilinear, spiral/helical, and branched forms), elongate microscopic etch-tunnels/tubes known as "ambient inclusion trails" are known to develop within microcrystalline silica (e.g., agates and cherts) by the migration of pyrite grains and/or organic materials through the process of abiotic, chemical etching, possibly caused by the corrosive products resulting from the diagenetic breakdown of organic matter [93, 124]. Moreover, experimental microscopic etch-tunnelling of volcanic glass (and tektite glasses) is routinely

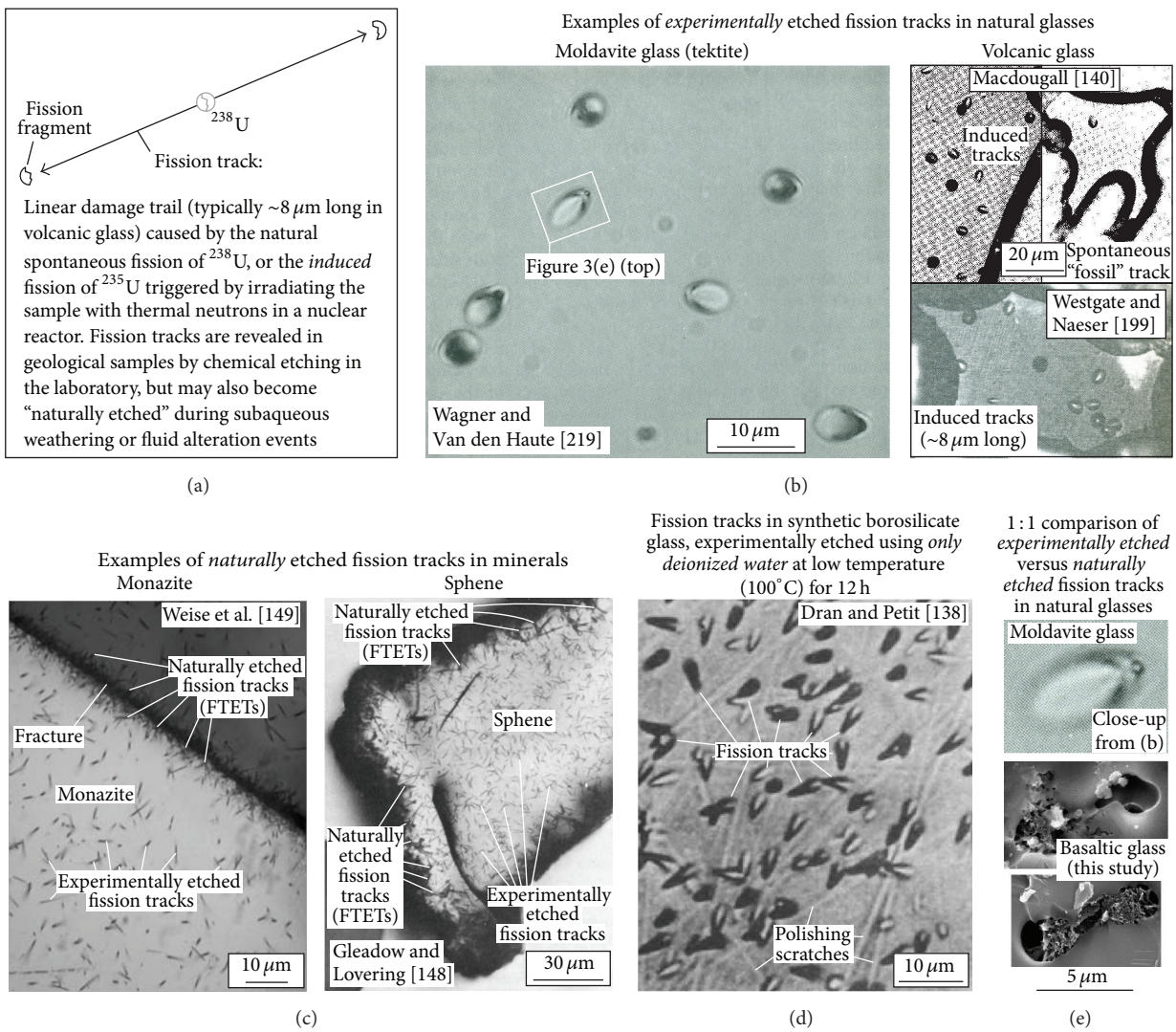

Figure 3: Background on fission tracks and examples of fission track etching. (a) Schematic illustration of a fission track. (b–d) Transmitted light photomicrographs of experimentally etched fission tracks in natural glasses (b), naturally etched fission tracks in minerals (c) (i.e., revealed by fluid alteration along a fracture in monazite (left) or by weathering and corrosion around the outer surface of a sphene grain (right)), and fission tracks in synthetic borosilicate glass (simulated nuclear waste glass) etched only with deionized water (d). (e) Scale comparison (1 : 1) of an experimentally etched fission track in natural moldavite glass (top), with two "naturally etched" fission tracks in submarine volcanic glass (sample *DSDP-418A-75-3[120–123]*; see close-ups and petrographic context of these two fission track etch-tunnels in Figures 11 and 13).

carried out in the laboratory during fission track dating studies (Figure 3), in which the polished surfaces of volcanic glass samples etch preferentially along elongate (typically ~6–8 μm long) latent damage trails in the glass caused by the spontaneous fission of ^{238}U during aging of the sample (or the induced fission of ^{235}U) [125–128]. Similarly, experimental chemical etching of alpha-recoil tracks (Figure 4) caused by the radioactive decay of U and Th (e.g., in alpha-recoil track dating studies of micas [129–134]) represents another style of etch-tunnelling of geological samples that could potentially be relevant to understanding the origin of naturally formed etch-tunnels in minerals and glasses. Furthermore, radiation damage in synthetic borosilicate nuclear waste glasses (for which basaltic glass is an ideal natural analog: [135, 136]), including fission tracks and simulated alpha-recoil damage, also leads to preferential etching of glass in a matter of hours, even at low temperatures (20–100°C) and using very weak etchants including deionized water or seawater (Figure 3(d)) [137, 138]. In fact, preliminary research indicates that preferential etching and corrosion of randomly distributed fission tracks and alpha-recoil tracks in submarine volcanic glasses—that is, during the *abiotic* encroachment of seawater during palagonitization along fractures—is a feasible abiotic geochemical process to form such "biogenic-looking" tubular and granular microtextures (e.g., p. 10 in French and Muehlenbachs [107] [111–113, 139]).

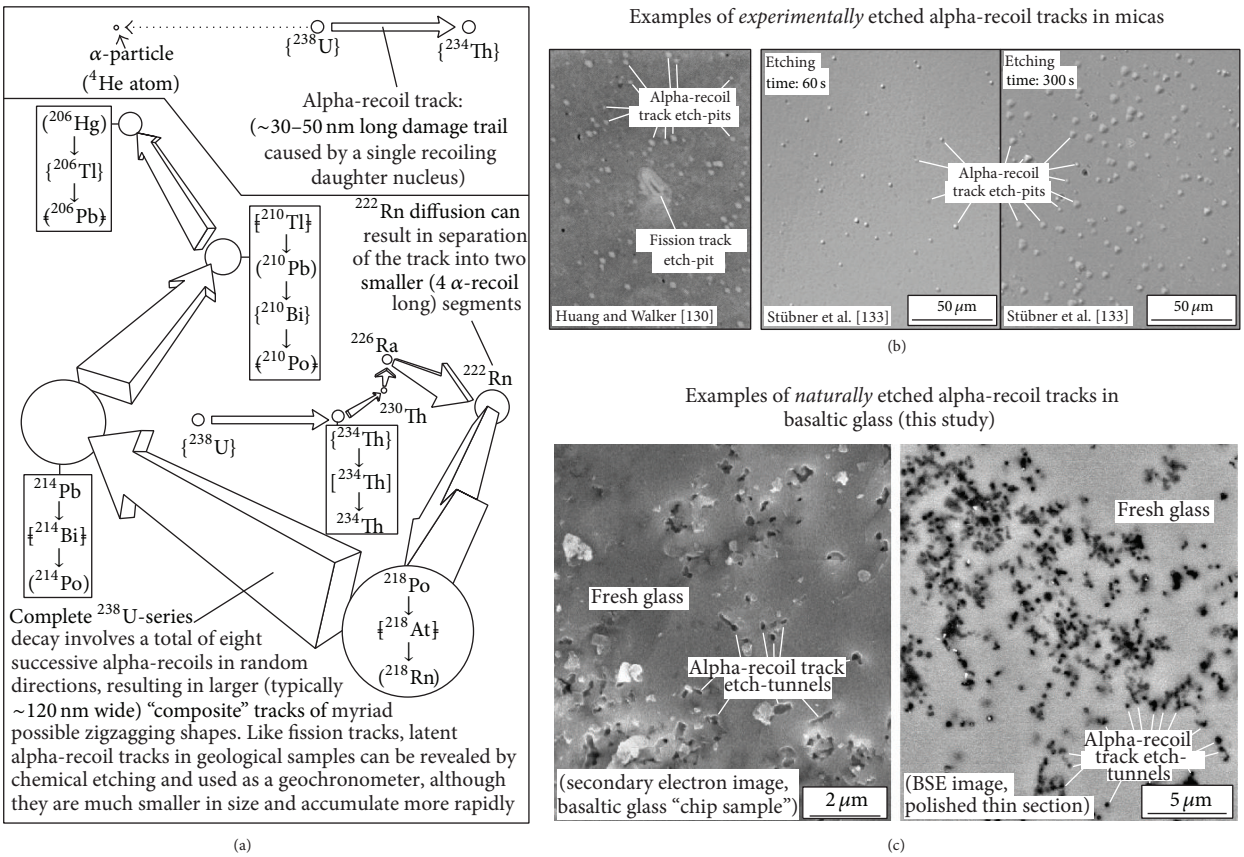

Figure 4: Background on alpha-recoil tracks and examples of alpha-recoil track etching. (a) Schematic illustration of alpha-recoil track development during complete ^{238}U-series radioactive decay (note: alpha-recoil tracks also originate from ^{235}U- and ^{232}Th-series decay—not shown). Beta decays are indicated by small arrows pointing down (enclosed in boxes/circles), while alpha decay parent-daughter pairs are denoted by identical bracket styles. (b) Etched alpha-recoil tracks in micas, revealed by experimental chemical etching of fresh cleavage surfaces. The image at left is of muscovite (etched for 2 hours at 20°C using 48% HF) and was obtained using phase contrast microscopy [130] (no scale bar is available for this image). The other two images (center and right) are of phlogopite (etched using 40% HF and then coated with a thin layer of carbon and imaged via an optical microscope equipped with an incident light device combined with Nomarski-Differential Interference Contrast [133]). Note the increase in average size of alpha-recoil track etch-pits with time, which is evident when comparing the 60 s and 300 s images. (c) Naturally occurring alpha-recoil track etch-tunnels (ARTETs)—identified at the glass-palagonite interface in the glassy margins of midocean ridge pillow basalts (this study). Left image: sample *DSDP-418A-75-3[120–123]* (see Figure 11 for petrographic context). Right image: sample *DSDP-418A-68-3[40–43]*.

Consequently, in the present study, we evaluate the origin of complex microscopic alteration textures commonly observed at the glass-palagonite interface in submarine basaltic glasses worldwide (i.e., tubular and granular textures: Figures 1 and 2), from a strictly nonbiological standpoint. In particular, we consider the likely effects of the accumulation of radiation damage—that is, in the form of randomly distributed spontaneous fission tracks and alpha-recoil tracks caused by radioactive decay of U and Th—on the process of natural abiotic corrosion (i.e., low temperature alteration) and dissolution (i.e., etch-tunnelling) of basaltic glass by seawater. Rationale for this study comes from the well-known fact that spontaneous fission tracks and alpha-recoil tracks in silicate glasses are known to etch preferentially over undamaged regions of glass [137, 138, 140–145], commonly resulting in microscopic etch-pits (e.g., Figures 3(b), 3(d), and 3(e)). Coupled with the observations that midocean ridge basaltic glasses worldwide are known to contain trace amounts of U and Th [146] and are routinely dated by the fission track method [125, 127, 147], this provides direct evidence that radiation damage could potentially play a very important role in the natural corrosion and dissolution of basaltic glass by seawater (i.e., as opposed to microbial activity). Moreover, naturally etched fission tracks (i.e., fission track etch-tunnels formed during low temperature aqueous weathering or fluid alteration) have also been documented previously in a variety of minerals including the outer surfaces of sphene grains (Figure 3(c)) [148], along fractures within monazite (Figure 3(c)) [149], and also within apatite grains [150].

Numerous previous studies of submarine volcanic glasses have claimed that "tubular" and "granular" corrosion microtextures are simply "too complex and too reminiscent of biological processes to be explicable by an abiotic process" [59],

that "abiotic" palagonitization produces only very simple (i.e., straight and sharp) glass-palagonite interfaces without such tubular or granular textures (e.g., Section 4.1 in Furnes et al. [59]; Figure 1 in Staudigel et al. [75]; Figure 13(a) in Furnes et al. [11]; Figure 1 in Furnes et al. [26]; Figure 2 in McLoughlin et al. [31]; Figure 1 in Staudigel et al. [27]), and that (other than microbial etching) no alternative abiotic process has yet been proposed to explain such globally distributed complex microtextures found in volcanic glasses worldwide [25]. In the present study, we challenge these three points by demonstrating unequivocally that such complex corrosion microtextures at the glass-palagonite interface in submarine volcanic glasses (e.g., see Figures 1 and 2) can form as a direct consequence of the preferential dissolution (etch-tunnelling) and corrosion of randomly distributed spontaneous fission tracks and alpha-recoil tracks (i.e., radiation damage) in the glass by seawater and are therefore *not* necessarily a consequence of biological processes such as microbial boring. Accordingly, in this study we question the widely accepted "biocorrosion" model for the development of complex alteration microtextures in submarine volcanic glass and, therefore, the biogenicity of such "tubular" and "granular" corrosion microtextures found in basaltic glasses worldwide.

To accomplish these objectives, we have focussed this multidisciplinary petrographic (rock-textural) and theoretical modelling study on partially palagonitized, 120.6 Ma basaltic glass "pillow margin" samples recovered from drill core of Deep Sea Drilling Project (DSDP) Hole 418A, in the southwestern North Atlantic Ocean (Figure 5)—a drill hole which in several previous studies has yielded many such basaltic glass samples exhibiting classic "tubular" and "granular" microtextures attributed to microbial activity (e.g., Figures 1(a), 1(c), 2(a), and 5(b)) [11, 26–28, 31, 33, 59, 61, 93, 94, 100]. Our study combines petrographic observations, high resolution SEM imaging, considerations of the geological setting, determination of trace element concentrations (U and Th) in fresh basaltic glass by Inductively Coupled Plasma-Mass Spectrometry (ICP-MS), and theoretical modelling of radiation damage in basaltic glass caused by radioactive decay of U and Th (i.e., the distribution of spontaneous fission tracks and alpha-recoil tracks in the glass). Ultimately, we discuss the implications that this new abiotic "U–Th–Pb radiogenic" paradigm for basaltic glass corrosion and dissolution has on the understanding of microbial ecology and microbial trace fossil identification on Earth (particularly within volcanic basement rocks of *in situ* Layer 2 oceanic crust, ophiolites, Archean greenstone belts, or impact glasses), as well as the vital implications that this new paradigm has for the future astrobiological exploration of Mars—a planet that importantly, appears to be dominated at the surface (geologically) by the widespread occurrence of basalt [151–155], palagonite [151, 152, 156], weathered volcanic/basaltic glass [151, 153, 157], and evidence for past action of liquid water [154, 155, 158, 159]—and which therefore may contain volcanic or impact glasses bearing analogous *microgrooves*, *granular* palagonite textures, or *tubular* etch-tunnels.

The natural breakdown and corrosion of basaltic glass have also long been considered to represent an important natural analog process pertinent to understanding the long-term breakdown of high level nuclear waste glasses stored in geological repositories [135, 136]. Therefore, we also highlight that our discovery/identification of naturally etched fission tracks and alpha-recoil tracks in 120.6 million-year-old submarine basaltic glass at DSDP 418A—formed by incremental encroachment of seawater through radiation damaged sites—also has profound implications for predicting the long-term behaviour of borosilicate nuclear waste glasses stored in deep geological aquifers (i.e., repositories), providing an ideal "natural laboratory" for carrying out such long-term studies.

2. Geological Setting

2.1. Sample Locations and Previous Work on DSDP-418A Basaltic Glasses. For this case study on the origin of complex microtextures at the glass-palagonite interface in submarine volcanic glasses, partially palagonitized basaltic glass pillow margin samples showing evidence of "tubular" and "granular" microtextures (cf. [11, 25–28, 31, 33]) were selected from rocks recovered from DSDP Hole 418A. The drill hole is situated under 5511 m of water in the western North Atlantic Ocean (Figure 5; latitude: 25°02.10′N; longitude: 68°03.44′W) and was drilled to a depth of 868 m below the seafloor [160]. At this site, sediments of Layer 1 oceanic crust are 324 m thick, below which occurs 120.6 Ma (for age constraints, see Figures 5(c) and 5(d) and Section 2.2), Layer 2 volcanic basement [160] that is considered to represent typical eruptive oceanic crust, comprising a succession of basaltic pillow lavas and massive flows, with lesser intercalations of breccias and sediments, as well as cross-cutting mafic dykes lower down in the succession (Figure 5(b)) [161]. Basaltic glass pillow margin samples from this study originate from core samples *DSDP-418A-68-3[40–43]*, *DSDP-418A-72-4[13–15]*, and *DSDP-418A-75-3[120–123]* collected from depths of 732, 760, and 785 m below the seafloor, respectively (Figure 5(b)). Detailed geochemical analyses (i.e., determination of major element oxide compositions) of pillow rim basaltic glasses throughout much of the entire sequence of lava flows at DSDP 418A—along with a comprehensive evaluation of the observed down-hole variations in volcanic chemical stratigraphy and delineation of volcanic eruptive units for these ancient midocean ridge pillow basalts, flows, and breccias—was carried out previously [161, 162]. According to their down-hole depths and relative positions in the volcanostratigraphic sequence at DSDP 418A (Figure 5(b)), all three of the basaltic glass pillow margin samples in the present study occur within chemical (i.e., glass) type "J" [162] of lithologic unit "13" of volcanic eruptive unit "Vb" [161]. Type "J" basaltic glasses are characterized by an average glass composition of 51.03 ± 0.35 wt.% SiO_2, 14.19 ± 0.14 wt.% Al_2O_3, 11.31 ± 0.24 wt.% FeO(T), 7.13 ± 0.09 wt.% MgO, 11.86 ± 0.11 wt.% CaO, 2.34 ± 0.04 wt.% Na_2O, 0.11 ± 0.01 wt.% K_2O, 1.54 ± 0.03 wt.% TiO_2, and 0.14 ± 0.01 wt.% P_2O_5 ($n = 18$, errors given in standard deviation [162]). Of particular interest to the present study (aimed at understanding the likely role of self-incurred radiation damage on the development of complex corrosion microtextures in submarine basaltic

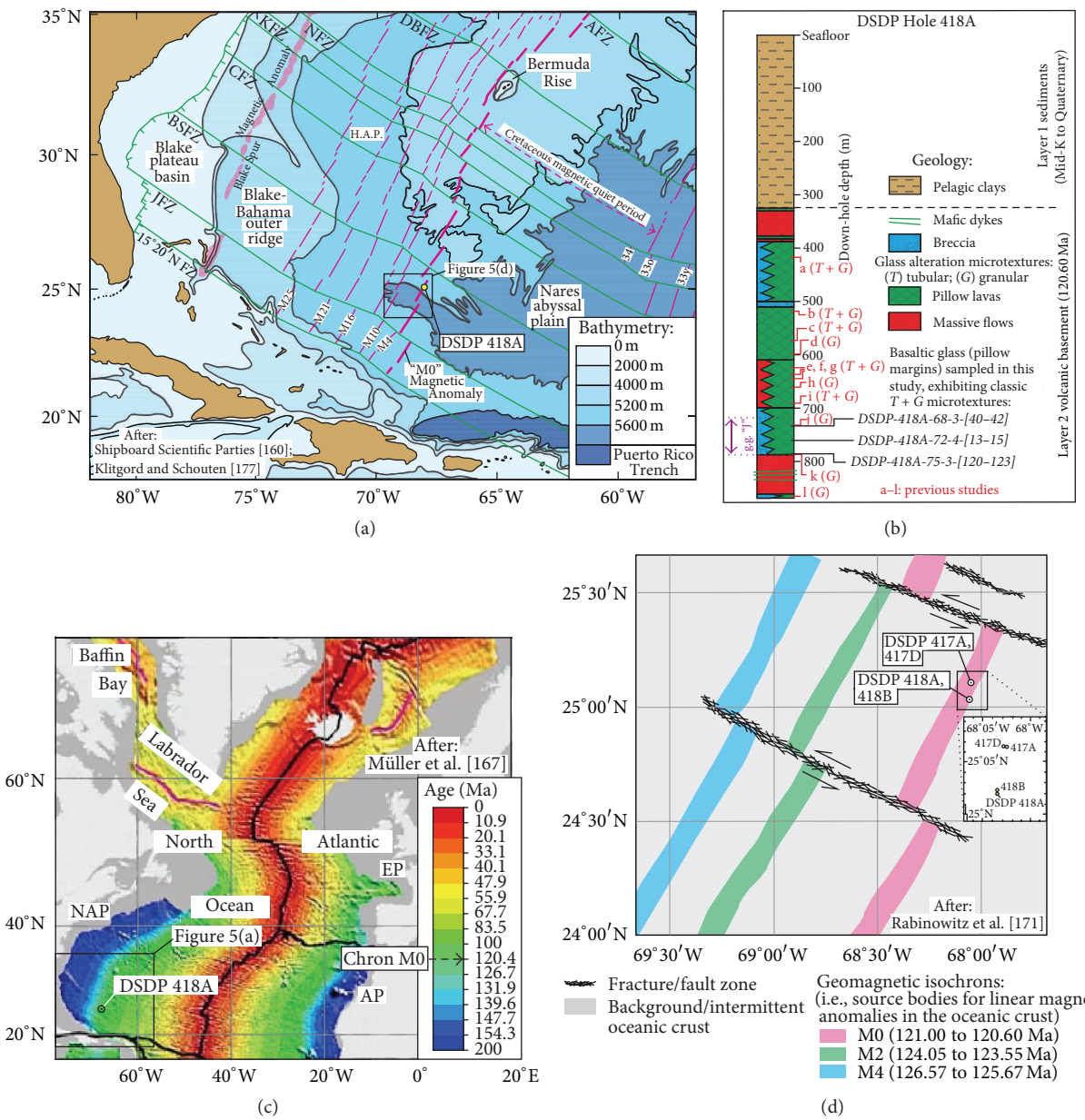

Figure 5: Geological maps (and stratigraphic column) of the North Atlantic region highlighting the position of DSDP Hole 418A within the context of regional patterns of lithospheric age and seafloor spreading magnetic anomalies. (a) Bathymetry, seafloor spreading magnetic anomalies (pink lines), and fault/fracture zones (green lines) of the southwestern North Atlantic Ocean (after [160, 177]). HAP denotes Hatteras Abyssal Plain. Fracture zones (FZ) include the Atlantis (AFZ), Delaware Bay (DBFZ), Norfolk (NFZ), Kane (KFZ), Carolinas (CFZ), Blake Spur (BSFZ), Jacksonville (JFZ), and 15°20′N FZ. (b) Stratigraphic column for DSDP 418A (after [160–162]) showing the locations of basaltic glass pillow margin samples in which classic "tubular" (*T*) and "granular" (*G*) alteration microtextures have been documented at the glass-palagonite interface in this (black) and previous studies (red). The black dashed line demarcates the top of volcanic basement, and zigzags represent interbedding of lithologic units. The volcanostratigraphic zone in which glass group "J" occurs [161, 162] is denoted in purple (g.g. "J") and corresponds to a geochemically coherent volcanic (glass) interval from which all three glass samples were collected in this study. Samples a–l from previous studies (shown in red) correspond to a—*418A-30-3-[4–6]* in Furnes and Staudigel [33] and Furnes et al. [59]; b—*418A-43-1-[80–82]* in Fliegel et al. [100]; c—*418A-49-2-[41–45]* in Staudigel et al. [27] and Furnes et al. [59]; d—*418A-52-5-[75–80]* in Furnes et al. [11] and Furnes et al. [59]; e—*418A-55-4-[112–114]* in Furnes et al. [11], Staudigel et al. [27], Furnes et al. [59], and Fliegel et al. [100]; f—*418A-56-5-[129–132]* in McLoughlin et al. [28] and Furnes et al. [59]; g—*418A-57-5-[12-13]* in Furnes et al. [59]; h—*418A-59-3* in Furnes et al. [59]; i—*418A-62-4-[64–70]* in Furnes et al. [11], Staudigel et al. [27], McLoughlin et al. [28], McLoughlin et al. [31], Furnes et al. [59], and Furnes et al. [61]; j—*418A-68-3-[32–38]* in Furnes et al. [59]; k—*418A-76-1-[4–7]* in Furnes et al. [59]; l—*418A-86-5-[24–32]* in Furnes et al. [59]. (c) Map showing lithospheric age in the North Atlantic Ocean, highlighting the location of DSDP 418A and Chron "M0" on which it lies (after Müller et al. [167]). Tectonic plates: AP: African Plate; EP: Eurasian Plate; NAP: North American Plate. (d) Close-up geological/geophysical map showing the location of DSDP 418A (and other nearby holes) in the context of local patterns of seafloor spreading magnetic anomalies and fracture/fault zones [160, 171]. The age intervals for geomagnetic isochrons M0, M2, and M4 are from Channell et al. [176].

glass), fission track dating of basaltic glasses from DSDP 418A was actually carried out early on as well [125]. In that study, it was found that spontaneous fission tracks (revealed by experimental chemical etching) are abundant enough in DSDP 418A basaltic glass to successfully carry out fission track dating, which (along with glasses from nearby holes 417A and D) yielded a thermally corrected, combined fission track age of 108.3 ± 1.3 Ma [125]. Furthermore, U concentrations in basaltic glass samples *DSDP-418A-30-2[71-72]* and *DSDP-418A-45-2[34–37]* (stratigraphically higher up in the volcanic succession than the rocks from this study) were determined to be 21.4 and 18.4 ppb, respectively [125]. The success of this early fission track dating study, coupled with the measurement of trace U in basaltic glasses at DSDP Hole 418A, provides important rationale for the present study on the corrosion of radiation damage in DSDP 418A basaltic glasses—because it already proves for us that such radiation damage (and U) is actually there, implying that fission tracks might indeed play an important role in controlling the microscopic patterns of corrosion during preferential dissolution and palagonitization of basaltic glass by seawater.

The present study on corrosion of DSDP 418A basaltic glasses also compliments a previous companion study [107] of branching, nanoscopic grooves on vesicle walls in basaltic glass from sample *DSDP-418A-75-3[120–123]* that we believe represent another variety of "abiotic" microtextural features in basaltic glass that could potentially be misidentified as microbial etch features (see Section 6.5).

Several previous studies on basaltic glass pillow margin samples from DSDP 418A have documented widespread evidence of granular and/or tubular alteration microtextures at the glass-palagonite interface throughout much of the entire succession of volcanic basement rocks encountered by this drill hole (Figure 5(b)) and universally attributed the origin of these tubular and granular microtextures to microbial activity/biocorrosion (Figures 1(a), 1(c), 2(a), and 5(b)) [11, 26–28, 31, 33, 59, 61, 93, 94, 100]. The down-hole depths at which such putative tubular and granular bioalteration microtextures have been documented in these previous studies are indicated in Figure 5(b) (in red), along with the positions of basaltic glass pillow margins sampled in this study (in black) in which we document the occurrence of identical but clearly *abiotic* tubular and granular microtextures arising from preferential corrosion of randomly distributed fission tracks and alpha-recoil tracks in basaltic glass.

2.2. Constraints on the Age of DSDP-418A Pillow Lavas and the M0 Magnetic Anomaly. In order to carry out accurate theoretical modelling (below in Section 5) of the accumulation of randomly distributed radiation damage (i.e., fission track and alpha-recoil track areal densities) in DSDP 418A basaltic glass in this study, it is imperative to know the exact age (t) of quenching of basaltic glasses (i.e., pillow eruption) at DSDP 418A. Because the amount of material we had for each pillow margin sample in this study is quite small, and no suitable U-bearing minerals are present in these glasses (such as zircon or baddeleyite), we were not able to carry out precise and accurate U–Pb isotopic dating of these rock samples (e.g., by Isotope Dilution Thermal Ionization Mass Spectrometry or Laser Ablation-Inductively Coupled Plasma-Mass Spectrometry). Nevertheless, there are several previous studies that do provide a number of different age estimates for the timing of formation of Layer 2 volcanic basement at DSDP 418A—employing various geochronological techniques including fission track, ^{40}Ar–^{39}Ar, and Rb/Sr radiometric dating, microfaunal biostratigraphy, and global correlation of linear magnetic anomalies in the oceanic crust (and their associated isotopic ages)—from which we can place somewhat reliable constraints on the timing of quenching of these DSDP 418A basaltic glass samples.

Direct dating of pillow rim basaltic glasses from DSDP 418A was actually carried out in a previous study by Storzer and Sélo [125] using the fission track method, which yielded a relatively precise—albeit thermally corrected, mean—age of 108.3 ± 1.3 Ma determined on a combination of basaltic glass samples originating from nearby DSDP Holes 417A, 417D, and 418A (Figure 5(d)). Accordingly, this fission track age was interpreted in that study as a reasonable estimate for the timing of pillow eruption, glass quenching, and formation of the M0 linear magnetic anomaly (intersected by these drill holes: Figures 5(a) and 5(d)), all of which formed during ancient (ca. Mid-Cretaceous) seafloor spreading during early ocean opening of the central Atlantic (Figure 5(c)). Presumably, the entire vertical sequence of pillow eruption recorded in DSDP Hole 418A (some 40 eruptive units [161]) represents a relatively contemporaneous lava succession that was emplaced during a relatively short (<100,000 year) geological timespan (i.e., by comparison with the fission track ages reported for samples from the FAMOUS area—see Storzer and Sélo [125] and references therein). Therefore, taken at face value, the fission track age of 108.3 ± 1.3 Ma reported by Storzer and Sélo [125] *could* effectively be used to estimate the age of eruption and glass quenching of all pillow lavas sampled from DSDP Hole 418A. Another radiometric dating study focussed on DSDP 418A volcanic basement rocks [163], employed Rb–Sr isotopic dating of secondary smectites, which yielded a similar but less precise Rb–Sr isochron age of 108 ± 17 Ma—adding support to the fission track age of Storzer and Sélo [125]. However, additional radiometric dating of secondary analcites, celadonites, and smectites showing greater overall Rb–Sr enrichments that originate from volcanic basement rocks of nearby DSDP Hole 417A (situated on the same M0 linear magnetic anomaly: Figure 5(d)) yielded a much more well-constrained Rb–Sr isochron age of 108 ± 3 Ma [163]—again, adding further support for the idea that the age of volcanic basement at DSDP Hole 418A is about 108 Ma. Although these smectites dated by Rb–Sr constitute "secondary" minerals originating from the extensive alteration of igneous basement rocks, they were considered in that study [163] to have formed more or less contemporaneously with volcanic basement (given the agreement between various age determinations at ~108 Ma). Consequently, according to this interpretation, the three basaltic glass pillow margin samples investigated in the present study from this drill hole (*DSDP-418A-68-3[40–43]*, *DSDP-418A-72-4[13–15]*, and *DSDP-418A-75-3[120–123]*)

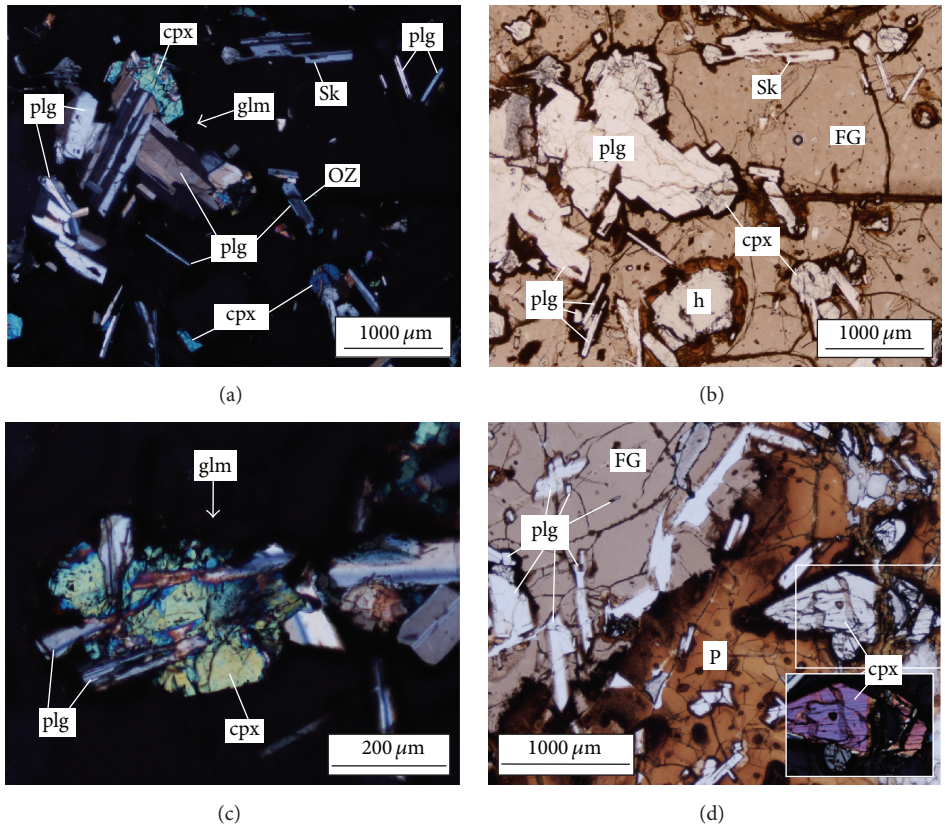

Figure 6: Photomicrographs of polished petrographic thin sections of DSDP 418A basaltic glass pillow margins, highlighting various igneous petrographic features. The photomicrographs shown in (a, c) and (d—"inset") are taken in cross polarized light (crossed nicols), whereas (b) and (d) are in plane polarized light (uncrossed nicols). (a-b): sample *DSDP-418A-75-3[120–123]*. (c-d): sample *DSDP-418A-68-3[40–43]*. Note that (a) and (b) depict the same petrographic area. cpx: clinopyroxene; FG: fresh basaltic glass; glm: glomerocryst; h: artificial hole in the petrographic section; OZ: oscillatory zoned plagioclase; plg: plagioclase phenocryst; Sk: skeletal plagioclase crystal.

would appear to have been emplaced at 108 ± 3 Ma (i.e., in agreement with the fission track age of 108.3±1.3 Ma, which is the radiometric age used in our original interpretation during previous preliminary work on these glasses [111, 112])—and indeed most previous geomicrobiological studies of DSDP 418A basaltic glasses have also considered the age of these glasses to be about 110 Ma [11, 26–28, 31, 33, 59, 94, 100]. However, given the occurrence of fresh basaltic glass in some pillow margin samples (e.g., the partially palagonitized samples in the present study, such as in Figures 6(b) and 6(d)), the timing of formation of some secondary smectites in volcanic basement rocks at DSDP 418A may not necessarily have been soon after pillow eruption, and so, in detail, the Rb–Sr age of 108 ± 3 Ma can only really be considered to represent a "minimum estimate" for the age of pillow eruption (e.g., could conceivably be millions or even tens of millions of years too young). Further evidence to support this type of scenario comes from the observation of a second generation of late-stage "off-axis" celadonite formation associated with renewed/continued alkali fixation documented locally in the oceanic crust [164]. It is also notable that due to problems associated with variable amounts of fission track fading, the initial (individual) fission track ages reported for various samples of basaltic glass in the study by Storzer and Sélo [125] ranged widely between 46 and 76 Ma—collectively requiring the derivation of a series of quite significant "age corrections" that varied systematically according to depth, which could potentially affect the accuracy of the final "thermally corrected" fission track age of 108.3 ± 1.3 Ma because of the additional assumptions inherent in the derivation of these age corrections. Therefore, the widely accepted age of ~108 Ma (or ca. 110 Ma) for the timing of formation of volcanic basement at DSDP 418A (e.g., [11, 26–28, 31, 33, 59, 94, 100, 111, 112, 125, 163]) may not necessarily be that accurate based on these original age constraints—and this idea is furthered if we consider another ^{40}Ar–^{39}Ar radiometric dating study carried out on drilled basalts from DSDP Holes 417D and 418A [165], additional biostratigraphic controls from overlying Layer 1 sediments [166], and, most importantly, the regional tectonic setting during the formation of oceanic crust (and associated linear magnetic anomalies) in the western North Atlantic region, in the context of global models of seafloor spreading in the Mesozoic Era [167].

Firstly, another radiometric dating study of DSDP 418A (and 417D) basalts was carried out early on [165], which employed an ^{40}Ar–^{39}Ar stepwise degassing method of dating

that was performed on seven whole rock samples of crystalline rocks (basalts) recovered from these drill holes. However, useful age information was only obtained for one of these samples (*417D-22-3-[134–139]*)—a plagioclase phyric basalt—and therefore age constraints on the timing of pillow lava eruption at DSDP 418A can only be made by assuming that the timing of emplacement of Layer 2 basalts at these two nearby (within 8 km of one another) drill holes was about the same—which is a reasonable assumption given that both drill sites are situated on the same regional linear magnetic anomaly "M0" (Figure 5(d)). Stepwise ^{40}Ar–^{39}Ar dating of this basalt sample from DSDP Hole 417D yielded a relatively complex spectrum of apparent ages ranging from 98.6 to 185.3 Ma, although five out of seven fractions were found to plot along a ~120 Ma reference isochron [165], possibly indicating that the age of the rock (and the M0 anomaly) is about 12 million years older than was determined by the aforementioned fission track dating study [125] of basaltic glasses from DSDP Holes 417A, 417D, and 418A.

Additional support for a slightly older age of eruption of pillow basalts at DSDP 418A comes from paleontological (biostratigraphic) arguments derived from observations of calcareous nanofossils present within the 324 m succession of Layer 1 pelagic sediments overlying the volcanic basement containing these pillow lavas. Gartner [166] documented the presence of a distinctive nanofossil species (*Lithastrinus floralis*) in sediments, a short distance above the volcanic basement/sediment contact at DSDP 418A, 418B, and 417D, that are known to have first appeared in Middle Aptian times and to be common in the Upper Aptian. Accordingly, based on these biostratigraphic constraints, the age of volcanic basement intersected by these drill holes was estimated to be not younger than ~112 Ma (i.e., at least as old as about Late Aptian [166])—again, in contrast with the slightly younger fission track age of 108.3 ± 1.3 Ma determined by Storzer and Sélo [125]. Furthermore, the occurrence of another important nanofossil datum (*Corrolithion acutum*) even lower down in the sedimentary succession intersected by two of these three drill holes (417D and 418A) was interpreted to indicate that earliest sedimentation above volcanic basement began in lower Aptian times (i.e., closer to ~125 Ma; Figures 1 and 2 in Gartner [166]).

Probably one of the best methods for estimating the age of eruption of pillow lavas at DSDP 418A that is currently available right now (until precise and accurate U–Pb isotopic ages become available for these rocks) is to consider the geological context of these lavas within the broader scale regional age patterns of development of the oceanic crust (and associated linear magnetic anomalies) in the North Atlantic Ocean. Global correlation of geomagnetic isochrons (linear magnetic anomalies in the oceanic crust linked with seafloor spreading and the reversal history of Earth's magnetic field that often show twin "tape-recorder" like symmetries about the central axis of the spreading ridge in ocean basins [168, 169]; Figure 5(c)), coupled with plate tectonic theory, has become a very useful tool in determining the age of formation of vast regions of the oceanic crust and lithosphere [170], and in fact the general age patterns of the oceanic crust and lithosphere present beneath all the world's oceans are already quite well-established [167]. Significant here is that one of the primary reasons for situating the DSDP 417 and 418 drill holes where they are (Figure 5(d)) was to intersect oceanic crust situated precisely on the Mid-Cretaceous linear magnetic anomaly/isochron "M0"—at a latitude of about 25°N [171, 172]. Therefore, before drilling was carried by the DV *Glomar Challenger*, early reconnaissance geophysical survey work was carried out by the USNS *Lynch*, in order to provide the necessary scientific means for drill site targeting [171]. From this reconnaissance work, a small geological/geophysical map was produced, highlighting local magnetic anomalies and fracture/fault zones, which situated the DSDP 417A, 417D, 418A, and 418B drill sites precisely on linear magnetic anomaly M0—with DSDP 418A situated right at the young (eastern) edge of the anomaly (Figure 5(d)). Consequently, the age of eruption of DSDP 418A pillow lavas and quenching of associated pillow rim basaltic glasses in this study coincides with the age of oceanic crust formation associated with the final stages of development of the M0 magnetic anomaly.

Linear magnetic anomalies recorded in the oceanic crust associated with the M0 Chron have now been correlated globally across the oceanic portions of several major tectonic plates—and beneath several different oceans [167, 173], notably including the North American, Eurasian, and African plates beneath the North Atlantic Ocean (note: in magnetostratigraphy, "chrons" are short intervals of geologic time, typically <1 million years in duration, often associated with a specific time period between reversals in polarity of the Earth's magnetic field [174]). On the basis of these global correlations of the M0 anomaly worldwide [167, 173], these narrow belts of oceanic crust/lithosphere are at present considered to have formed in the Mid-Cretaceous Period precisely at 120.4 Ma [167]—although some authors indicate a slightly older and more prolonged time interval of 121.00–120.60 Ma for the M0 Chron [175]. During the 1970's, 80's, and 90's, as more and more geochronological and geophysical data became available and as global models of seafloor spreading became continually more refined, age estimates for the time interval during which the globally correlated M0 magnetic anomaly was formed changed progressively between successive models from 109.01 to 108.19 Ma (LH75), from 118.7 to 118.0 Ma (KG85), from 124.88 to 124.32 Ma (GTS89), from 120.10 to 119.15 Ma (GRAD93), from 120.98 to 120.38 Ma (GRAD94), and from 121.00 to 120.60 Ma (CENT94) (see a summary of these data in Channell et al. [176]). The 121.00–120.60 Ma interval (i.e., from the base to the top of the M0 anomaly) proposed by Channell et al. [176] (based on global correlations of oceanic anomaly block models and magnetostratigraphy) is still currently considered to represent a robust estimate for the age of formation of the M0 linear magnetic anomaly worldwide [175], and it also coincides closely with the age of 120.4 Ma suggested by Müller et al. [167] (Figure 5(c)) for the age of this global magnetic anomaly. Therefore, in the present study on DSDP 418A basaltic glasses, we also consider this time interval of 121.00–120.60 Ma proposed by Channell et al. [176] to represent the current best estimate for the age of formation of the

M0 magnetic anomaly in the western North Atlantic Ocean. Accordingly, because DSDP Hole 418A was drilled directly into the "top" (or young edge) of magnetic anomaly M0 (Figure 5(d)), the timing of formation of volcanic basement at DSDP 418A is interpreted to coincide precisely with an age of 120.60 Ma. Consequently, we consider the timing of eruption of pillow lavas at DSDP 418A to be 120.60 Ma—which therefore coincides with the time of glass quenching and the age of basaltic glass "pillow margin" samples in this study (namely, *DSDP-418A-68-3[40–43]*, *DSDP-418A-72-4[13–15]*, and *DSDP-418A-75-3[120–123]*).

Here, it is important to note that the M0 Chron and associated seafloor spreading linear magnetic anomalies are quite crucial to understand many aspects of Earth evolution and plate tectonic theory, especially regarding the origin and opening of the Atlantic Ocean. In the North Atlantic Ocean, the M0 linear magnetic anomaly forms a prominent feature in the oceanic portions of both the North American (Figures 5(a) and 5(c) [167, 177]) and African (Figure 5(c)) plates and shows pronounced symmetry about the Mid-Atlantic ridge (Figure 5(c) [167]; also see Figure 1 in Bird et al. [175]) and in the southwestern North Atlantic Ocean (i.e., where DSDP Hole 418A is situated) it forms a well-defined linear magnetic anomaly that is traceable for a few thousand kilometers (Figures 5(a) and 5(c) [167, 177]). In terms of the geomagnetic and tectonic histories of the ocean basins (especially the North Atlantic), the linear magnetic anomaly M0 is quite significant, because it marks the commencement of the Cretaceous Magnetic Quiet Period (CMQP) [178, 179]—a relatively long time interval in Earth history between Chrons M0 and C34 (~120–84 Ma) during which no magnetic reversals took place (and consequently no linear magnetic anomalies are present in the oceanic crust—this CMQP is labelled in Figure 5(a))—which is also referred to as the "Cretaceous Normal Superchron" [180]. Furthermore, the M0 anomaly also coincides with an important time interval (Chron) in the geological history of the South Atlantic Ocean, because it corresponds to the time of initial ocean opening and seafloor spreading at ~120 Ma, which took place after the rifting of Africa from South America during the breakup of Gondwana, and therefore the M0 magnetic anomaly now fringes certain parts of the Atlantic-facing edges of these two continents [181]. In addition, the base of the globally correlated M0 magnetic anomaly, which is currently estimated at 121.00 Ma [175], is also an important stratigraphic time marker in that it is interpreted to coincide precisely with the Barremian–Aptian boundary of the Early Cretaceous Period [176].

3. Petrographic and SEM Studies of Dissolution/Alteration Microtextures in Basaltic Glass

To study and characterize alteration microtextures preserved in basaltic glass pillow margin samples in this study, we prepared polished petrographic thin sections and studied them (Sections 3.1–3.3) using both transmitted light microscopy (Figures 6–10; also see Figures 1(b), 1(d), and 1(f)) and SEM analysis (Figures 8–10; also see Figures 2(b), 2(d), and 4(c)—right, and 7(c)). For the SEM studies (including backscattered electron (BSE) imaging and secondary electron imaging), polished sections were first coated with ~40 Å of iridium using a Xenosput XE200 and then analysed using a JEOL 6301F field emission scanning electron microscope equipped with a PGT IMIX model X-ray analysis system—the instrument used to obtain the energy dispersive X-ray spectroscopy (EDS) spectra shown in Figure 8(j). We also carried out high resolution SEM studies (secondary electron imaging) of corrosion microtextures exposed on freshly fractured surfaces of basaltic glass "chip samples" that we prepared—which are explained later (in Section 3.4).

In polished petrographic thin section, all three glassy pillow margin samples are very similar in appearance and comprise an original igneous assemblage of ~70% sideromelane (pale brown basaltic glass) with a phenocryst modal mineralogy of ~25% plagioclase and ~5% clinopyroxene (Figure 6)—similar to other previous petrographic descriptions of pillow basalts from lithologic Unit 13 [161]. Plagioclase crystals are typically euhedral (although rare skeletal crystals are also present, "Sk" in Figures 6(a) and 6(b)), show polysynthetic albite twinning (some grains show weak oscillatory zoning, "OZ" in Figure 6(a)), and exhibit a somewhat bimodal distribution with regards to crystal size, shape, and abundance. This bimodal distribution is defined by a few large (~0.5–1 mm across) subequant/stubby plagioclase crystals (i.e., phenocrysts) dispersed amongst a larger population of small and elongate plagioclase laths (~10–100 μm wide by a few hundred μm long), thus defining an overall porphyritic texture (Figures 6(a) and 6(b)). Clinopyroxene crystals are equant, range from subhedral to euhedral in form, vary in size from <100 μm up to ~1 mm across (Figure 6(d)), and are commonly observed to partially overgrow/envelope previously formed plagioclase grains (i.e., form "glomerocrysts" with plagioclase: "glm" in Figures 6(a) and 6(c); as noted by Flower et al. [161] as well), and this is true for both the large equant plagioclase crystals (Figure 6(a)) and also the smaller clusters of plagioclase laths (Figure 6(c)), thereby defining a sort of protoophitic petrographic texture. For the most part, all plagioclase and clinopyroxene crystals are fresh and unaltered in these pillow lavas; however, basaltic glass is variably altered to both orange-brown palagonite ("P" in Figures 6(d) and 7) and white (K-Al-Si)-rich devitrified zones ("D" in Figures 7(a), 7(b), and 8(a)–8(f)).

The most striking petrographic feature exhibited by these glassy pillow margin samples is pronounced irregular palagonitization (corrosion/alteration of basaltic glass) along fractures (e.g., Figures 1(b), 6(d), 7(a), 9(m)–9(o), and 10(a)). Accordingly, the basaltic glass in these samples ranges locally from fresh unaltered glass (e.g., "FG" in Figures 6–10) to highly altered zones along fractures (e.g., "P" in Figures 6–10), and at least two distinct episodes of fracturing and alteration/devitrification have affected these glasses: (1) early fracturing (labelled "f_1" in Figures 7–9) associated with incipient and ongoing palagonitization and (2) late fracturing (labelled "f_2" in Figures 7 and 8) associated with white (K-Al-Si)-rich devitrified zones (Figures 7(a), 7(b), and 8). Palagonitization refers to the formation of

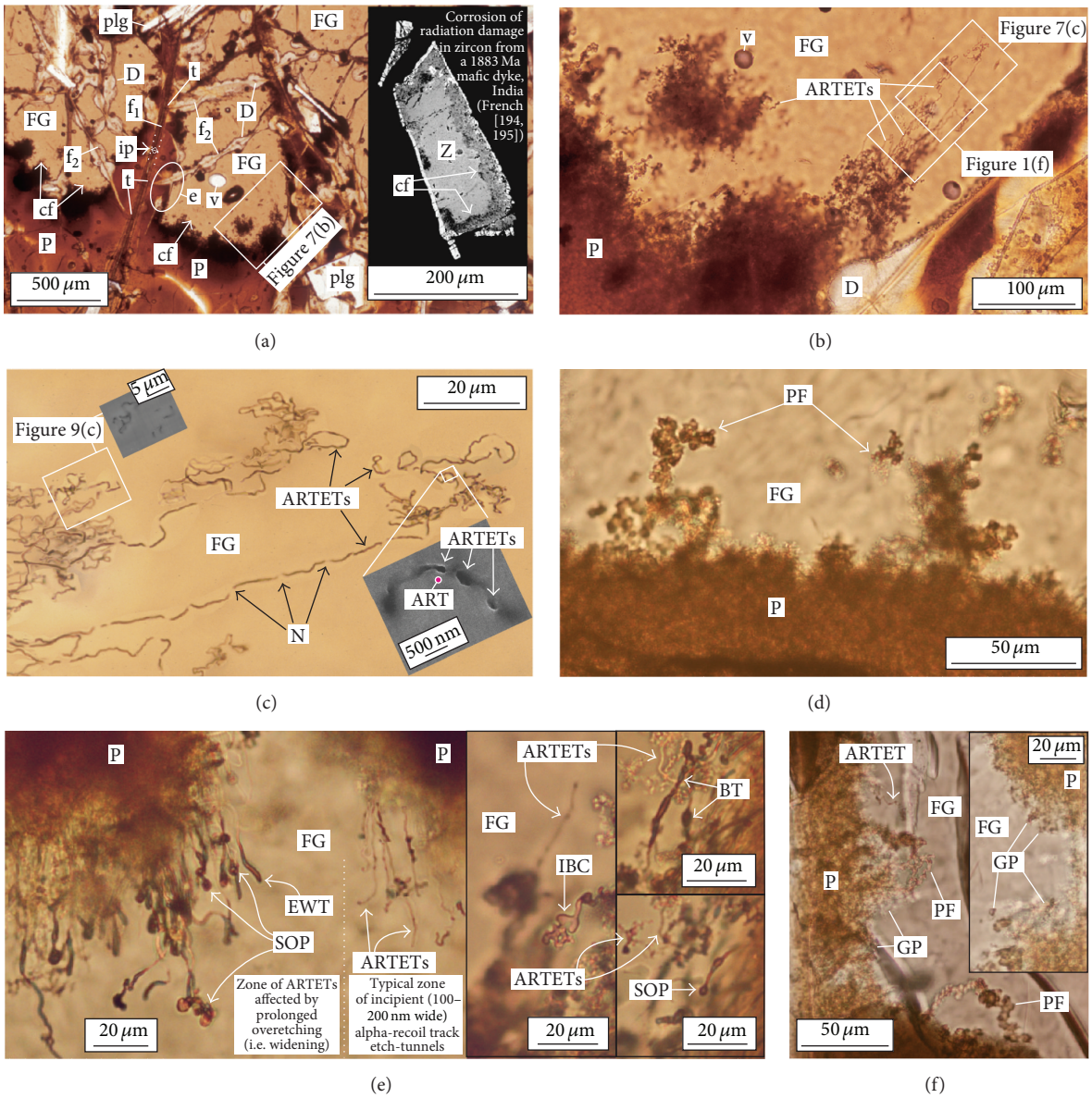

Figure 7: Diversity of *abiotic* corrosion microtextures in DSDP 418A basaltic glass linked with palagonitization (all thin section photomicrographs are taken in plane polarized light (uncrossed nicols); (a–e): sample *DSDP-418A-75-3[120–123]*; (f): sample *DSDP-418A-72-4[13–15]*). (a) Overview, highlighting fresh basaltic glass (FG), vesicles (v), plagioclase phenocrysts (plg), early fracturing (f_1) associated with incipient (ip) and ongoing palagonite (P), late fracturing (f_2) associated with white (K-Al-Si)-rich devitrified zones (D), regions where white devitrified zones have been enveloped (labelled "e") by ongoing palagonitization, and the corrosion front (cf) associated with etched radiation damage. Inset BSE image: Paleoproterozoic (1883.0 ± 1.4 Ma) zircon (Z) from the BD2 mafic dyke swarm, India, highlighting a similar corrosion front developed in the relatively U- and Th-rich (radiation damaged) zircon core during recent tropical weathering (Appendix A in French [194]; Figures 1 and 2 in French [195]). (b) Close-up from (a) highlighting fresh basaltic glass, vesicles, white (K-Al-Si)-rich devitrified zones exhibiting weak evidence of axiolitic internal microtextures, palagonite, and alpha-recoil track etch-tunnels (ARTETs). (c) Close-up from (b) highlighting the characteristic tortuosity of ARTETs in fresh basaltic glass and places where necking (N) has pinched off certain portions of these nanotunnels. This image is a photomosaic of numerous image fragments taken at 15 different focal depths throughout the entire depth of the ~30 μm thick petrographic thin section (a single image from this same area—see (b)—is shown in Figure 1(f), in which the alpha-recoil tracks appear to dive in and out of focus). Two inset SEM (secondary electron) images highlight the tiny size of these ARTETs, where they intersect the surface of the polished thin section (~100–200 nm wide), that is, about the same size as an alpha-recoil track (or ART; see ~120 nm pink dots in Figures 7(c) and 9(d)). (d) Region where palagonite fingers (PF) have now "overprinted" previously existing ARTETs. (e) Four regions where incipient ARTETs have been affected by prolonged overetching (i.e., etch-tunnel widening), possibly in relation to pressure solution, resulting in a diversity of etch-tunnel sizes and shapes, including elongate wide tunnels (EWT), string-of-pearls texture (SOP), irregular bulbous cavities (IBC), and boudinaged tunnels (BT). Note: the zone of incipient ARTETs (at right in the left image) is a photomosaic of five focal depths, and the two small images at far right are of the same region but different focal depths. (f) Two photomicrographs highlighting development of "granular palagonite ART alteration" (GP), as well as additional examples of palagonite fingers (PF) and a single (ARTET).

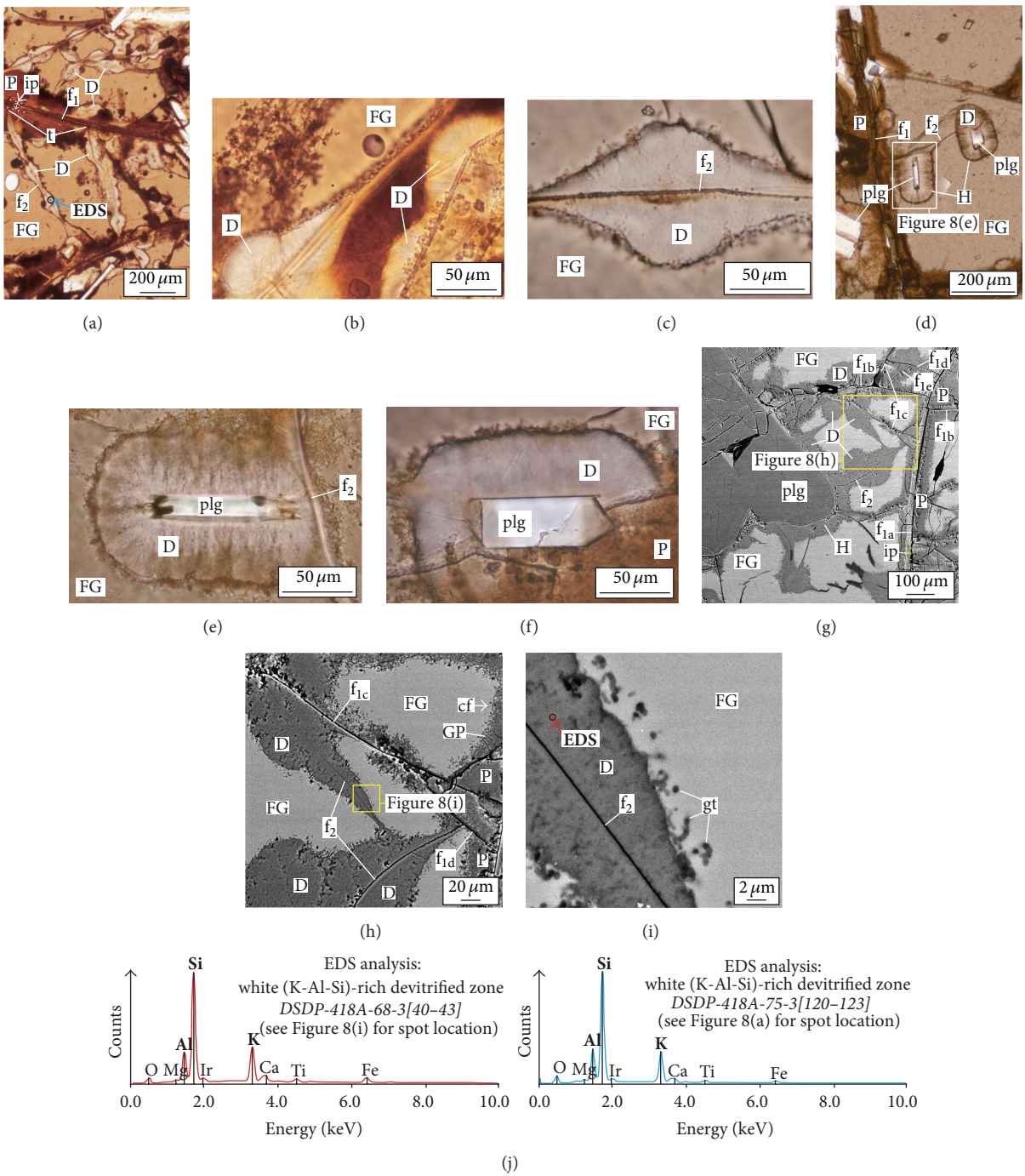

FIGURE 8: Petrographic and SEM study of white (K-Al-Si)-rich devitrified zones (in thin section). (a–f) Photomicrographs in plane polarized light, highlighting development of "lip-shaped" (K-Al-Si)-rich devitrified zones along late (f_2) fractures (a–c), as well as halos around some plagioclase crystals (d–f). (a, b): sample *DSDP-418A-75-3[120–123]*; (d, e): sample *DSDP-418A-68-3[40–43]*; (c, f): sample *DSDP-418A-72-4[13–15]*. (g–i) SEM (BSE) images of a polished thin section of sample *DSDP-418A-68-3[40–43]*, highlighting white (K-Al-Si)-rich devitrified zones. Note: palagonitization of basaltic glass along early (f_1) fractures (a, d, g, and h) and the stepwise/punctuated "cracking" of basaltic glass (from f_{1a} through f_{1e} in (g, h) and from f_1 through f_2 in (a, d, g, and h)), inferred based on the pattern of termination of successively younger fractures against older ones. (j) SEM EDS spectra for white (K-Al-Si)-rich devitrified zones (see petrographic context in (a, i)), showing abundant Si, Al, and K—consistent with microcrystalline K-feldspar ± quartz or cristobalite. cf: corrosion front; D: white (K-Al-Si)-rich devitrified zones; f_1 (including f_{1a}–f_{1e}): early fractures along which palagonite is rooted; f_2: late fractures along which white (K-Al-Si)-rich devitrified zones are rooted; FG: fresh basaltic glass; GP: granular palagonite ART alteration; gt: minor granular corrosion texture associated with devitrified zones; H: halos of white (K-Al-Si)-rich devitrified zones around plagioclase; ip: initial palagonite; P: palagonite; plg: plagioclase.

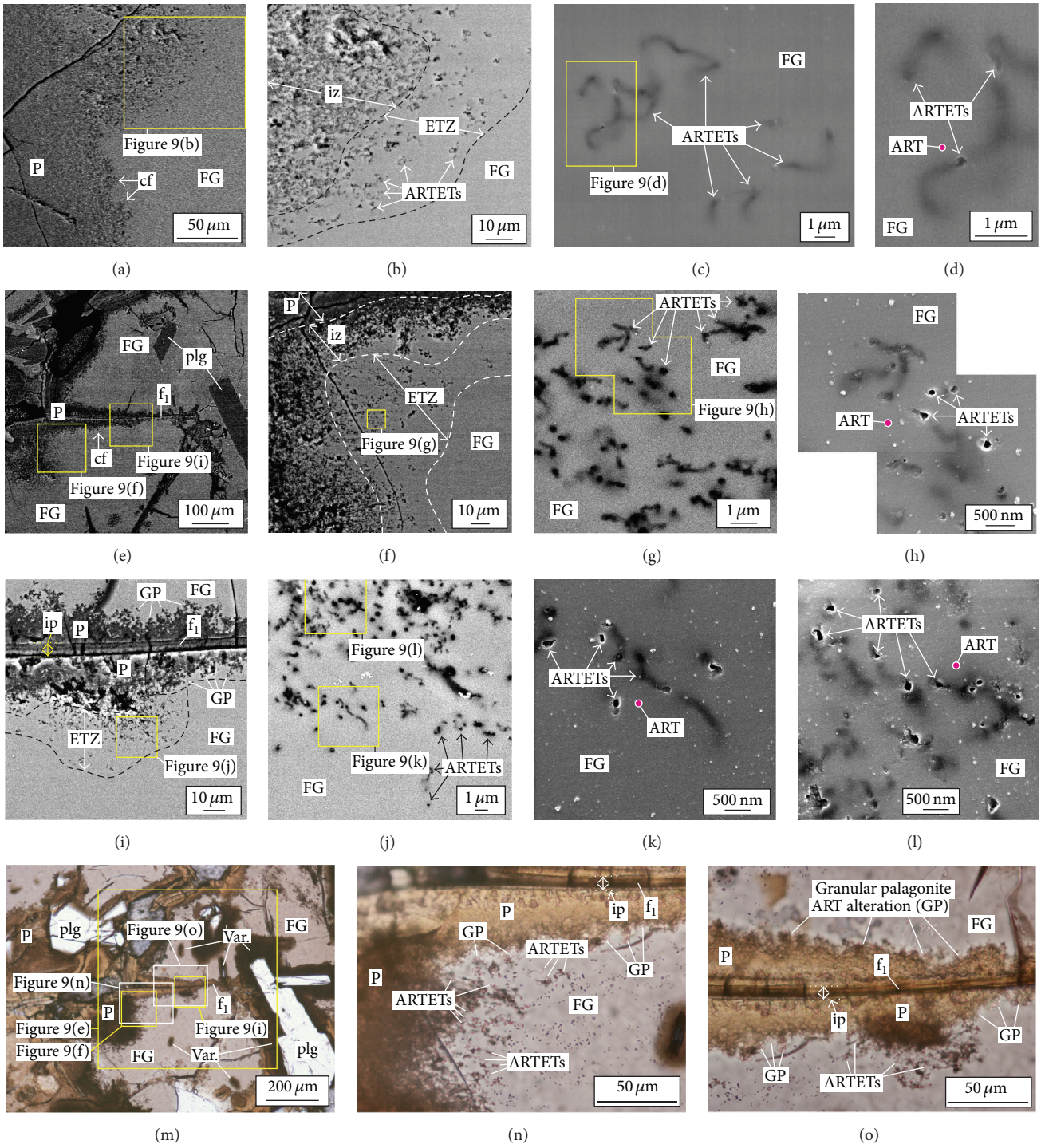

FIGURE 9: Petrographic and SEM study of the alpha-recoil track etch-tunnel (ARTET) zone at the glass-palagonite interface (in polished petrographic thin section). (a–d): sample *DSDP-418A-75-3[120–123]*; (e–o): sample *DSDP-418A-68-3[40–43]*. The images shown in (a, b, e–g, i, and j) are BSE images, while (c, d, h, k, and l) are secondary electron images. Note: (c) and (d) are close-ups from Figure 7(c). Pink dots in (d, h, k, and l) represent hypothetical ARTs—note the striking similarity in size between the real etch-tunnels and the ARTs. Photomicrographs (taken in plane polarized light) in (m–o) show the same petrographic area shown in (e–l). ART: alpha-recoil track; ARTETs: alpha-recoil track etch-tunnels; cf: corrosion front; ETZ: etch-tunnel zone; f_1: early fractures associated with palagonite; FG: fresh basaltic glass; GP: granular palagonite ART alteration; ip: initial palagonite; iz: intermediate zone (between the etch-tunnel and palagonite zones); P: palagonite zone; plg: plagioclase; Var.: varioles.

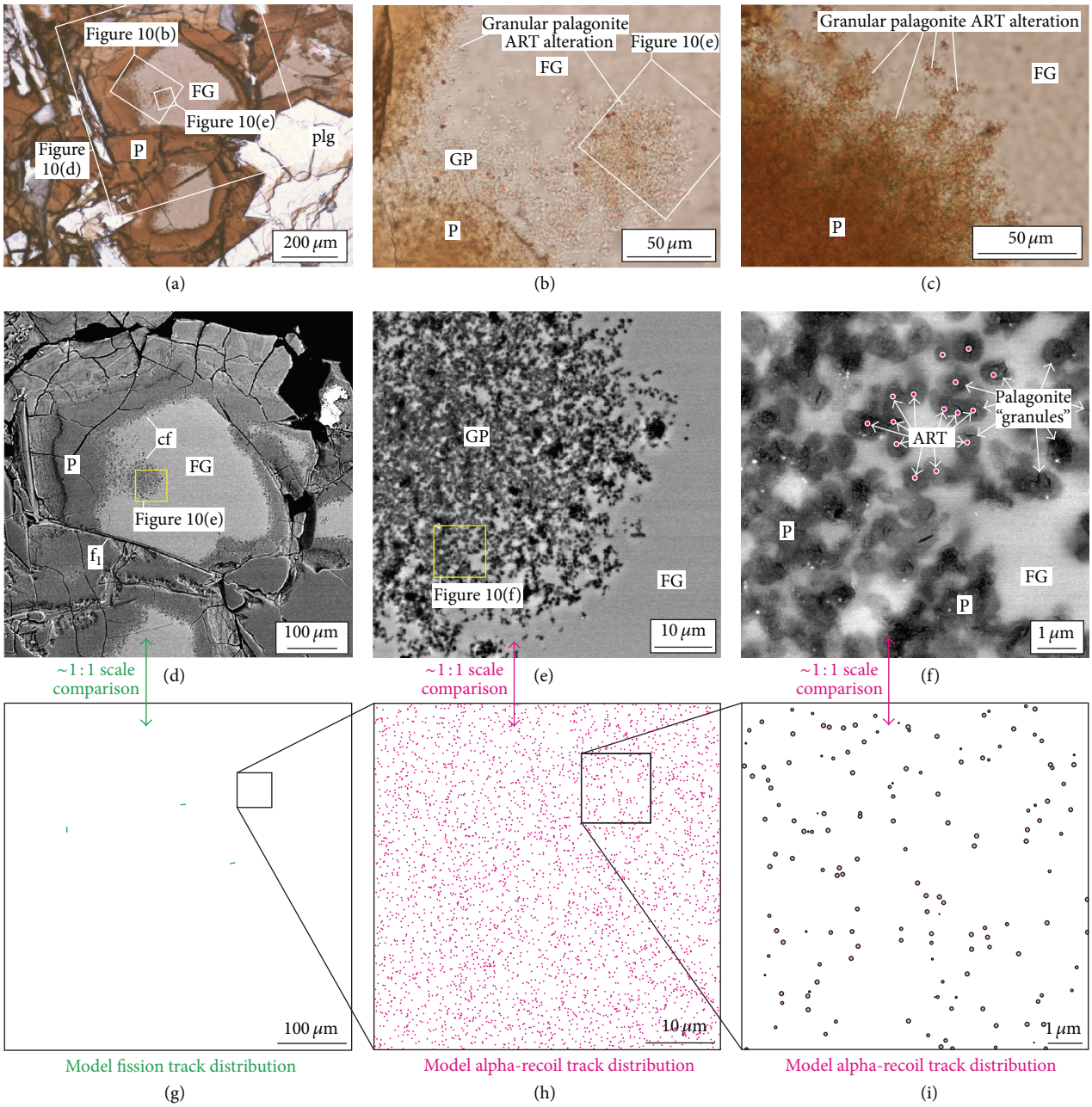

Figure 10: Petrographic, SEM, and theoretical modelling study of "granular palagonite ART alteration" microtexture in DSDP 418A basaltic glass. (a–c) Thin section photomicrographs (in plane polarized light) of samples *DSDP-418A-68-3[40–43]* (a, b) and *DSDP-418A-75-3[120–123]* (c), highlighting "granular palagonite ART alteration." (d–f) Close-up SEM (BSE) images from (a, b). (g–i) Theoretical plots of model fission track (g) and alpha-recoil track (h, i) areal distributions in DSDP 418A basaltic glass (calculated using (1) and (2); fission tracks are shown in green (g) and alpha-recoil tracks in pink (h, i)). The model track distributions in (g–i) are shown at approximately the same scale as the SEM images in (d–f), respectively—see green and pink arrows. Note that fission tracks are quite sparse (g), but alpha-recoil tracks are quite abundant and correlate very well with the observed pattern of development and areal distribution of ~0.3–1.0 μm palagonite "granules" (i.e., compare (h) and (e), and (i) and (f)), thus indicating that, during corrosion of basaltic glass by seawater, granular palagonite microtextures develop through selective palagonitization of alpha-recoil tracks (and not microbial activity). To emphasize this idea, several hypothetical, previously existing alpha-recoil tracks (120 nm pink dots) are plotted in (f), which would have acted as ideal "point sources" of radiation damage amenable to preferential corrosion/palagonitization. ART: alpha-recoil track; cf: corrosion front; f_1: early fractures associated with palagonite; FG: fresh basaltic glass; GP: granular palagonite ART alteration; P: palagonite; plg: plagioclase.

secondary orange-brown palagonite along fractures during low temperature aqueous alteration/corrosion, hydration, and dissolution of basaltic glass by infiltrating seawater (Figure 7; see further explanation in Sections 3.2 and 3.3—also see reviews on palagonite/palagonitization in Crovisier et al. [136] and Stroncik and Schmincke [182]), and the formation of white (K-Al-Si)-rich devitrified zones is explained below in Section 3.1. The development of such orange-brown palagonite during aqueous alteration of basaltic glass is a common feature in both submarine [44] and terrestrial (e.g., Icelandic [136, 183] and Hawaiian [110]) basaltic glasses, and data on the mineralogical and chemical characteristics of typical palagonites formed from weathered/altered basaltic glass can be found elsewhere [44, 110, 136, 182, 183].

3.1. White (K-Al-Si)-Rich Devitrified Zones. The white devitrified zones ("D" in Figures 7(a), 7(b), and 8) are typically lip-shaped (i.e., pinch and swell shaped and symmetrical about a central fracture/axis: Figures 8(a)–8(c)) or occur as ~50 μm thick rims/halos surrounding plagioclase phenocrysts ("H" in Figures 8(d)–8(g)), range up to ~100 μm in thickness at the swells (e.g., Figure 8(c)), have relatively sharp curvilinear contacts with basaltic glass (i.e., smooth and sharp glass–devitrification interfaces: Figure 8(c)), and are composed primarily of microcrystalline K-feldspar (i.e., are K-, Al-, and especially Si-rich based on EDS analysis (by SEM): see Figure 8(j)) (±quartz or cristobalite?)—similar in composition to some other examples of devitrified volcanic glass (p. 418 in Cas and Wright [184], [185]).

Locally, these white (K-Al-Si)-rich devitrified zones exhibit a weakly fibrous internal microtexture, visible with transmitted light microscopy (Figure 8(b)) and define an overall axiolitic structure (i.e., with fibers growing outward from the observed linear fractures along the central axis of the pinch and swell structures)—similar in nature to the axiolitic devitrification textures commonly observed in rhyolitic glasses [185]. Similarly, the white devitrified zones that form halos around plagioclase phenocrysts also exhibit a fibrous internal microtexture, but in this case the fibers appear to radiate around the phenocrysts, maintaining perpendicularity to the plagioclase contact (Figures 8(d) and 8(e)). High resolution SEM imaging of these white devitrified zones does not reveal any evidence of this fibrous/axiolitic microstructure and instead shows a more mottled and even textured material (Figures 8(h) and 8(i)); however, this is in keeping with the definition of axiolitic structure defined by A. Allaby and M. Allaby [185], which states that such axiolitic fibers are typically only visible by petrographic microscope.

The white (K-Al-Si)-rich devitrified zones described here are similar in size, shape, geological context, and chemical composition to light coloured K-rich zones documented in a previous study of DSDP 418A basaltic glasses [186], where they were also found to occur in basaltic glass along some fractures and as rims around some plagioclase phenocrysts and interpreted as poorly crystalline, secondary K-feldspar.

Although the glass-devitrification interface is for the most part quite sharp and curvilinear (e.g., see boundary between "D" and "FG" in Figure 8(c)), close-up SEM imaging reveals the presence of a minor amount of "granular textured" corrosion features (defined by ~0.5–1 μm wide granules) that extend outwards (typically <10 μm) into fresh basaltic glass ("gt" in Figure 8(i)), which we interpret as incipient corrosion of previously formed alpha-recoil tracks in the glass during devitrification. This interpretation is based on the similarity in size and form of these corrosion microtextures to other such "granular textures" described from the glass-palagonite interface that are considered to have formed by preferential corrosion of multitudes of randomly distributed alpha-recoil tracks (see Figure 10 and Section 3.3.2). However, because the formation of these white devitrified zones is presumed to have taken place relatively early on in the alteration history of these rocks (<~1 million years after pillow eruption—possibly during burial beneath the overlying volcanic pile—see below), only a minor amount of alpha-recoil tracks were likely to have been present during devitrification—resulting in only minor/sparse development of granular corrosion microtextures at the glass-devitrification interface (Figure 8(i)).

Aside from being the possible end product of the solid-state transformation of basaltic glass into poorly crystalline materials (i.e., secondary K-feldspar ± quartz or cristobalite?) during devitrification [185], the formation of these white axiolitic devitrified zones (and associated f_2 fractures) and halos in DSDP 418A basaltic glass might have been triggered as a diagenetic/low-grade-metamorphic response (cf. p. 418 in Cas and Wright [184]) to deep burial (to 408–461 m) of these glasses beneath the overlying volcanic pile (Figure 5(b)), late in the history of the spreading ridge. High temperature devitrification of submarine glasses (i.e., penecontemporaneous with eruption and quenching) commonly results in the formation of varioles (also known as "variolites" [184] or "spherulites"—in glasses with more felsic compositions [187, 188]), which are typically comprised of tiny radiating crystals of clinopyroxene and/or plagioclase (±quartz or cristobalite) [184, 187, 188], but this can be ruled out in the present case because the fractures along which these white devitrified zones occur (i.e., "f_2" in Figures 7 and 8) clearly truncate ("t" in Figures 7(a) and 8(a)) against an earlier-formed set of fractures ("f_1" in Figures 7(a) and 8(a)) along which "low temperature" palagonite had already formed (e.g., "ip" in Figures 7(a), 8(a), and 8(g)) and, moreover, the mere fact that these white devitrified zones occur along fractures suggests that they must have formed sometime after the glass had cooled below the glass transition temperature (i.e., ~600–700°C [189]) to allow the fracturing to occur in the first place. Furthermore, the composition of these white (K-Al-Si)-rich devitrified zones is consistent with poorly crystalline K-feldspar (Figure 8(j)) and not plagioclase or clinopyroxene, and they do not form masses of coalescing spheroidal bodies (of radiate fibers) that are typical of high temperature devitrification textures (e.g., Figures F14, F15, F23, and F31 in Shipboard Scientific Party [187]). However, some minor occurrences of varioles do exist locally in some of the basaltic glass pillow margin samples studied (e.g., "var." in Figure 9(m)), and although they also occur as halos around some plagioclase phenocrysts, they are distinctly different from the white (K-Al-Si)-rich devitrified zones in

that they are dark brown in colour (i.e., resemble very dark brown basaltic glass: Figure 9(m)) and are interpreted as primary (high temperature) igneous quench features—similar in nature to the dark-coloured varioles described by Fisk and McLoughlin [103]. Another possible explanation for the origin of the white (K-Al-Si)-rich devitrified zones (Figure 8) in DSDP 418A glasses (i.e., aside from diagenetic/low-grade metamorphic response to deep burial—alluded to above) is that they are more externally linked to an episode of late alkalic hydrothermal alteration (i.e., metasomatism) affecting these pillow basalts, given that late-stage (i.e., renewed or continued) "off-axis" alkali fixation is known to occur in the alteration history of the oceanic crust [164] and that K-feldspar can be a product of hydrothermal alteration of glassy volcanic rocks [190].

3.2. Stepwise Development of Fracturing, White Devitrified Zones, and Palagonitization. The textural relationships observed between different generations of fractures (f_1 and f_2), development of white (K-Al-Si)-rich devitrified zones, and stepwise/incremental encroachment of orange-brown palagonite alteration zones in these volcanic glasses are somewhat complex (e.g., Figures 7(a), 7(b), 8(a), 8(d), 8(g), and 8(h)). Initially (sometime soon after pillow eruption and quenching of basaltic glass), these glassy pillow margins underwent f_1 fracturing followed by infiltration of seawater and incipient palagonitization along these fractures, resulting in thin (typically 10–50 μm thick), straight, *initial* palagonitic layers ("ip" in Figures 7(a), 8(a), 8(g), 9(i), 9(n), and 9(o)) that are parallel to (and occur along) f_1 fractures. Some *later* "f_1" fractures probably formed during the initial stages of development of the volcanic pile (early burial) and are considered to have formed as a series of individual discrete curviplanar fractures (i.e., not occurring in parallel sets) that represent incremental "cracking" of glass in stages (e.g., see f_{1a} to f_{1e} in Figure 8(g)). The formation of initial orange-brown palagonitic layers along f_1 fractures ("ip" in Figures 7(a), 8(a), 8(g), 9(i), 9(n), and 9(o)) is interpreted to have occurred during the first several thousand years of glass alteration (palagonitization) by infiltrating seawater, during which radiation damage in the glass was quite minimal and therefore the glass-palagonite interface on either side of the f_1 fractures remained quite sharp and parallel to the f_1 fractures—essentially equivalent to the straight, fracture-parallel, palagonite alteration textures observed in young Icelandic basaltic glasses (see Figure 1 in Crovisier et al. [136]) and also in some submarine basaltic glasses (i.e., so-called "abiotic" palagonite alteration described in Section 4.1 of Furnes et al. [59], Figure 1 in Staudigel et al. [75], Figure 13(a) in Furnes et al. [11], Figure 1 in Furnes et al. [26], Figure 2 in McLoughlin et al. [31], and Figure 1 in Staudigel et al. [27]). These relict "sharp contacts" can still be seen ("ip" in Figures 7(a), 8(a), 8(g), 9(i), 9(n), and 9(o)), even though they have now been overgrown by a subsequent/ongoing stage of palagonitization ("P" in Figures 7(a), 8(a), 8(g), 9(i), 9(n), and 9(o)) discussed below (in Section 3.3). Such slow advancement of the glass-palagonite interface (i.e., on the order of microns over timescales of thousands or millions of years) is a well-known aspect of the palagonitization process [136] and is probably in part due to the protective effect of the alteration layer [136, 191] and has even prompted some to consider using palagonite rind thickness as an archaeological dating tool for certain basaltic glass/obsidian artefacts [40].

Subsequent to the development of these narrow incipient (i.e., initial) palagonitic layers along f_1 fractures in basaltic glass ("ip" in Figures 7(a), 8(a), 8(g), 9(i), 9(n), and 9(o)), a second stage of fracturing (f_2) of these glasses took place along which white (K-Al-Si)-rich devitrified zones developed (Figures 7(a), 7(b) and 8) and as highlighted above (in Section 3.1) this probably took place in response to deep burial of these pillow lavas beneath some 450 m of overlying lavas (perhaps 50 to 100 thousand years after their initial eruption, during the building up of ancient "axial volcanic ridges" (which may be up to ~600 m high [192]) on the floor of the median valley of the Early Cretaceous Mid-Atlantic Ridge). Where they intersect the earlier-formed (f_1) fractures (along which palagonite is rooted), these second-stage (f_2) fractures are observed to terminate against them ("t" in Figures 7(a) and 8(a))—thus indicating their "younger" relative age—which is consistent with late-stage (f_2) "cracking" (and associated devitrification) of the intervening basaltic glass that occurs between preexisting f_1 fractures (i.e., during deep burial).

Ongoing palagonitization of basaltic glass by infiltrating seawater (i.e., *still* rooted along f_1 fractures) then appears to have continued long after the formation of white (K-Al-Si)-rich devitrified zones and associated f_2 fractures, as evidenced by the advancement of orange-brown palagonite ("P" in Figure 7(a)) that has partially enveloped/overgrown preexisting white (K-Al-Si)-rich devitrified zones (oval labelled "e" in Figure 7(a)). Unlike the early-formed, narrow (<50 μm) layers of incipient palagonite ("ip" in Figures 7(a), 8(a), 8(g), 9(i), 9(n), and 9(o)), which seem to exhibit relict "sharp contacts" with preexisting glass, this next stage of continued (and ongoing) palagonitization of basaltic glass ("P" in Figures 7–10) extends for distances of up to several hundred microns away from the f_1 fractures and appears to have been advancing in the wake of an irregular and complex corrosion front ("cf" in Figures 7(a), 8(h), 9(a), 9(e), and 10(d)) that occurs at the present-day glass-palagonite interface. This corrosion front is locally characterized by a pronounced etch-tunnel zone (Figures 1(b), 1(d), 1(f), 7, and 9) that extends out in front of the palagonite zone into fresh basaltic glass for distances of up to a few hundred microns (e.g., Figure 7(b))—in addition to regions characterized by "granular" palagonite microtextures (Figures 7(f), 8(h), 9(i), 9(n), 9(o), and 10(a)–10(f)). The nature and origin of this complex corrosion front—and associated "etch-tunnel zone" and "granular palagonite microtexture"—is the main focus of the present study on DSDP 418A basaltic glass, because in many previous studies of basaltic glasses from this drill site, such alteration microtextures have classically been interpreted as evidence for microbial activity (i.e., biocorrosion/bioalteration) [11, 26–28, 31, 33, 59, 61, 93, 94, 100]—whereas we think that they instead represent evidence of "abiotic" corrosion (palagonitization and etch-tunnelling: by seawater) of dense concentrations of randomly distributed,

radiation damaged sites in the glass (p. 10 in French and Muehlenbachs [107], [111–113, 139]).

Therefore as a first step, in the next few Sections we provide a range of detailed observations of complex corrosion microtextures that occur at the glass-palagonite interface in these studied samples of basaltic glass pillow margins from DSDP 418A.

3.3. Complex Corrosion Microtextures Associated with Ongoing Palagonitization. Palagonitization is interpreted to have started early—soon after quenching (in the Early Cretaceous), in association with f_1 fracturing (as outlined in Section 3.2)—but also to have been episodic and ongoing in these rocks, possibly right up until the point of drilling and sample collection. The present-day glass-palagonite interface is very irregular and mottled in form due to the presence of a complex corrosion front that occurs there ("cf" in Figures 7(a), 8(h), 9(a), 9(e), and 10(d))—the formation of which seems to occur in advance of the encroaching orange-brown palagonite by some kind of initial corrosion/dissolution/etch-tunnelling process that takes place within fresh basaltic glass. Similar alteration microtextures have also been observed in the interior of some zircon grains caused by preferential corrosion of high U and Th (radiation damaged) regions during weathering (e.g., "cf" in Figure 7(a) (inset BSE image); Figure 9 in Lumpkin [193]; Appendix A in French [194]; Figure 1(d) in French [195]), and thus, by comparison, the irregular corrosion front observed here ("cf" in Figures 7(a), 8(h), 9(a), 9(e), and 10(d)) may also have been caused by preferential corrosion of radiation damaged regions of basaltic glass by seawater. In polished petrographic thin section, this corrosion front at the glass-palagonite interface in DSDP 418A basaltic glass can be subdivided into two distinct microtextural varieties including an "etch-tunnel zone" (i.e., "ARTETs" in Figures 1, 7, and 9) and a "granular palagonite alteration zone" (i.e., "granular palagonite ART alteration" or "GP" in Figures 2(b), 2(d), 7(f), 8(h), 9(i), 9(n), 9(o), and 10(a)–10(f)), which are described below in Sections 3.3.1 and 3.3.2, respectively.

3.3.1. The Etch-Tunnel Zone at the Glass-Palagonite Interface. Palagonite at the glass-palagonite interface locally appears to be superficially much darker in colour (i.e., almost black)—when viewed under plane polarized light by petrographic microscope—because it grades into a complex network of nanoscopic etch-tunnels that scatter and absorb light (Figures 1(b), 7(a), 7(b), and 9(m)–9(o)). These etch-tunnels extend outwards into the fresh glass for up to several hundred microns past the palagonite zone (Figure 7(b)), tracing out intricate 3-dimensional curvilinear pathways through the glass (Figure 7(c)) that exhibit a high degree of tortuosity (i.e., highly anastamosing patterns), which allows only a small portion of them to be brought into focus at a given time under petrographic microscope (e.g., Figure 1(f)). A mosaic of many photomicrographic image fragments taken at 15 different focal depths shows a more complete "in focus" representation of the tunnel networks observed in a ~30 μm thick petrographic section (Figure 7(c)). SEM imaging reveals that where they intersect the surface of the thin section, the tunnels imaged in these photomicrographs of sample *DSDP-418A-75-3-[120–123]* (Figures 1(f) and 7(a)–7(c)) are ~120 nm wide (see Figures 7(c) (inset secondary electron images) and 9(c), 9(d))—essentially identical in size as a typical alpha-recoil track (~120 nm in diameter [129]; see pink dots in Figure 7(c) (inset) and in Figure 9(d)). Similar SEM imaging of the etch-tunnel zone preserved at the glass-palagonite interface in a polished petrographic section of sample *DSDP-418A-68-3[40–43]* (Figures 9(e)–9(o)), ~50 m higher up in the volcanostratigraphic succession (Figure 5(b)) also reveals that these etch-tunnels at the glass-palagonite interface are typically ~120 nm wide (i.e., compare the diameters of hypothetical alpha-recoil tracks (pink dots) with those of the etch-tunnels—i.e., "ARTETs"—in Figures 9(h), 9(k), and 9(l)). The similarity in diameter between hypothetical alpha-recoil tracks and the observed etch-tunnels (i.e., circa 120 nm in both cases; Figures 9(d), 9(h), 9(k), and 9(l)) at the glass-palagonite interface in two different DSDP 418A pillow margin samples provides compelling evidence that this etch-tunnelling and corrosion which takes place in advance of the palagonitization front occurs primarily due to preferential dissolution (by seawater) of multitudes of randomly distributed alpha-recoil tracks in the glass—in contrast with previous biogenic (i.e., microbial trace fossil) interpretations (i.e., of "tubular" texture at DSDP 418A [11, 26–28, 31, 33, 59, 61, 93, 94, 100]. For that reason (also see Sections 3.4 and 5), we propose that the majority of etch-tunnels observed at the glass-palagonite interface in polished petrographic sections of DSDP 418A basaltic glass (e.g., Figures 1(a)–1(d), 1(f), 7(a)–7(c), 7(e), and 9) can now be interpreted as "alpha-recoil track etch-tunnels" (ARTETs).

Subsequent to their formation at the glass-palagonite interface, late secondary modification of some of these alpha-recoil track etch-tunnels has also locally taken place. For instance, postdissolutional "necking" of tunnel walls ("N" in Figure 7(c)) has healed/closed-off many portions of these alpha-recoil track etch-tunnels ("ARTETs" in Figure 7(c)) into what are now isolated, elongate (several microns long), narrow (~120 nm wide) fluid inclusions that presumably contain seawater. In addition, at many places along the glass-palagonite interface, encroachment of palagonite appears to have completely overprinted/destroyed preexisting alpha-recoil track etch-tunnels, preserving their elongate curvilinear form as "palagonite fingers" that extend outward into fresh glass (Figures 7(d) and 7(f)). Furthermore, prolonged overetching (perhaps caused by pressure solution etch-tunnelling—this idea is explored further in Section 5.3) has apparently widened some incipient alpha-recoil track etch-tunnels to significantly larger tunnels of myriad shapes (Figure 7(e)), including elongate wide tunnels (EWT), string-of-pearls (SOP) texture (cf. string-of-beads texture in Figure 1(f) of Fisk et al. [24], and string-of-pearls texture described in Figure F68 of Shipboard Scientific Party [60] and Banerjee and Muehlenbachs [64]), irregular bulbous cavities (IBC), and boudinaged tunnels (BT: i.e., shaped like sausage links—but not "stretched" as in other examples of boudinaged rocks in the field of structural geology). In the studied samples, these larger "overetched" tunnels (Figure 7(e)) are

somewhat rare and atypical in comparison to the more common ~120 nm wide "incipient" alpha-recoil track etch-tunnels (Figures 1(b), 1(d), 1(f), 7(b), 7(c), 7(e), and 9), which represent >95% of all tunnels observed in the etch-tunnel zone at the glass-palagonite interface in basaltic glass pillow margins in this study.

3.3.2. Granular Palagonite ART Alteration Microtextures. In many places along the glass-palagonite interface, alpha-recoil track etch-tunnels are abundant (e.g., Figures 7 and 9)—but equally common along this interface is a distinctly different type of corrosion microtexture: granular palagonite ART (alpha-recoil track) alteration (Figure 10; also see Figures 2(b), 2(d), 7(f), 8(h), 9(i), 9(n), and 9(o)). For instance, along the f_1 fracture highlighted in Figures 9(e), 9(i), and 9(m)–9(o), a prominent alpha-recoil track etch-tunnel zone occurs at the glass-palagonite interface on one side (i.e., the bottom side: "ETZ" in Figures 9(f) and 9(i) and "ARTETs" in Figures 9(n) and 9(o)) in addition to abundant granular palagonite ART alteration ("GP" in Figures 9(i), 9(n), and 9(o)). In contrast, the glass-palagonite interface on the opposite side of this fracture exhibits only "granular palagonite ART alteration" microtextures (i.e., "GP," top side of the fracture in Figure 9(i), and "granular palagonite ART alteration" in Figure 9(o)).

Although such "granular" palagonite alteration microtextures may occur adjacent to alpha-recoil track etch-tunnels (as in the previous example), this style of corrosion/palagonitization of basaltic glass is not considered to form by any kind of prior dissolution (e.g., etch-tunnelling) process—in contrast with "palagonite fingers" (e.g., Figures 7(d) and 7(f)) which appear to form by overprinting of alpha-recoil track etch-tunnels by encroaching palagonite (Figures 11(a)–11(c)). Instead, "granular" palagonite seems to represent a distinct type of low temperature aqueous *alteration* (i.e., palagonitization) by seawater that takes place in a very spotty/mottled/granular fashion by preferential leaching, diffusion, hydrolysis, and reaction of chemical components at specific nucleation sites in the glass (i.e., numerous "point sources" of damage in the glass, which we attribute (below) to the presence of randomly distributed alpha-recoil tracks: Figures 10(e), 10(f), 10(h), and 10(i)). The individual palagonite spots (or granules) reported here range from about ~0.3 to ~1.0 μm in diameter but are most commonly ~0.6 μm across (Figures 10(e) and 10(f))—similar in size to other known examples of granular palagonite alteration in submarine glasses worldwide (i.e., those attributed to microbial activity: ~0.1–1.3 μm, but most commonly ~0.2–0.6 μm [11, 26, 28, 34, 59]; e.g., compare Figures 2(c) and 2(d))—and they tend to occur in dense constellations that form a spotty/mottled transition zone between fresh basaltic glass ("FG" in Figures 10(a)–10(d)) and glass that has been completely altered to palagonite ("P" in Figures 10(a)–10(d)). We interpret this pattern of alteration as evidence that the infiltration of seawater into the glass during palagonitization takes place not only by preferential etch-tunnelling through alpha-recoil track damaged sites in the glass (i.e., as described in Section 3.3.1 and Figure 9), but also through "selective palagonitization" of multitudes of randomly distributed alpha-recoil tracks—which represent ideal point sources of radiation damage that are more amenable to chemical attack than surrounding glass—resulting in a characteristic "granular" palagonite microtexture (Figures 10(e), 10(f), 10(h), and 10(i)). Key evidence to support this claim comes from the observation that the areal density and distribution of palagonite granules imaged by SEM (e.g., Figures 10(e) and 10(f)) matches closely the calculated areal density and distribution of "model" alpha-recoil tracks in DSDP 418A basaltic glass (Figures 10(h) and 10(i))—predicted in our theoretical modelling study (Section 5). In addition, the characteristically small size of these palagonite "granules" (~600 nm) is only slightly larger than the diameter of these putative previously existing alpha-recoil tracks (typically ~120 nm [129]; see pink dots labelled "ART" in Figure 10(f)); that is, the ~120 nm alpha-recoil tracks provide ideal "point sources" for selective palagonitization that are inherent in these old glasses. However, during the process of selective palagonitization, some of the surrounding glass is evidently also palagonitized, resulting in a slightly larger size of ~600 nm for these preferentially palagonitized alpha-recoil tracks (i.e., "palagonite granules" in Figure 10(f)). Therefore, we propose that granular palagonite alteration microtextures found in submarine volcanic glasses worldwide (e.g., [11, 28, 34, 59] and this study) do not represent evidence of microbial activity/bioalteration or the presence of a global lithoautotrophic microbial community thriving at the glass-palagonite interface in submarine glasses (e.g., [11, 28, 34, 59]) but instead are a reflection of the preferential *abiotic* corrosion/palagonitization of multitudes of randomly distributed alpha-recoil tracks in submarine glasses by seawater—which appears to take place at the global scale because midocean ridge basaltic glasses are known to contain trace amounts of U and Th worldwide [146] and thus accumulate alpha-recoil tracks very quickly. Consequently, we suggest that the recently proposed microbial trace fossil (i.e., ichnospecies) *Granulohyalichnus vulgaris* and, in fact, the entire *Granulohyalichnus* ichnogenus [28] are now more or less in doubt in terms of biogenicity (see further discussion in Section 6.1).

3.4. High Resolution Scanning Electron Microscopy of Basaltic Glass "Chip Samples". Due to the polishing process used in the fabrication of polished petrographic thin sections, some of the more tiny (<0.1 μm) details preserved within corrosion microtextures and etch-tunnels have the potential to become slightly obscured/modified and thus difficult to image at high resolution by SEM. Therefore, in order to circumvent this problem in the present study, we also prepared hand-crushed (i.e., via mortar and pestle), sand-sized basaltic glass "chip samples" from *DSDP-418A-75-3-[120–123]* to allow for more detailed high resolution SEM imaging of corrosion microtextures (Figures 11–15)—to compliment the SEM studies of the surfaces of polished petrographic sections that we carried out above (Figures 8–10). In this way, fracture surfaces generated during crushing of the sample into small chips exposed "fresh surfaces" of the interior of the basaltic glass pillow margin for

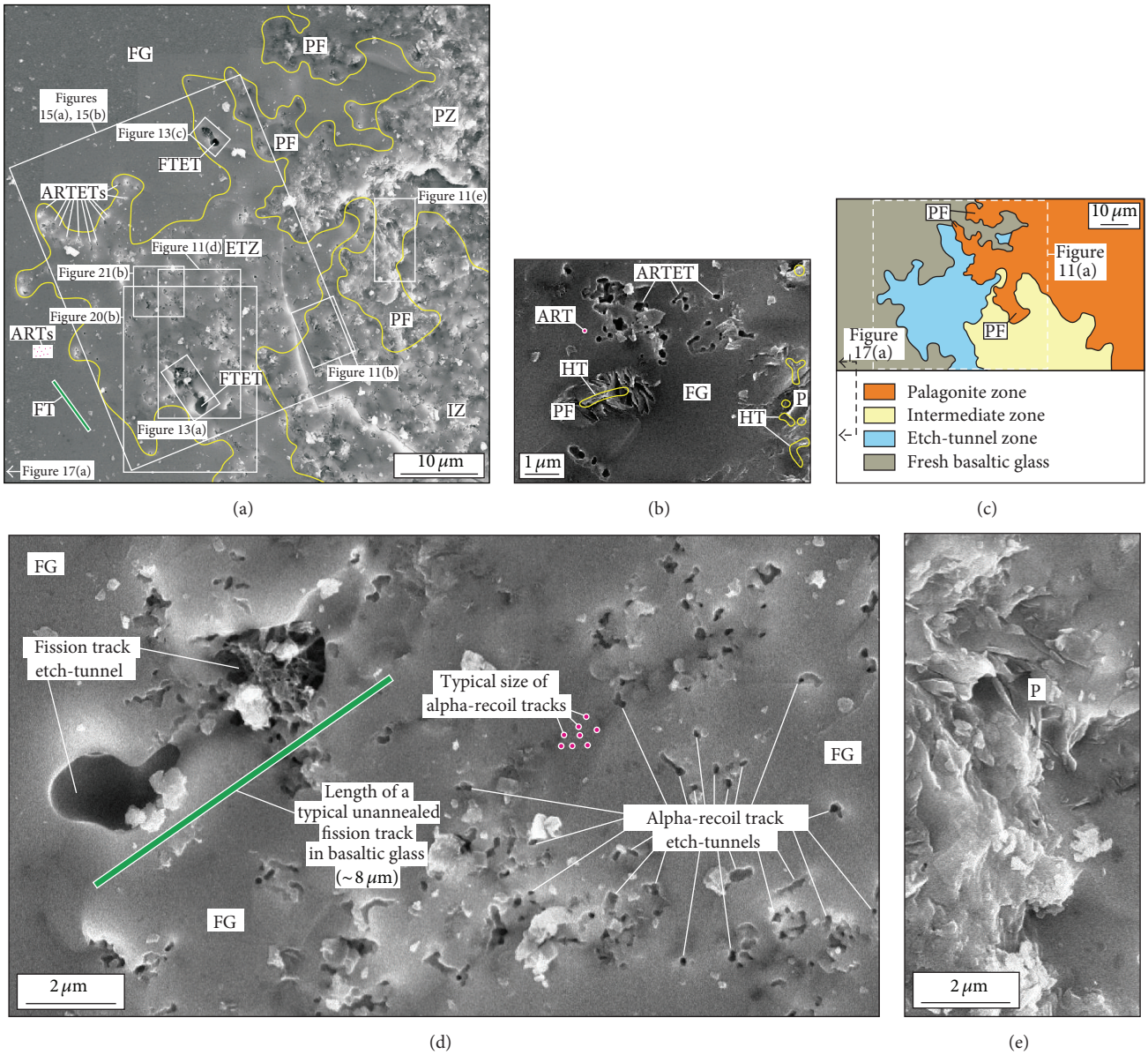

Figure 11: High resolution SEM mapping of the glass-palagonite interface and associated etch-tunnel zone (as observed on the freshly fractured surface of a basaltic glass "chip sample" of *DSDP-418A-75-3[120–123]*). (a, b, d, and e) Secondary electron images. (a) Overview of a representative region of the glass-palagonite interface, highlighting four microtextural domains (boundaries shown as yellow lines; also see (c)) that include two large FTETs and several hundred smaller ARTETs. (b) Close-up from (a) highlighting where the palagonite zone is encroaching upon (overprinting) the etch-tunnel zone. (c) Alteration map, showing the distribution of the four microtextural domains outlined in (a). (d) Close-up (from (a)) of the etch-tunnel zone, highlighting one FTET and several ARTETs. Note the similarity in size between the hypothetical fission track (green bar) and the FTET and between the hypothetical ARTs (pink dots) and the ARTETs. (e) Representative close-up (from (a)) of the palagonite zone. ARTs: alpha-recoil tracks; ARTETs: alpha-recoil track etch-tunnels; ETZ: etch-tunnel zone; FG: fresh basaltic glass; FT: fission track; FTET: fission track etch-tunnel; HT: hypothetical preexisting alpha-recoil track etch-tunnel; IZ: intermediate zone (between the ETZ and the PZ); P: palagonite; PZ: palagonite zone.

the high resolution SEM studies of corrosion microtextures (Figures 11–15; also see Figures 3(e) and 4(c)—left, and some images introduced in later Sections: Figures 17, 20(b), 21(b), 21(c), 21(e), and 21(f)). The sub-millimeter-sized glassy pillow margin fragments (i.e., chip samples) analysed by SEM in this study were sputtered with a 20 Å coating of iridium using a VCR group Inc IBS/TM200S Ion Beam Sputterer and analysed using a JEOL 6301F field emission scanning electron microscope equipped with a PGT IMIX model X-ray analysis system (images presented in Figures 11(a), 11(d), 11(e), 13(a), 15(a) and some images introduced in later Sections: Figures 17, 20(b), 21(b), 21(c), 21(e), and 21(f)) or a Hitachi S-4000 scanning electron microscope (Figures 11(b), 12(d)–12(h), 13(b)–13(e), and 14(e)–14(h)), or alternatively coated

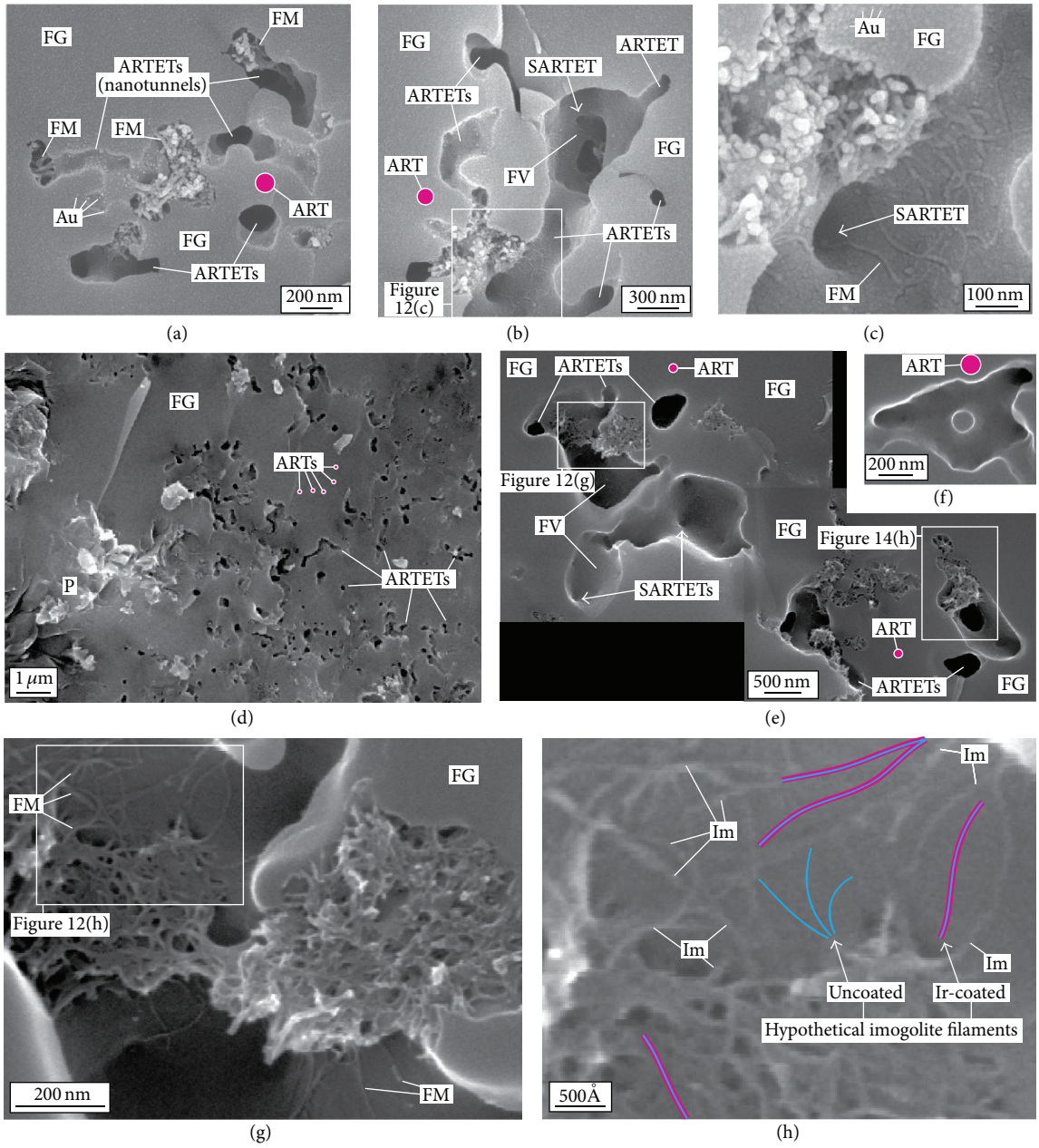

Figure 12: High resolution SEM (secondary electron) images of alpha-recoil track etch-tunnels (ARTETs) at the glass-palagonite interface (as observed on freshly fractured surfaces of basaltic glass "chip samples" from *DSDP-418A-75-3[120–123]*). (a–c) Representative close-up images of typical ARTETs found at the glass-palagonite interface. Note the meandering, branching nature of the etch-tunnels and the occurrence of FM within them, and note that tunnel diameters are about the same size as a typical alpha-recoil track (~120 nm pink dots labelled "ART"). Other features include "pockmarks" that represent new side-tunnels (SARTETs), and flare-out voids (interpreted as etch-tunnelling of locally dense regions of ARTs or as ARTETs affected by prolonged "overetching" ± pressure solution). (d) Overview image, showing a typical region of the glass-palagonite interface where abundant ARTETs occur, which are being encroached upon and overprinted by palagonite. (e) Overview of a region where numerous ARTETs, FVs, and SARTETs occur. (f) A region where an ARTET forms an etched-out "loop." (g) Close-up from (e), highlighting abundant FM lining tunnel walls and draping/bridging across tunnel void spaces. (h) Close-up from (g). For comparison, several hypothetical imogolite filaments are drawn to scale (in blue) (i.e., 20 Å wide, the exact thickness of a single strand of imogolite), some of which also depict the 20 Å thick coating of iridium (magenta). Note the identical thickness of these hypothetical, iridium-coated imogolite filaments and the real nanofilaments imaged by SEM. ART: alpha-recoil track; ARTETs: alpha-recoil track etch-tunnels; Au: granules of gold sputtering; FG: fresh basaltic glass; FM: filamentous material; FV: flare-out voids; Im: imogolite; P: palagonite; SARTETs:"starting" alpha-recoil track etch-tunnels.

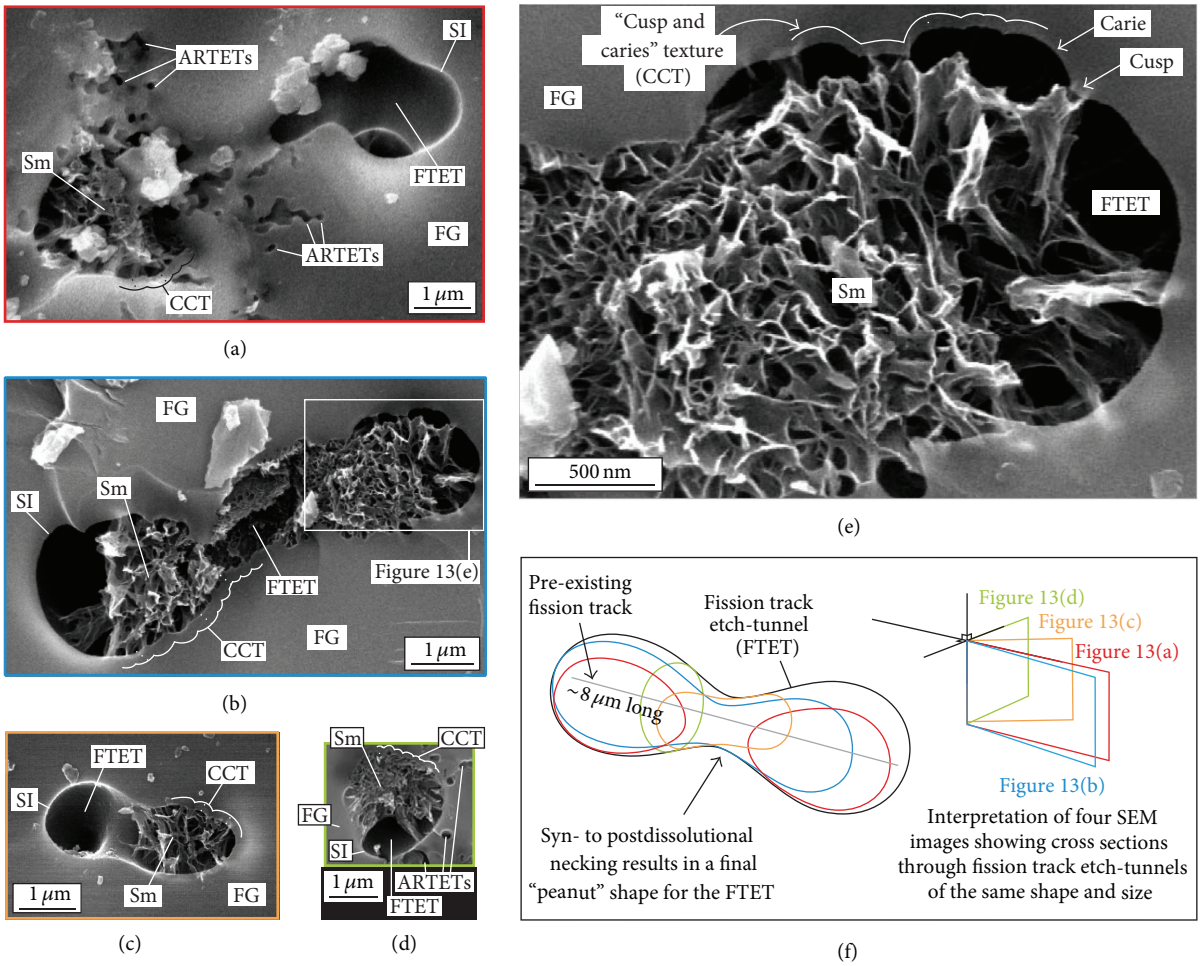

Figure 13: High resolution SEM (secondary electron) imaging of fission track etch-tunnels (FTETs) at the glass-palagonite interface (as observed on the freshly fractured surfaces of basaltic glass "chip samples" of *DSDP-418A-75-3[120–123]*). (a–d) Images of four FTETs shown at the same scale, all of which contain authigenic platy smectite. Note how two of these FTETs ((a) and (d)) are interconnected to several smaller ARTETs as a part of the same porosity/etch-tunnel network. In addition, all four FTETs exhibit two contrasting types of glass-dissolution interface: (1) a smooth interface (labelled "SI") at regions distal to secondary smectite growth and (2) a "cusp and caries" textured interface (labelled "CCT") at regions undergoing dissolution in the vicinity of secondary smectite growth (see Figure 14 for further explanation of CCT). (e) Close-up from (b), highlighting authigenic platy smectite within an FTET, as well as well-developed cusp and caries microtexture. (f) Interpretation of the four large etch-tunnels shown in (a–d) as variably oriented cross sections through FTETs of essentially the same shape and size (i.e., peanut-shaped and ~8 μm long). ARTETs: alpha-recoil track etch-tunnels; CCT: "cusp and caries" texture; FTET: fission track etch-tunnel; SI: smooth interface; Sm: platy smectite.

with ~150 Å of gold using a Nanotech Semprep2 and then analysed using the aforementioned JEOL 6301F instrument (Figures 12(a)–12(c) and one image introduced in a later Section: Figure 21(a)). During high resolution SEM imaging, the samples sputtered with a ~150 Å thick layer of gold showed a slight artificial granulation of the sample surface (see nanogranules of "Au" in Figures 12(a)–12(c)), which is why most of the chip samples in this study were coated with ~20 Å of iridium—allowing resolution of much finer details (as small as ~20 Å across: e.g., see the nanofilaments in Figure 12(h)).

3.4.1. Overview of the Glass-Palagonite Interface and Associated "Etch-Tunnel Zone". We surveyed a large number of fresh fracture surfaces of various basaltic glass chip samples (from *DSDP-418A-75-3-[120–123]*) and located partially palagonitized basaltic glass (and associated etch-tunnels) on several different grains, and a high resolution SEM overview of a representative region of the glass-palagonite interface is shown in Figure 11(a). Many of the corrosion/dissolution microtextures observed in polished petrographic thin section at the glass-palagonite interface (e.g., Figures 7 and 9) were also identified within this representative region (Figure 11(a)), which can be subdivided into four distinct textural domains, including fresh basaltic glass, an etch-tunnel zone, a palagonite zone, and an intermediate zone where the latter two coexist (Figures 11(a)–11(c)). The etch-tunnel zone occurs between the palagonite zone and fresh basaltic glass

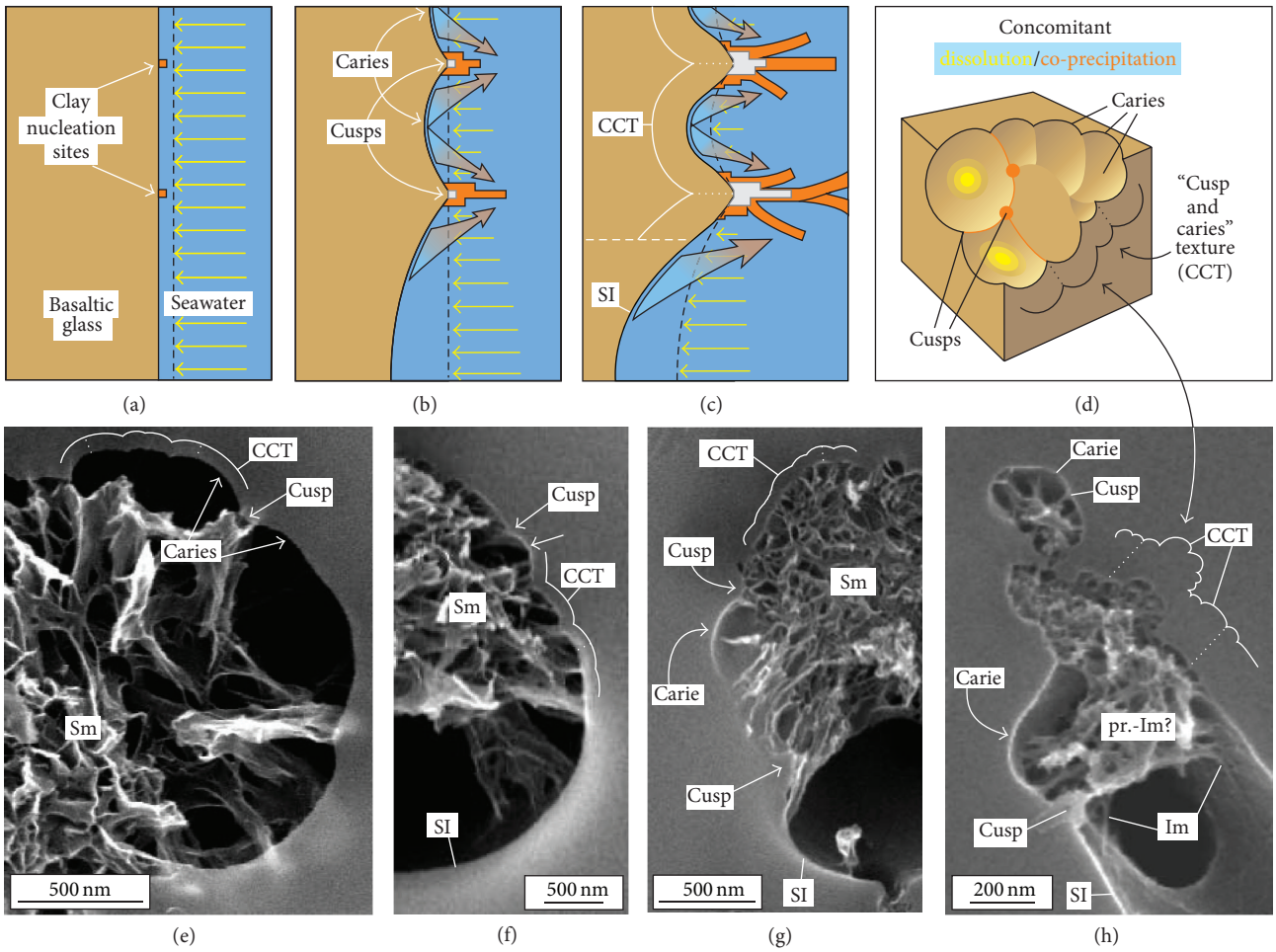

Figure 14: SEM images and a schematic model (a–d) explaining the origin of "cusp and caries" texture observed along the walls of fission track etch-tunnels (FTETs) and alpha-recoil track etch-tunnels (ARTETs) in basaltic glass. The secondary electron images in (e–h) are all close-up SEM images from other figures: (e) and (f) are close-up images from Figure 13(b); (g) is a close-up from Figure 13(d); and (h) is a close-up from Figure 12(e). Schematic model (a–d): at locations distal to the nucleation sites of secondary clays, the glass-water interface (i.e., dissolution front) is quite smooth and featureless (see "SI" in (c) and (f–h) and also in Figures 13(a)–13(d)). In contrast, where glass dissolution (yellow) is accompanied by the nearby nucleation and growth of secondary clays (orange), the protective effect of the newly formed clay minerals (±the kinetics of the dissolution/co-precipitation process—see orange/blue and yellow arrows in (b) and (c)) results in the formation of "cusps" along the dissolution front that are separated by "caries" (b)—the latter of which form by dissolution of glass as a concave front/incursion (slightly distal to secondary clay formation). In the case of FTETs, the secondary clay that forms during development of cusp and caries texture is platy smectite (e–g), whereas for ARTETs the secondary mineral is filamentous imogolite ((h); Figures 12(e), 12(g), and 12(h)). CCT: "cusp and caries" texture; Im: imogolite; pr.-Im?: proto-imogolite?; SI: smooth interface; Sm: platy smectite.

(Figures 11(a)–11(c)) and consists of fresh basaltic glass that is riddled with porosity (i.e., etch-tunnels: Figure 11(d)). These textural relationships indicate that advancement of the palagonite alteration front took place in the wake of a prominent dissolution/etch-tunnelling front caused by the infiltration of seawater into fresh basaltic glass (preferentially along radiation damaged regions—see Section 3.4.2). Furthermore, in some places the etch-tunnel zone has been completely overprinted by this encroachment of secondary palagonite, which locally forms palagonite fingers ("PF" in Figures 11(a)–11(c)) that extend outward into the etch-tunnel zone and fresh basaltic glass (akin to those shown in Figures 7(d) and 7(f)).

3.4.2. Nature of Alpha-Recoil Track Etch-Tunnels (ARTETs) and Fission Track Etch-Tunnels (FTETs). Porosity in the etch-tunnel zone occurs in the form of a complex 3-dimensional network of anastamosing nanoscopic tunnels (i.e., "ARTETs" in Figures 11 and 12) that are typically ~120 nm in diameter (Figures 11(d), 12(a), 12(b), and 12(d)), exhibit a high degree of tortuosity (Figures 12(a), 12(b), and 12(d)), commonly branch (Figures 12(a) and 12(b)), occasionally flare out into larger irregular voids up to ~1 μm across ("FV" in Figures 12(b) and 12(e)) that have small "pockmarks" on their interior surface ("SARTETs" in Figures 12(b), 12(c), and 12(e)), and in one instance occur in the form of an etched-out loop

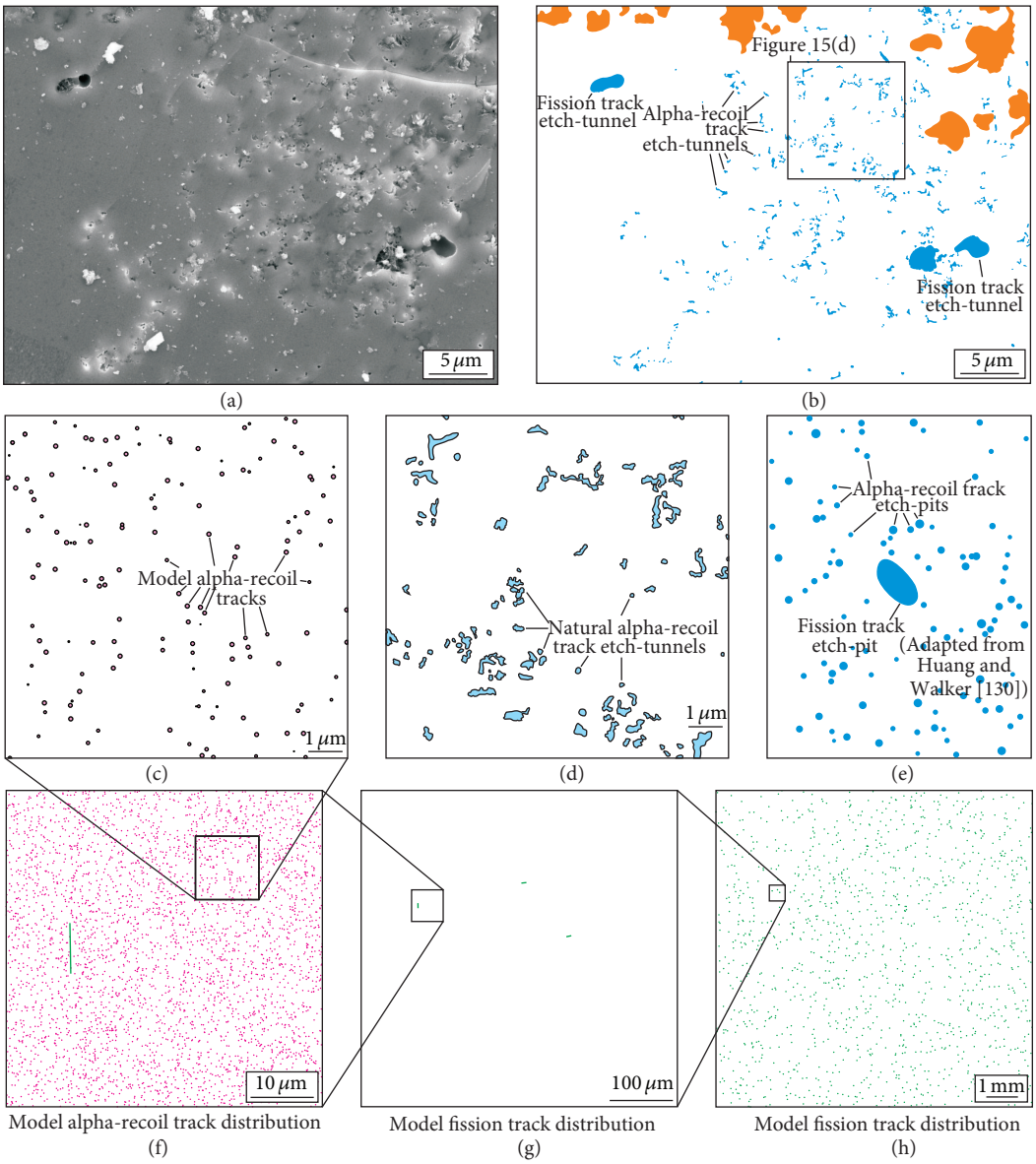

Figure 15: Comparison of theoretical modelling of radiation damage in DSDP 418A basaltic glass with the observed distribution of natural etch-tunnels at the glass-palagonite interface. (a) Representative SEM (secondary electron) image of the etch-tunnel zone (close-up from Figure 11(a)). (b) Porosity map (constructed from (a)) highlighting the distribution of fission track etch-tunnels (FTETs) and alpha-recoil track etch-tunnels (ARTETs) observed at the glass-palagonite interface. (c) Theoretical areal distribution of alpha-recoil tracks (ARTs) in DSDP 418A basaltic glass intersecting a hypothetical flat fracture plane through the glass (calculated using (1)). In this close-up theoretical plot (c), the individual model ARTs are plotted as randomly distributed 120 nm diameter spheres, resulting in pink circles of varying size (up to 120 nm), depending on their depth relative to the plane of the page (i.e., flat fracture surface). (d) Close-up porosity map from (b), highlighting a representative region of the etch-tunnel zone that is predominated by ARTETs. Note the similarity in size and areal distribution of the natural ARTETs (d) with the theoretically modelled ARTs (c), indicating a causal relationship. Many of the ARTETs in (d) exhibit elongate anastamosing shapes, the result of seawater "etching out" several nearby alpha-recoil tracks in cumulative succession (see "step 10a" in the lower left panel of Figure 18). (e) Etch-pit map, showing the observed distribution of experimentally etched ARTs and one etched-out fission track, on the cleavage surface of a mica crystal (adapted from Figure 1(b) of Huang and Walker [130], no scale bar available). (f–h) Theoretical models of the present-day distribution of randomly distributed ARTs (pink) and fission tracks (green) intersecting a hypothetical flat fracture plane through DSDP 418A basaltic glass, as determined using (1) and (2). For clarity, ARTs are not shown in (g) and (h) because of their exceptionally high numbers. Note how in (f), one single large fission track is surrounded by a multitude of smaller ARTs, similar in nature to the *bimodal* size versus population distributions of experimentally etched ARTs and fission tracks in mica (e) and naturally formed ARTETs and FTETs in DSDP 418A basaltic glass (b), a key argument for the "radiation damage" origin of the ARTETs and FTETs in DSDP 418A basaltic glass (see Sections 3.4.2, 5.2, and 6.1 for discussion). Colours in (b) and (d): blue = ARTETs and FTETs; white = fresh basaltic glass; orange = palagonite. Colours in (c), (f), (g), and (h): white = fresh basaltic glass not affected by radiation damage; pink = model ARTs; green = model fission tracks (randomly oriented lines in (f) and (g); dots in (h)). Colours in (e): white = fresh cleavage surface of mica; blue = ART etch-pits and one fission track etch-pit.

(Figure 12(f)). Rare larger chambers/tunnels that are ~1-2 μm in diameter and typically peanut-shaped (i.e., dumbbell shaped) and up to ~8 μm long (i.e., "FTETs" in Figures 11(a), 11(d) and 13) are also interconnected with this complex network of anastamosing nanoscopic tunnels. In cross section (i.e., on a large, freshly formed "chip"/fracture surface of basaltic glass pillow margin), these two contrasting types of exposed etch-tunnels show a bimodal size versus population distribution (Figures 11(a), 11(d), 15(a), and 15(b)) and also contain different types of infilling authigenic minerals. The typically peanut-shaped larger tunnels (i.e., fission track etch-tunnels or "FTETs") are much less abundant than the smaller tunnels (i.e., compare: 2 FTETs versus 379 ARTETs in Figures 15(a) and 15(b)) and contain platy material that is interpreted based on morphology, EDS analysis by SEM, geological context, and textural relationships with surrounding glass to be authigenic platy smectite ("Sm" in Figures 13 and 14). SEM images of four cross sections through the larger variety of etch-tunnel (Figures 13(a)–13(d)) may all be interpreted to represent variably oriented planar sections through a single type of peanut-shaped void space (i.e., fission track etch-tunnel) with the same overall shape and size in each case (Figure 13(f)). The smaller etch-tunnels (i.e., alpha-recoil track etch-tunnels or "ARTETs") predominate in the etch-tunnel zone (e.g., Figures 11(d) and 12(d)) and commonly contain filamentous material that forms cobweb-like bundles that drape across the tunnel void spaces and line tunnel walls ("FM" in Figures 12(a), 12(c), and 12(g)). On the basis of morphology, size, geological context, and textural relationships with surrounding glass, this filamentous material is interpreted to be authigenic imogolite (Figures 12(e), 12(g), 12(h), and 14(h); also see Figure 17(c) and 17(f)—introduced in a later Section—and [111, 139]). For instance, imogolite is typically described as the initial weathering product of glassy volcanic ash [196], and so it is logical that this mineral should also be forming here at the glass-water interface in submarine glasses that are undergoing corrosion/dissolution by seawater. In a close-up view of many imogolite filaments draped across the wall of a larger flare-out void that is a part of the smaller (alpha-recoil track) etch-tunnel network (Figure 12(h)), cross sections through hypothetical imogolite filaments are shown to scale as 20 Å thick (the known outer diameter of natural imogolite tubes [196]) filaments (blue) with an additional 20 Å of thickness on either side in order to represent the iridium coating (magenta). In this comparison, it is clear that the thickness of a hypothetical imogolite filament matches the size of the filaments draped across the tunnel walls in the SEM image given that they are coated with 20 Å of iridium (Figure 12(h); also see Figures 17(c) and 17(f)—introduced in a later Section). In SEM images of a different basaltic glass "chip" (also from sample *DSDP-418A-75-3-[120–123]*) coated in gold (Figures 12(a)–12(c)), similar-sized filaments also show through the relatively thicker and irregular coating formed on the sample during gold sputtering ("FM" in Figures 12(a)–12(c)).

The authigenicity of these imogolite filaments and platy smectite occurring within small versus large etch-tunnels, respectively (i.e., ARTETs versus FTETs), is constrained by the occurrence of pronounced "cusp and caries" texture (CCT) at the glass-water interface ("CCT" in Figures 13 and 14). This distinctive microtexture occurring at the glass-water interface (i.e., "cusp and caries texture" along etch-tunnel walls) is interpreted to arise from two concomitant processes taking place simultaneously during etch-tunnelling: dissolution (of glass) and coprecipitation (of secondary clays—i.e., smectite within FTETs and imogolite within ARTETs). According to this model (Figures 14(a)–14(d)), "cusps" form along the etch-tunnel walls at the sites of nucleation and growth of secondary clays (imogolite or smectite), whereby the protective effect of the secondary clays prevents dissolution from taking place directly at those regions, while "caries" (or "incursions" into the glass) form slightly adjacent to these sites of nucleation and growth (Figure 14(b)) through dissolution of nearby glass in a concave fashion. In regions sufficiently distal to the sites of clay nucleation and growth, glass dissolution proceeds without hindrance, resulting in a smooth interface ("SI" in Figures 13 and 14). This type of "cusp and caries" microtexture is a term traditionally used by microscopists in the study of ore deposits, in cases where a primary mineral is being replaced by a secondary (alteration) mineral, such that the new mineral forms concave incursions into the host, "as if the secondary mineral had bitten into the host" (p. 141 in Guilbert and Park Jr. [197]) and actually originates from a dental analogy—with the "caries" representing the concave incursions in a tooth cavity and the relict protuberences between them being "cusps" (p. 141 in Guilbert and Park Jr. [197]).

The smaller (~120 nm diameter) and more abundant variety of etch-tunnels (i.e., "ARTETs" in Figures 11(d) and 12) observed on the surfaces of these "chip" samples are essentially identical in size to the etch-tunnels identified at the glass-palagonite interface in polished petrographic thin sections in this study (Figure 9) and, therefore, also have incidentally the same size as a typical alpha-recoil track (~120 nm in diameter [129]—see "ARTETs" and pink dots labelled "ART" in Figures 9(d), 9(h), 9(k), 9(l), 11(a), 11(b), 11(d), 12(a), 12(b), and 12(d)–12(f)). This adds further support for our conclusion in Section 3.3.1 that the etch-tunnel zone at the glass-palagonite interface forms in advance of the palagonitization front primarily due to preferential etch-tunnelling (by seawater) of randomly distributed alpha-recoil tracks in the glass resulting from radioactive decay of U and Th—again, in contrast with previous biogenic (i.e., microbial trace fossil) interpretations (i.e., of "tubular" texture at DSDP 418A [11, 26–28, 31, 33, 59, 61, 93, 94, 100]). Additional support for a "radiation damage origin" for this etch-tunnel zone comes from the coincidence in size of the rare, larger (~1-2 μm wide by up to ~8 μm long) etch-tunnels ("FTETs" in Figures 11(a), 11(d) and 13) with the typical size of a "pristine" fission track in volcanic/impact glass (i.e., ~8 μm in length—see a direct comparison in Figure 3(e); "Pristine" means naturally occurring *spontaneous* fission tracks in volcanic/impact glass originating from the natural radioactive decay (spontaneous fission) of ^{238}U that have not been affected by subsequent thermal annealing/track-shortening or in the case of *induced* fission tracks in volcanic glass, originating from the induced

fission of ^{235}U triggered by irradiating the sample with thermal neutrons in a nuclear reactor—fission tracks which are also typically ~8 μm in length: see Figure 1 in Sandhu et al. [198], Figure 8(b) in Westgate and Naeser [199], Figure 3 in this study, and descriptions in Arias et al. [126] and Sandhu and Westgate [128]). As such, we interpret the etch-tunnel zone at the glass-palagonite interface (Figures 7, 9, 11–13, 15(a), 15(b), and 15(d); also see Figures 1(b), 1(d), 1(f), 3(e), 4(c)—left) to have formed by preferential dissolution and etch-tunnelling (by seawater) through radiation damaged regions of basaltic glass (i.e., randomly distributed alpha-recoil tracks and spontaneous fission tracks)—in advance of the encroaching palagonitization front that formed along fractures during low temperature subaqueous alteration of these glassy margins of midocean ridge pillow lavas—long after their initial eruption and quenching.

It is also important to highlight at this point that the *bimodal* distributions observed for "etch-tunnel size" versus "etch-tunnel population/areal density" in this study (i.e., a multitude (379) of small (~120 nm wide) etch-tunnels versus only a few (2) large (~8 μm long) etch-tunnels: Figures 11(a), 15(a), and 15(b)) also provides strong "microtextural" evidence that the etch-tunnel zone at the glass-palagonite interface is abiotic in origin and the result of preferential etching (by seawater) of radiation damaged regions of glass. For instance, because fossil fission tracks in most geological materials are produced by the spontaneous fission of ^{238}U, they should occur amongst a much larger population of relatively smaller alpha-recoil damage tracks caused by the eight alpha-recoil events (Figure 4(a)) that are a part of the ^{238}U–^{206}Pb radioactive decay chain (e.g., [130]; Figures 4(b): left and 15(e)). A contrast in relative abundance of the two types of radiation damage occurs (i.e., several orders of magnitude more alpha-recoil tracks than fission tracks) mostly because of the difference in half-lives for spontaneous fission of ^{238}U and the ^{238}U–^{206}Pb alpha/beta decay chain, which are 8.2×10^{15} and 4.468×10^{9} y, respectively [200, 201]. But this is also in part because a significant number of additional alpha-recoil tracks are caused by the radioactive decay of other isotopes present such as ^{235}U to ^{207}Pb and ^{232}Th to ^{208}Pb, which for these particular decay chains involves a total of seven and six alpha-recoil events, respectively [202]. This bimodal size/population distribution for alpha-recoil tracks versus fission tracks was recognized early on in the studies of experimentally etched fission tracks and alpha-recoil tracks on the cleavage surfaces of micas ([130]; i.e., one large fission track etch-pit surrounded by a multitude of tiny alpha-recoil track etch-pits: Figures 4(b): left and 15(e)). Further discussions on the significance of these "bimodal distributions" of corrosion microtextures—linked to the differences in size and areal density of fission tracks versus alpha-recoil tracks—can be found in Sections 5.2, 6.1, and 6.2.2, including the observation of bimodal distributions of "granular" palagonite textures in glasses from the Costa Rica Rift (Section 6.1).

In summary, there are three lines of microtextural evidence identified thus far—from the "etch-tunnel zone" at the glass-palagonite interface in DSDP-418A basaltic glass—that support a *radiation damage origin* for these etch-tunnels and *not a microbial origin*. (1) The smaller variety of etch-tunnels (~120 nm diameter "ARTETs" in Figures 9(d), 9(h), 9(k), 9(l), 11(a), 11(b), 11(d), 12, 13(a), 13(d), 15(a), 15(b), and 15(d)) are typically about the same size as an alpha-recoil track (~120 nm in diameter [129]). (2) The larger variety of etch-tunnels ("FTETs" in Figures 11(a), 11(d), 13, 15(a), and 15(b)) range in length up to ~8 μm long, that is, the same size as a typical unannealed fission track in volcanic glass (as well as in tektite glasses, that is, ~8 μm in length; see Figures 3(b) and 3(e) (this study), Figure 1 in Sandhu et al. [198], Figure 8(b) in Westgate and Naeser [199], and descriptions in Arias et al. [126] and Sandhu and Westgate [128]). (3) The smaller (~120 nm diameter) variety of etch-tunnels are several orders of magnitude more abundant than the larger (up to ~8 μm long) variety (e.g., 379 "ARTETs" versus 2 "FTETs" in Figures 15(a) and 15(b))—consistent with the well-known concept (outlined above) that the areal density of alpha-recoil tracks (i.e., #tracks/cm^2) accumulates several orders of magnitude faster than fission track areal densities.

In light of these similarities between natural etch-tunnels in DSDP-418A basaltic glass and alpha-recoil tracks and fission tracks, it is important to evaluate precisely how much radiation damage should actually be present in these glasses (i.e., in the form of randomly distributed fission tracks and alpha-recoil tracks) based on the known age of these pillow lavas (~120.6 Ma; for age constraints, see Figures 5(c) and 5(d) and Section 2.2) and the measured concentrations of U and Th present in fresh basaltic glass, and that is the subject of the following two Sections (4 and 5).

4. Determination of U and Th Concentrations in Fresh Basaltic Glass by ICP-MS

For theoretical modelling of radiation damage in the glassy margins of pillow basalts in this study, the concentrations of U and Th in fresh glass from sample *DSDP-418A-75-3-[120–123]* were measured by ICP-MS. A few fragments of this basaltic glass pillow margin sample (each several mm across) were crushed in ethanol to achieve a smaller grain size using an agate mortar and pestle. The resulting rock powder was then sieved in ethanol using a silkscreen mesh to remove the fines (material less than ~50 μm in grain size). Crushing and sieving were necessary to isolate numerous fragments of only fresh basaltic glass that were of adequate size. The grains were then hand-picked in ethanol under binocular microscope, using a custom built pipette made of Tygon and Teflon. Selecting fresh material required sorting through and picking grains of basaltic glass that contained no alteration (e.g., palagonitized or devitrified zones), no evidence of still attached fragments of mineral inclusions (e.g., clinopyroxene and plagioclase), and only those grains that were devoid of vesicles.

In all, 827 individual fragments of pristine basaltic glass were picked for U and Th analysis, ranging in size from ~50 to ~300 μm (Table 1). They are described as fresh shards of basaltic glass that are light tan brown (smallest shards) to dark brown (largest shards) in colour. Grain surfaces invariably

Table 1: ICP-MS results for U and Th concentrations in DSDP 418A basaltic glass.

Sample name	Sample grain size; {# grains}	Sample description	Sample weight (mg)	Th (ppm)	U (ppm)	Th/U
DSDP-418A-75-3-[120–123]-ICP–MS #1	~0.3–1.0 mm; {13}	(a)	5.3	0.097	0.037	2.66
DSDP-418A-75-3-[120–123]-ICP–MS #2	~0.3–1.0 mm; {42}	(a)	10.4	0.129	0.037	3.51
DSDP-418A-75-3-[120–123]-ICP–MS #3	~1.5 × 3 × 4 mm; {1}	(a)	17.8	0.164	0.053	3.10
DSDP-418A-75-3-[120–123]-ICP–MS #4	~1 × 1 × 1 mm; {1}	(a)	1.6	0.112	0.038	2.97
DSDP-418A-75-3-[120–123]-ICP–MS #5	~1 × 1 × 1 mm; {1}	(a)	1.1	0.107	0.040	2.67
DSDP-418A-75-3-[120–123]-ICP–MS #6	~50–300 μm; {266}	(b)	0.9	0.132*	0.042*	3.16*
DSDP-418A-75-3-[120–123]-ICP–MS #7	~50–300 μm; {263}	(b)	0.9	0.117	0.035	3.31
DSDP-418A-75-3-[120–123]-ICP–MS #8	~50–300 μm; {298}	(b)	1.2	0.108	0.032	3.35

For Th and U determinations (ppm), the external reproducibility is 5–10% (2σ level) of the quoted abundances.

Sample descriptions:

(a) Test fractions: they comprise predominantly fresh basaltic glass, which also contains numerous small (<100 μm) vesicles and their inclusions (e.g., vesicles commonly contain numerous ~1 μm sized Fe-sulfide spherules) and possibly some small domains (~a few % by volume) that comprise altered (palagonitized/devitrified) zones and/or phenocryst inclusions such as clinopyroxene and plagioclase.

(b) Pristine, fresh basaltic glass, devoid of alteration, inclusions, or vesicles: the shards of glass are transparent and light tan brown (thinnest shards) to dark brown (thickest shards) in colour. Surfaces invariably show a vitreous luster and comprise curviplanar to conchoidal fractures that impart a myriad of shapes to the grains. All of these grains were found to be isotropic when viewed under petrographic microscope with crossed nicols.

*values used for theoretical modelling of alpha-recoil track (Figures 10(h), 10(i), 15(c), and 15(f)) and fission track (Figures 10(g), 15(g), and 15(h)) areal densities in DSDP 418A basaltic glass in this study.

show a vitreous luster and because they are curviplanar to conchoidal fractures they impart a myriad of shapes to the grains from elongate blades with razor sharp edges to more equant shapes. As an additional precautionary measure after picking, all of the grains were then examined with crossed polars using a petrographic microscope to ensure that they were isotropic. This was also done to exclude any fragments that might still contain attached splinters of other minerals (e.g., plagioclase) that were difficult to see under binocular microscope. It was found that all of the grains were indeed isotropic, as expected for basaltic glass, although ~2% of the grains had tiny inclusions, or fragments on their edges, which were readily visible as bright birefringent material (likely phenocryst fragments). These grains were removed leaving the final population of 827 fresh basaltic glass fragments that was split into three 0.9 to 1.2 mg fractions for trace element analysis (Table 1).

To ensure that these fractions would comprise an adequate amount of material for successful analysis by ICP-MS, a series of five test fractions was run first. These also originate from sample *DSDP-418A-75-3-[120–123]* and ranged in weight from 1.1 to 17.8 mg (Table 1). These fractions comprised larger grains (one to several mm in size) of pillow margin that contained predominantly fresh basaltic glass, which also contained a significant amount of vesicles, altered domains, and mineral inclusions (Table 1).

Before dissolution, the grains were transferred into Savillex beakers in MilliQ H_2O (18.6 MΩ) and placed into an ultrasonic bath for several minutes. The water was decanted and the grains rinsed again in MilliQ H_2O. This was followed by addition of four parts 49% HF and one part 68% HNO_3 into the Savillex beakers for dissolution on a hot plate for 48 hours at 135°C. Solutions were then evaporated to dryness and then reequilibrated in 1 mL of 2% HNO_3, and an internal standard solution (Bismuth) was added before analysis.

For determination of U and Th concentrations, solutions were analysed on a Perkin Elmer Elan 6000 quadrupole ICP-MS. Operating conditions are as outlined in Simonetti et al. [203], with the exception that dwell times for Th and U were 120 and 60 ms, respectively. Each sample analysis consisted of 35 sweeps/reading (3 replicates) for a total analysis time of 21 s per sample, and the external reproducibility is 5–10% (2σ level) of the quoted abundances (Table 1).

The five test samples yielded positive results and so the three small fractions of fresh basaltic glass were also analysed by ICP-MS. The results for these eight samples were quite similar overall, and they are shown in Table 1. For the test fractions, Th concentration ranged from 0.097 to 0.164 ppm and U concentrations from 0.037 to 0.053, with Th/U values between 2.66 and 3.51. The fresh glass showed a more narrow range of trace element concentrations, with 0.108–0.132 ppm Th, 0.032–0.042 ppm U, and an exceptionally narrower range of Th/U values of 3.16–3.35. The broader range of values for the test fractions likely resulted from the inclusion of minor amounts of altered glass, mineral inclusions, and vesicles. Because—as highlighted in Section 2—all three basaltic glass pillow margin samples in this study belong to the same chemical (i.e., glass) type "J" [162] of lithologic unit "13" of volcanic eruptive unit "Vb" [161], it is reasonable to make the geochemical prediction that the U and Th contents of fresh basaltic glass from samples *DSDP-418A-68-3[40–43]* and *DSDP-418A-72-4[13–15]* in this study are probably quite similar to the values reported here for sample *DSDP-418A-75-3[120–123]* (i.e., U = 0.032–0.042 ppm; Th = 0.108–0.132 ppm). Consequently, we consider our theoretical modelling study (Section 5) of the present-day distribution of radiation damage in fresh basaltic glass—which utilizes these U and Th concentrations determined here by ICP-MS—to apply to all three pillow margin samples.

The Th/U ratios and U and Th contents in DSDP-418A basaltic glass determined in this study are similar to other previous results for midocean ridge basaltic glass. For example, fresh basaltic glass from globally widespread, dredged samples of normal MORB have U concentrations

that range from 0.0215 to 0.129 ppm, with Th/U rising smoothly from 1.4 to 3.1 as Th concentrations increase from 0.03 to 0.399 ppm [146]. The measured U concentrations in basaltic glasses from other pillow margins higher up in the volcanostratigraphic sequence at DSDP-418A are also quite similar (0.018–0.037 ppm [125]).

5. Theoretical Modelling of Present-Day Radiation Damage in Fresh Basaltic Glass

In order to evaluate in a more quantitative way the role of radiation damage on microtextural development during the natural corrosion/palagonitization of DSDP-418A basaltic glasses by seawater, we carried out a theoretical modelling study of the present-day distribution of radiation damage in these glasses (i.e., areal densities of alpha-recoil tracks and spontaneous fission tracks intersecting a hypothetical flat fracture surface in the glass), based on the known age of these pillow lavas (~120.6 Ma; for age constraints, see Figures 5(c) and 5(d) and Section 2.2) and the measured concentrations of U and Th in fresh basaltic glass determined by ICP-MS (Table 1).

5.1. Modelling Methodology. As they grow—for example, during the eight successive alpha-recoil events during the complete radioactive decay chain of ^{238}U to ^{206}Pb—alpha-recoil tracks typically "zigzag" through their host material (Figure 4(a)), ~30–50 nm in new random directions with each successive alpha-recoil event (e.g., Figure 3 in Jonckheere and Gögen [131]; Table 1 in Stübner and Jonckheere [132]), resulting in a final composite cluster of radiation damage measuring about 120 nm across (e.g., estimates for the mean diameter of alpha-recoil tracks derived from the complete decay of ^{238}U to stable ^{206}Pb in micas range from ~110 nm [132] to ~120 nm [129] and to ~125 nm [131]). In this theoretical modelling study of the distribution of alpha-recoil tracks in DSDP 418A basaltic glass, we consider each alpha-recoil track to be the end result of complete U- or Th-series decay. For example, even though a total of eight alpha-recoil events take place during the complete radioactive decay of ^{238}U to ^{206}Pb, because they are all interconnected they are considered as a "single" composite ~120 nm wide alpha-recoil track (Figure 4(a) [129, 131, 132]). In addition, for simplicity in this high spatial resolution theoretical modelling study (Figures 10(i) and 15(c)) each alpha-recoil track is modelled as a ~120 nm diameter sphere (instead of as myriad different geometric varieties of zigzagging structures) and this is in keeping with the observation that when fully etched, alpha-recoil tracks tend to form relatively equant etch-pits (e.g., see Figure 4(b); Figure 1 in Stübner et al. [133]); that is, the theoretical nanoscopic "zigzagging" three-dimensional structure of alpha-recoil tracks is effectively destroyed upon etching. Furthermore, because these DSDP 418A basaltic glasses are inferred to have only experienced relatively low temperatures throughout their entire geological history (since quenching), we assume that (a) no ^{222}Rn diffusion has occurred (which can "split" the ^{238}U–^{206}Pb composite alpha-recoil track in half—see Figure 4(a)) AND (b) no alpha-recoil track "fading/shortening" has occurred.

The areal density of alpha-recoil tracks intersecting a hypothetical flat fracture plane through DSDP-418A basaltic glass (Figures 10(h), 10(i), 15(c), and 15(f)) was calculated using (1), which is adapted from (4) and (5) of Gögen and Wagner [129] with two additional exceptions. (i) The effects of partitioning of Th/U between mineral and melt are excluded in the present case because we are dealing with a quenched glass and (ii) we are calculating a theoretical alpha-recoil track areal density (ρ_a), not a volume density (ρ_v), and therefore multiply by R_e (the etchable range of an alpha-recoil track).

Accordingly, in (1), ρ_{ART} is the areal density of etchable alpha-recoil tracks (i.e., # of alpha-recoil tracks per cm^2), $^{238}\mathrm{U}_g$ is the weight concentration of ^{238}U in DSDP 418A basaltic glass (4.17×10^{-8} g/g, calculated from the ^{235}U/^{238}U isotopic abundance ratio of 0.00725 [204] and the U concentration of 42 ppb determined by ICP-MS: *DSDP-418A-75-3[120–123]-ICP-MS #6*, Table 1), n_s is the density of basaltic glass (3.0 g/cm^3: cf. [205]), N_A is Avogadro's number (6.02×10^{23} atoms/mol), M_{U} is the molar mass of uranium (238.0289 g/mol), λ_{238} is the decay constant for ^{238}U ($1.55125 \times 10^{-10}\ \mathrm{y}^{-1}$ [204]), λ_{230} is the decay constant for ^{230}Th ($9.158 \times 10^{-6}\ \mathrm{y}^{-1}$ [206]), λ_{235} is the decay constant for ^{235}U ($9.8485 \times 10^{-10}\ \mathrm{y}^{-1}$ [204]), λ_{234} is the decay constant for ^{234}U ($2.8262 \times 10^{-6}\ \mathrm{y}^{-1}$ [206]), λ_{232} is the decay constant for ^{232}Th ($4.9475 \times 10^{-11}\ \mathrm{y}^{-1}$ [204]), t is the time since quenching of the glass (120,600,000 y; for age constraints see Figures 5(c), 5(d) and Section 2.2), $(\mathrm{Th/U})_{\mathrm{glass}}$ is the Th/U ratio of the glass (3.16, determined from the ICP-MS data: *DSDP-418A-75-3-[120–123]-ICP-MS #6*, Table 1), I is the ^{235}U/^{238}U isotopic abundance ratio (0.00725 [204]), and R_e is the etchable range of an alpha-recoil track (0.000012 cm; i.e., 120 nm [129, 131]). The value for the total efficiency coefficient for alpha-recoil track revelation (η_{tot}) in conventional alpha-recoil track dating studies is assumed to be 1 [129], which holds true in the present case because the tracks are hypothetical and therefore automatically revealed. Consider

$$\begin{aligned}\rho_{\mathrm{ART}} = {} & \left\{\frac{\left[\left(^{238}\mathrm{U}_g\right)(n_s)(N_A)\right]}{(M_{\mathrm{U}})}\right\}\left(e^{\lambda_{238}t}\right)\left\{\left(1-e^{-\lambda_{238}t}\right)\right. \\ & + \left(\frac{\lambda_{238}}{\lambda_{234}}\right)\left(1-e^{-\lambda_{234}t}\right) + \left(\frac{\lambda_{238}}{\lambda_{230}}\right)\left(1-e^{-\lambda_{230}t}\right) \\ & \left. + I\left(1-e^{-\lambda_{235}t}\right) + \left(\frac{\mathrm{Th}}{\mathrm{U}}\right)_{\mathrm{glass}}\left(1-e^{-\lambda_{232}t}\right)\right\}(\eta_{\mathrm{tot}}) \\ & \cdot (R_e).\end{aligned} \tag{1}$$

Note that one particular subpart of this equation (and the same goes for (2) below) is equal to the atomic frequency of ^{238}U in basaltic glass (i.e., $^{238}\mathrm{U}_a$ in: #atoms of ^{238}U/cm^3), whereby $^{238}\mathrm{U}_a = \{[(^{238}\mathrm{U}_g)(n_s)(N_A)]/(M_{\mathrm{U}})\}$ (i.e., after (5) of Gögen and Wagner [129]).

The areal density of fossil fission tracks intersecting a hypothetical flat fracture plane through DSDP-418A basaltic glass (Figures 10(g), 15(g), and 15(h)) is calculated here using (2) (adapted from Bigazzi [207] and Galbraith and Laslett [208]), where ρ_{FT} is the areal density of etchable fossil fission tracks, λ_{238} is the decay constant for ^{238}U ($1.55125 \times 10^{-10}\,\mathrm{y}^{-1}$ [204]), t is the time since quenching of the glass (120,600,000 y; for age constraints see Figures 5(c), 5(d) and Section 2.2), λ_F is the decay constant for spontaneous fission of ^{238}U ($8.5 \times 10^{-17}\,\mathrm{y}^{-1}$ calculated from the half-life value of 8.2×10^{15} y reported for the spontaneous fission of ^{238}U by Holden and Hoffman [201] using the equation $T_{1/2} = \ln 2/\lambda$, that is, (4.10) of Faure [202]), $^{238}\mathrm{U}_g$ is the weight concentration of ^{238}U in g/g (4.17×10^{-8} g/g, calculated using the $^{235}\mathrm{U}/^{238}\mathrm{U}$ isotopic abundance ratio of 0.00725 [204] and the U concentration of 42 ppb determined by ICP-MS: *DSDP-418A-75-3[120–123]-ICP-MS #6*, Table 1), n_s is the density of basaltic glass (3.0 g/cm^3: cf. [205]), N_A is Avogadro's number (6.02×10^{23} atoms/mol), M_{U} is the molar mass of uranium (238.0289 g/mol), and R_F is the etchable length of a fission track in volcanic glass (0.0008 cm; i.e., ~8 μm: see Figures 3(b) and 3(e) (this study); Figure 1 in Sandhu et al. [198]; Figure 8(b) in Westgate and Naeser [199]; and descriptions in Arias et al. [126]; Sandhu and Westgate [128]). Consider

$$\rho_{\mathrm{FT}} = \left(\frac{1}{2}\right)\left[\frac{\left(e^{\lambda_{238}t}-1\right)}{\lambda_{238}}\right](\lambda_F) \cdot \left\{\frac{\left[\left(^{238}\mathrm{U}_g\right)(n_s)(N_A)\right]}{(M_{\mathrm{U}})}\right\}(R_F). \tag{2}$$

The 1/2 in (2) falls out of the Poisson line-segment model "in which the orientation distribution of a track is uniform with respect to solid angle, and the joint distribution of length and orientation of a track is independent of its location" [208], which holds true for basaltic glass because it is isotropic with a liquid like structure.

5.2. Modelling Results. From (1), we calculate the present-day alpha-recoil track areal density in DSDP-418A basaltic glass to be very high at 148,000,000 alpha-recoil tracks/cm^2, which indicates that these glasses are absolutely riddled with alpha-recoil track damage (Figures 10(h), 10(i), 15(c), and 15(f)) amenable to preferential dissolution/etch-tunnelling (e.g., Figures 1(b), 1(d), 1(f), 7(a)–7(c), 9, 11, 12, 15(a), 15(b), and 15(d)) and preferential palagonitization (e.g., Figure 10) during corrosion/alteration by infiltrating seawater. In our theoretical model, U and Th contributed about equally to the accumulation of alpha-recoil tracks, with the majority of tracks originating from radioactive decay of ^{238}U (accounting for ~71,700,000 alpha-recoil tracks/cm^2) and ^{232}Th (accounting for ~72,700,000 alpha-recoil tracks/cm^2). Comparatively, few alpha-recoil tracks originated from radioactive decay of ^{235}U (3,140,000 alpha-recoil tracks/cm^2), ^{234}U (~212,000 alpha-recoil tracks/cm^2), and ^{230}Th (~65,500 alpha-recoil tracks/cm^2).

A direct 1 : 1 scale comparison of the resultant map of theoretical alpha-recoil track distribution in DSDP 418A basaltic glass (Figure 15(c)) to the map of natural porosity in the etch-tunnel zone (Figure 15(d)) at the same scale reveals two very important similarities. Firstly, the model alpha-recoil tracks are about the same width as the natural etch-tunnels (circa 120 nm). Secondly, the model alpha-recoil track areal density (148 alpha-recoil tracks in a $10 \times 10\,\mu$m region: Figures 10(i) and 15(c)) is high and quite close to the observed areal density of natural nanoscopic etch-tunnels (94 nanotunnels observed in a representative $10 \times 10\,\mu$m region: Figure 15(d)). This indicates that the numerically predicted alpha-recoil track areal density is more than sufficient to account for the observed areal density of ~120 nm wide etch-tunnels. From these two observations, we conclude that the complex networks of nanoscopic etch-tunnels observed at the glass-palagonite interface in DSDP 418A basaltic glass (Figures 1(b), 1(d), 1(f), 7, 9, 11, 12, and 15(a)) are in fact naturally formed alpha-recoil track etch-tunnels (ARTETs) caused by the infiltration of seawater into the glass through preferential dissolution/etch-tunnelling along multitudes of randomly distributed alpha-recoil track damaged sites in the glass and therefore not the result of microbial activity (i.e., in the case of "tubular" microtextures in DSDP 418A basaltic glasses [11, 26–28, 31, 33, 59, 61, 93, 94, 100]).

Similarly, direct 1 : 1 scale comparisons of the model alpha-recoil track distribution in DSDP-418A basaltic glass (Figures 10(h) and 10(i)) with the observed distribution of "granular palagonite" (Figures 10(e) and 10(f)) reveal very similar "spotty" patterns of randomly distributed submicroscopic bodies; that is, the areal density of model alpha-recoil tracks (Figures 10(h) and 10(i)) is very similar to the observed areal density of palagonite granules (Figures 10(e) and 10(f)). This provides strong microtextural evidence to suggest that such granular palagonite microtextures at the glass-palagonite interface (both in DSDP-418A basaltic glass and probably in submarine basaltic glasses worldwide; see further discussion in Sections 3.3.2 and 6.1) originate by preferential alteration/corrosion (i.e., palagonitization) of randomly distributed alpha-recoil track damaged sites in the glass and, therefore, not by microbial activity/bioalteration as previously thought (e.g., [11, 26–28, 31]).

As expected (see Section 3.4.2), the model fission track areal density calculated from (2) is several orders of magnitude smaller at 1,310 fission tracks/cm^2 (Figure 15(h); also see Figures 10(g), 15(f), and 15(g)). This indicates that although they are larger, fission track etch-tunnels should be comparatively few with respect to the number of alpha-recoil track etch-tunnels found (e.g., compare track distributions in Figures 15(f) and 15(g)), and this is consistent with our observations (2 FTETs versus 379 ARTETs in Figures 15(a) and 15(b)), and indeed only 4 were found in our search for fission track etch-tunnels (Figures 13(a)–13(d)). This type of bimodal population versus size distribution of etched fission tracks versus etched alpha-recoil tracks was recognized early on in etching studies of micas (i.e., Figure 1 in Huang and Walker [130]; Figures 4(b): left and 15(e) in this study) and is reminiscent of the pattern of etch-tunnelling that we have observed here in DSDP 418A basaltic glass (i.e., compare

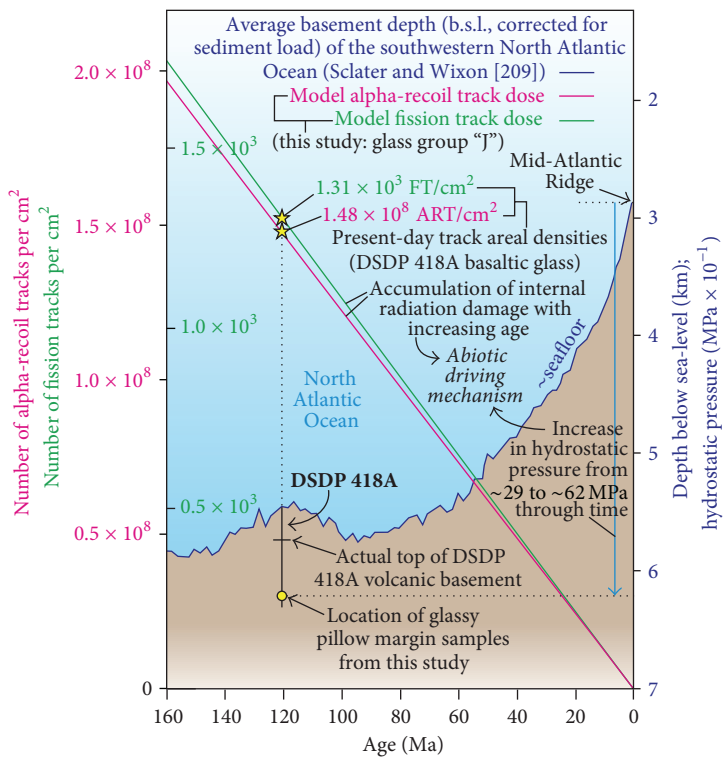

Figure 16: Diagram summarizing the "abiotic driving mechanism" for the formation of complex corrosion microtextures (i.e., microscopic etch-tunnels and granular palagonite) in DSDP 418A basaltic glass: the concomitant increase in hydrostatic pressure and accumulation of radiation damage in basaltic glass with aging of the oceanic crust. The following is depicted in this diagram: (i) the depth-age relationships for volcanic basement in the oceanic crust—depicted as the average depth to basement below sea level (b.s.l.) (corrected for sediment load) for the southwestern North Atlantic Ocean (jagged blue line; from Sclater and Wixon [209]); (ii) the location of DSDP Hole 418A (note that the actual top of volcanic basement in this drill hole is slightly lower than the southwestern North Atlantic average (jagged blue line)); (iii) the inferred hydrostatic pressure in the water column (which can be read at right, along with ocean depth); and (iv) curves (although they are nearly straight lines in this plot) depicting the accumulation (dose) of radiation damage in basaltic glass group "J" (g.g. "J" in Figure 5(b)) through time—that is, the systematic increase (with age) in model fission track and alpha-recoil track areal densities intersecting a hypothetical flat fracture plane through DSDP 418A basaltic glass (calculated using (1) and (2)).

Figures 15(b) with 15(e)). This similarity between the pattern of natural etch-tunnelling in DSDP 418A basaltic glass (e.g., Figure 15(b)) and etch-pit formation on the cleavage surface of experimentally etched micas (e.g., Figure 15(e)—adapted from Huang and Walker [130]) is taken as further microtextural evidence to support a "radiation damage origin" for the etch-tunnels observed at the glass-palagonite interface in DSDP 418A basaltic glass—vis-à-vis natural preferential etch-tunnelling of alpha-recoil tracks and spontaneous fission tracks in the glass by infiltrating seawater.

5.3. The Abiotic Driving Mechanism for the Development of Complex Corrosion Microtextures in Submarine Glasses. The "abiotic" driving mechanism for the formation of microscopic etch-tunnels and granular palagonite microtextures at the glass-palagonite interface in submarine glasses is really quite simple (Figure 16). As the oceanic crust ages and moves away from the spreading ridge, it subsides (e.g., [209]) causing the ambient hydrostatic pressure in volcanic basement rocks to rise incrementally with deepening of the overlying ocean, and this happens concomitantly as radiation damage in the rocks accumulates with time (Figure 16). Consequently, as basaltic glass ages and becomes more and more amenable to preferential corrosion along alpha-recoil track and fission track damaged regions, it may also become increasingly susceptible to the effects of pressure solution etch-tunnelling associated with increasing hydrostatic pressure. Classically, pressure solution in rocks—for example, during diagenesis—takes place in response to increasing *lithostatic* pressure (e.g., under "nonhydrostatic" stress conditions at grain-to-grain contacts, or between sedimentary layers in the case of stylolites [210]). As outlined in Section 3.1, the basaltic glass in this study appears to have undergone an episode of (f_2) fracturing and concomitant devitrification during the formation of white (K-Al-Si)-rich devitrified zones, and this appears to have taken place as a direct consequence of deep burial beneath the overlying volcanic pile (i.e., in response to increasing *lithostatic* pressure). Hence, the diagenetic/low-grade metamorphic response of volcanic glasses to increasing lithostatic load is not necessarily a form of pressure solution, but rather, the solid-state transformation of glass into microcrystalline K-feldspar (±quartz or cristobalite) during the process of "devitrification" (p. 418 in Cas and Wright [184],

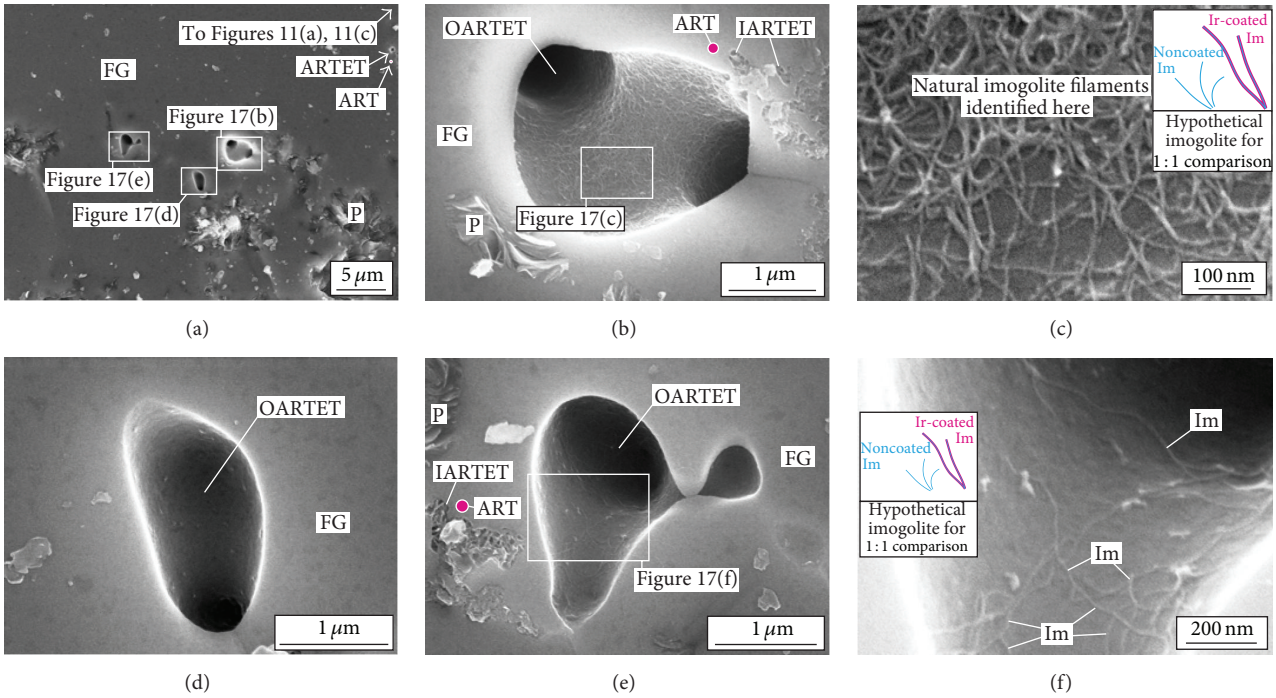

Figure 17: Examples of a peculiar class of etch-tunnels at the glass-palagonite interface that formed either by (i) prolonged overetching of alpha-recoil track etch-tunnels (i.e., are overetched ARTETs or "OARTETs") and/or (ii) by the advance of etch-tunnelling primarily through pressure solution (caused by increasing hydrostatic pressure through time: Figure 16). All images (a–f) are SEM (secondary electron) images, obtained from the freshly fractured surface of a basaltic glass "chip sample" from *DSDP-418A-75-3[120–123]*. Regardless of their origin, these etch-tunnels contain authigenic imogolite filaments within them (c, f) (similar in nature to the imogolite filaments found within ARTETs—see Figure 12), which seems to indicate possible links with alpha-recoil track etch-tunnelling. Note that the etch-tunnels in this region (a) actually occur along the same glass-palagonite interface and etch-tunnel zone shown in Figure 11 (which contains both FTETs and ARTETs) and occur nearby to some ARTETs (e.g., see ARTET at top right in (a)). Furthermore, some of the alteration features in the immediate vicinity of these tunnels are close to the same size as an alpha-recoil track (~120 nm) and are therefore interpreted as corroded or "infilled ARTETs" (see "IARTETs" at top right in (b) and at left in (e)). Although these comparatively large etch-tunnels (a, b, d, e) are closer in size to FTETs (~1-2 μm wide)—hinting at a possible "etched out" fission track cluster—they do not contain any authigenic platy smectite, which is observed ubiquitously within FTETs (see Figure 13). Therefore, these observations point to an origin that is different than fission track etch-tunnelling (i.e., (i) and/or (ii), above). Nevertheless, this peculiar class of etch-tunnels (OARTETs?) (b, d, e), is interpreted to be more or less equivalent to the variety of overetched microtunnels shown in Figure 7(e) that were imaged by transmitted light microscopy.

[185]). Nevertheless, here we suggest that some localized pressure solution of basaltic glass may actually be taking place—not in response to increasing lithostatic pressure—but rather, increasing *hydrostatic* pressure as the overlying Atlantic Ocean has deepened systematically with the passage of geologic time (Figure 16).

According to this hypothesis, the etch-tunnels in DSDP 418A basaltic glass have formed not only through preferential dissolution of radiation damage, but also by a process of pressure solution etch-tunnelling (e.g., enhancement or runaway dissolution of ARTETs)—as if the ever deepening Atlantic Ocean has been incrementally squeezing or "injecting" its way into the glass with microscopic etch-tunnelling "needles" of seawater that propagate preferentially through radiation damaged regions. In this regard, this type of "hydrostatic" pressure solution may be an important compounding factor in controlling pattern formation during etch-tunnelling (e.g., by connecting up nearby tracks during etch-tunnelling: see step 10a of Figure 18 and curvy blue arrows in Figure 19 (bottom), or by etch-tunnel "widening," as seen in Figures 7(e) and 17, and step 12d of Figure 18). Consequently, some etch-tunnels might start out by preferential etch-tunnelling of a single alpha-recoil track by seawater but then continue to propagate through the glass via the process of pressure solution etch-tunnelling (i.e., "runaway etch-tunnelling"), which could explain the occurrence of some relatively long and straight etch-tunnels (e.g., Figure 7(c)). Although testing this hypothesis regarding *hydrostatic* "pressure solution etch-tunnelling" in DSDP 418A basaltic glass is beyond the scope of this study, it does seem like a reasonable proposition given that (a) Since pillow eruption at the Mid-Atlantic ridge ~120.6-million-years-ago, the ambient hydrostatic pressure has more than doubled from ~29 MPa to ~62 MPa, and (b) "Classic" pressure solution is known to take place at around these conditions of pressure and temperature (e.g., during burial of quartzose sandstones: ~20–60°C and ~18–30 MPa—albeit "lithostatic" pressure [210]).

Therefore, we suggest that microscopic etch-tunnels and granular palagonite microtextures in submarine glasses are not microbial trace fossils, but rather, artefacts of three

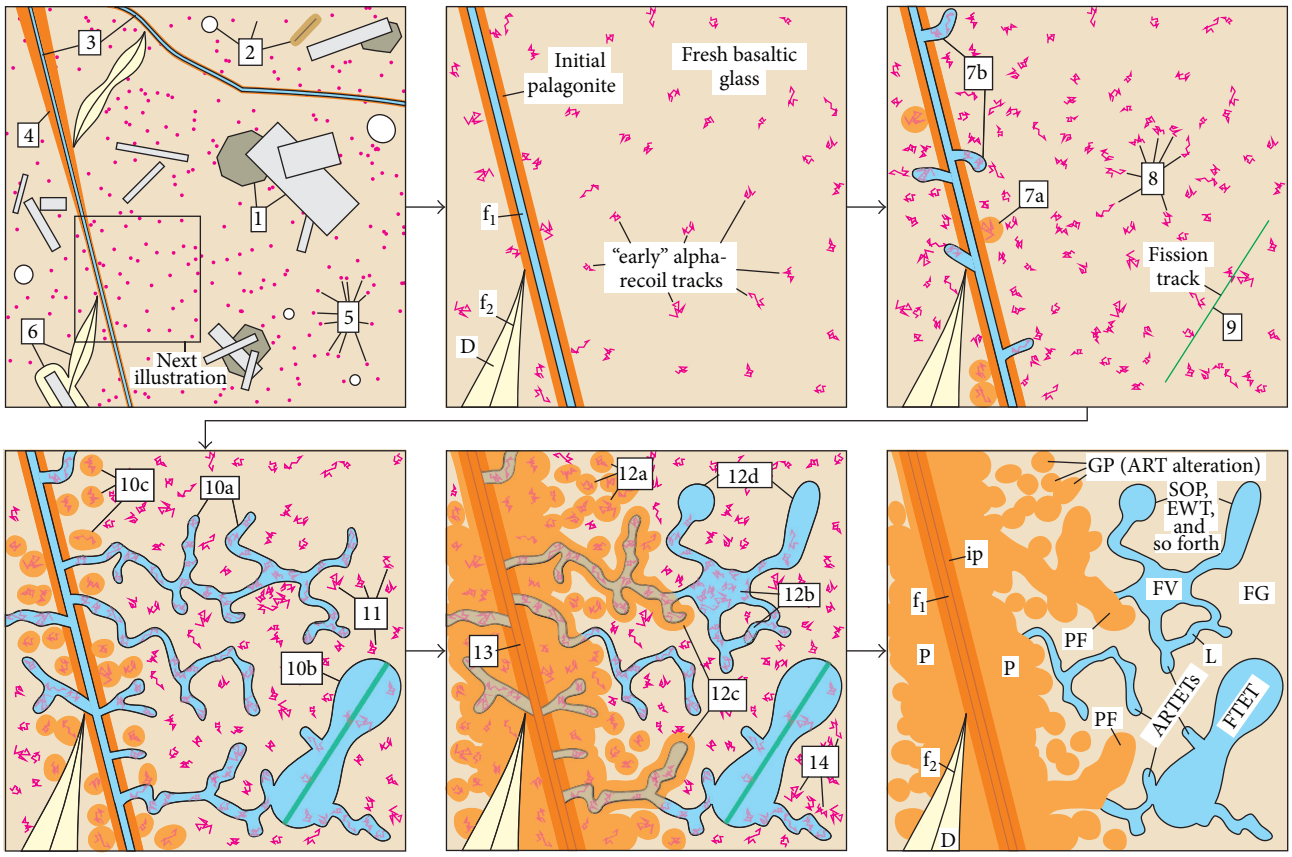

Figure 18: Schematic illustrations depicting the abiotic, stepwise development of complex petrographic microtextures in DSDP 418A basaltic glass (with emphasis on the corrosion of radiation damage). The final illustration (at lower right) highlights the key dissolution/palagonitization microtextures in DSDP 418A basaltic glass that are readily observable by transmitted light microscopy and SEM. Steps in microtextural/petrographic development: (1) nucleation and growth of plagioclase and clinopyroxene phenocrysts in the parent magma; (2) formation of basaltic glass, vesicles, and varioles, upon pillow eruption and quenching of glassy pillow margins; (3) early (f_1) fracturing of glass, allowing the infiltration of seawater into pillow margin interiors; (4) formation of inicipient (initial) palagonite—that is, before the onset of radiation damage—resulting in a sharp glass-palagonite interface; (5) the accumulation of significant numbers of alpha-recoil tracks (ARTs) in basaltic glass (originating from radioactive decay of U and Th) begins soon after pillow eruption (~23,500 ARTs/cm^2 after only the first 10,000 years); (6) deep burial of the pillow lavas being studied to depths of ~408–461 m beneath the overlying volcanic pile causes (f_2) fracturing and development of white (K-Al-Si)-rich devitrified zones, both along f_2 fractures and as halos surrounding plagioclase phenocrysts; (7) early-formed ARTs in the vicinity of f_1 fractures undergo preferential palagonitization (7a) and/or preferential dissolution/etch-tunnelling (7b); (8) ARTs continue to accumulate inside fresh basaltic glass; (9) eventually, fission tracks begin to accumulate in significant numbers within the glass, albeit in a much more sluggish fashion than ARTs (i.e., only ~11 fission tracks/cm^2 after the first 1,000,000 years); (10) over the passage of many tens of millions of years, basaltic glass becomes "riddled" with radiation damage. Meanwhile, the local oceanic crust ages and subsides under a deepening ocean (Figure 16), causing large incremental increases in hydrostatic pressure. The combination of these two processes leads to more advanced corrosion (dissolution and palagonitization) of basaltic glass, including development of a complex etch-tunnel network at the glass-palagonite interface defined by immense numbers of ARTETs (step 10a) interconnected with comparatively sparse FTETs (step 10b). In addition, multitudes of additional ARTs undergo "selective palagonitization" that collectively results in the development of a "granular palagonite ART alteration microtexture" (step 10c). (11-12) More ARTs and fission tracks would continue to form with the passage of time (step 11), ultimately resulting in an increase in complexity of both "granular palagonite ART alteration microtextures" (step 12a) and the ARTET-FTET network (step 12b). Eventually, some previously existing ARTETs/FTETs would become completely overprinted by the advancing palagonite zone, resulting in the formation of "palagonite fingers" that extend outwards into glass (step 12c; Figures 7(d) and 7(f)). Incremental increases in hydrostatic pressure could lead to "pressure solution" etch-tunnelling (step 12d), resulting in more peculiar etch-tunnel structures such as string-of-pearls (SOP), elongate wide tunnels (EWT), and overetched ARTETs (Figures 7(e) and 17). (13) Locally, the permeability of f_1 fractures could be reduced to zero by infilling of fractures with clays/palagonite, terminating the corrosion process. (14) Even after the termination of etch-tunnelling and alteration of the glass by seawater, additional ARTs (and fission tracks) would continue to form within fresh glass. ART: alpha-recoil track; ARTETs: alpha-recoil track etch-tunnels; D: devitrified zone; f_1: early fractures (associated with incipient/initial and ongoing palagonitization); f_2: late fractures (associated with devitrification); FTET: fission track etch-tunnel; FG: fresh glass; FV: flare-out void (formed by dissolution of multiple nearby ARTs); GP: granular palagonite; ip: initial palagonite; L: loop; P: palagonite; PF: palagonite fingers; SOP, EWT, and so forth: string-of-pearls texture, elongate wide tunnels, and other peculiar etch-tunnel varieties caused by prolonged overetching of alpha-recoil tracks and/or pressure solution etch-tunnelling; see Figures 7(e) and 17.

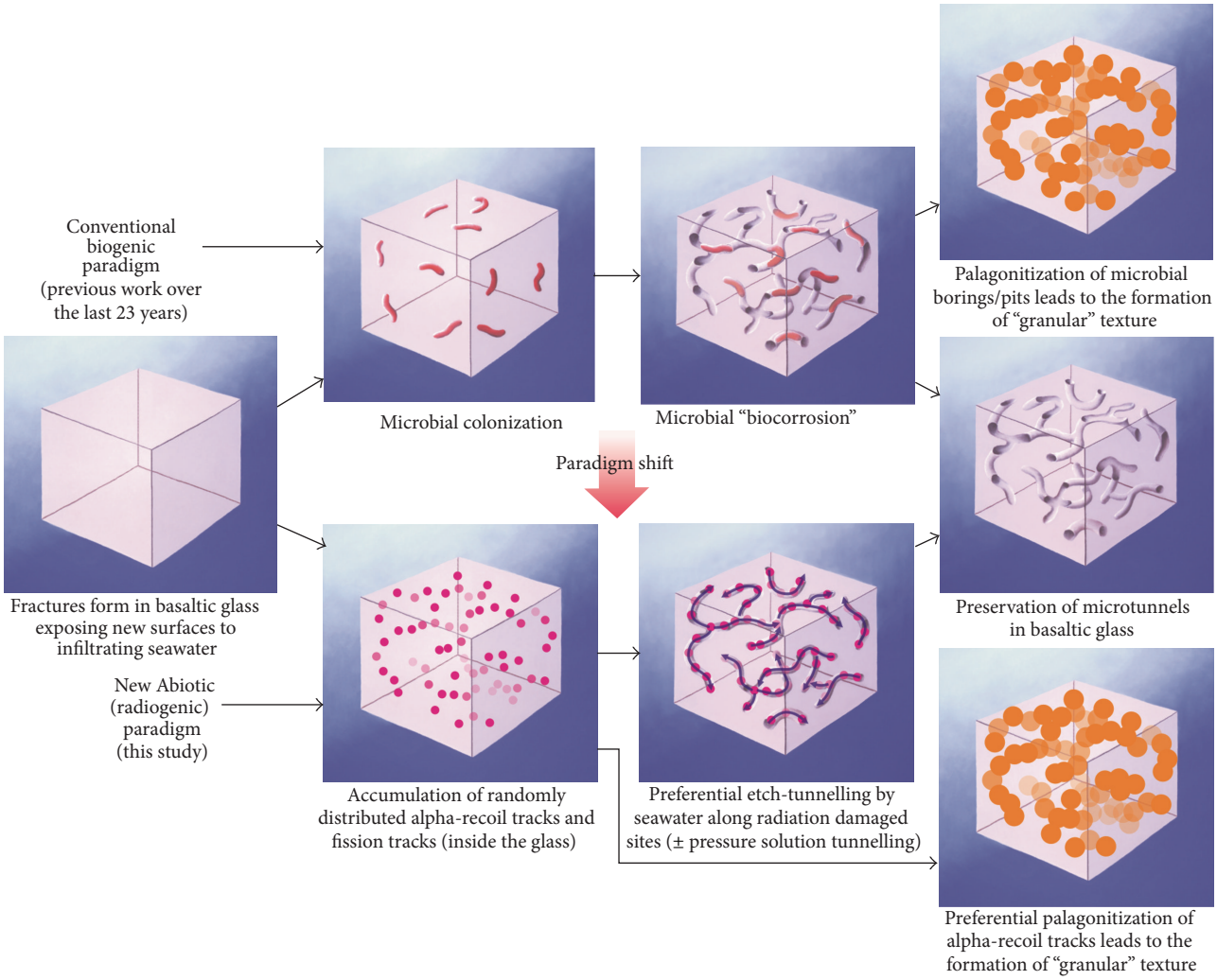

Figure 19: Diagram outlining a paradigm shift in scientific perspectives on the origin of complex corrosion microtextures in submarine basaltic glass—constrained in this study with our model for the preferential corrosion of radiation damage (by seawater) in basaltic glass pillow margins at DSDP 418A (i.e., new abiotic "Radiogenic" paradigm). The conventional "biogenic" paradigm is outlined in previous studies on microbial bioalteration of basaltic glass (e.g., see reviews in Furnes et al. [11], Furnes et al. [26], Staudigel et al. [27], McLoughlin et al. [28], and Furnes et al. [59]).

compounding "abiotic" geological processes: (1) accumulation of radiation damage (i.e., fission tracks and alpha-recoil tracks) in the glass by radioactive decay of U and Th; (2) preferential corrosion (i.e., palagonitization and dissolution) of radiation damage in the glass by seawater; (3) subsidence of the oceanic crust during the cooling and thickening of oceanic lithosphere as it moves away from the spreading ridge and the associated incremental increases in hydrostatic pressure under a deepening ocean—leading to localized pressure solution of glass (and alpha-recoil track etch-tunnel widening/enhancement).

As with the study of mm-scale pressure solution structures in fossiliferous shales by Lescinsky and Benninger [211]—which may be readily mistaken for predator traces (i.e., are *pseudo*ichnofossils or *pseudo*borings)—the pressure solution microstructures (i.e., enhanced alpha-recoil track etch-tunnels) described here may also be readily mistaken for microbial trace fossils (e.g., compare SOP texture in Figure 7(e) of this study with string-of-beads texture in Figure 1(f) of Fisk et al. [24]).

6. Discussion and Implications

6.1. Discovery of Naturally Etched Nuclear Tracks in Basaltic Glass: Implications for Geomicrobiology. The worldwide corrosion of basaltic glass throughout geological history on planet Earth has resulted in the development of a variety of distinct and complex alteration/dissolution microtextures preserved in submarine glasses of the *in situ* oceanic crust, ophiolites, and greenstone belts dating back to ~3.5 Ga, and, for about the last 20 years, the consensus has been that these globally widespread, complex petrographic microtextures in

volcanic glass (i.e., "tubular" etch-tunnels and "granular" palagonite) originate strictly through microbial activity [11, 23, 24, 26–28, 59, 104]). Therefore, our discovery in the present study that microscopic etch-tunnels and granular palagonite microtextures in DSDP-418A basaltic glass originate primarily by preferential corrosion of radiation damage (i.e., fission tracks and alpha-recoil tracks) has immediate implications for geomicrobiology, microbial ecology, and studies aimed at identifying microscopic morphological biomarkers in volcanic/impact glasses on planet Earth (or even Mars). For instance, alpha-recoil track etch-tunnels and granular palagonite "ART" alteration identified at the glass-palagonite interface in DSDP-418A basaltic glass in this study are basically indistinguishable from many previous reports of "tubular" and "granular" bioalteration (i.e., compare "tubular bioalteration" in Figures 1(a), 1(c), and 1(e), to "alpha-recoil track etch-tunnels" in Figures 1(b), 1(d), and 1(f), and compare "granular bioalteration" in Figures 2(a) and 2(c) to "granular palagonite ART alteration" in Figures 2(b) and 2(d)). What this means is that probably in many cases in the past, such "abiotic" corrosion microtextures in submarine basaltic glass have likely been mistaken for signs of microbial activity/bioalteration. In this regard, naturally etched fission tracks and alpha-recoil tracks in submarine glasses—including microscopic "fission track etch-tunnels" (e.g., Figures 11, 13, 15(a), and 15(b)), "alpha-recoil track etch-tunnels" (e.g., Figures 7, 9, 11, 12, 15(a), and 15(b)), and "granular palagonite ART alteration" (e.g., Figures 7(f) and 10)—can also be regarded as *pseudomicrobial trace fossils*—that is, abiotic microstructures that look conspicuously biogenic, but which are not (akin to previously described "*pseudo*borings/predator traces" documented in fossiliferous shales that are simply artefacts of pressure-dissolution [211]). Consequently, the depth of the biosphere (in the oceanic crust), the distribution of microbes and microbial habitat and the possible preservation of microbial trace fossils in volcanic glass within the *in situ* oceanic crust, ophiolites, and greenstone belts dating back to ~3.5 Ga now need to be completely reevaluated in light of our abiotic (i.e., U–Th–Pb radiogenic) model for the development of microscopic etch-tunnels (i.e., tubular textures) and granular palagonite microtextures in submarine basaltic glass. Therefore, our study marks the second "paradigm shift" in scientific perspectives on the origin of complex corrosion microtextures in submarine volcanic glass (Figure 19), from an early "abiotic" paradigm (i.e., before Thorseth et al. [23] [39], "mist zone" of Morgenstein and Riley [40], [41–44]), to the popular "biotic" paradigm which has dominated the scientific literature over the last 23 years (e.g., [11, 12, 23–28, 34, 49, 59, 64, 96, 104])—and now back to an "abiotic" (i.e., U–Th–Pb radiogenic) paradigm with the present study (Figure 19).

Probably in most previously documented cases, the notion of "granular bioalteration" of basaltic glass is now more or less in doubt—in light of our simple "abiotic" model of granular palagonite formation by the preferential palagonitization of multitudes of alpha-recoil tracks (Figures 2, 10, 18, and 19). Therefore, we suggest that the recently proposed trace fossil names for granular bioalteration of basaltic glass, including the *Granulohyalichnus vulgaris* ichnospecies and the *Granulohyalichnus* ichnogenus [28], can now essentially be challenged. These granular palagonite microtextures are quite clearly the result of preferential palagonitization of multitudes of randomly distributed alpha-recoil tracks in the glass (Figures 10 and 18), and they are basically identical (Figure 2) to previous reports of granular bioalteration microtexture—most notably those microtextures presented as "classic examples" of granular bioalteration (Figures 2(a) and 2(c) [11, 28, 59]).

We did not observe any examples of preferentially palagonitized fission tracks in DSDP 418A basaltic glass in this study (i.e., "granular palagonite FT alteration" as opposed to "granular palagonite ART alteration"), and this is probably due to the relatively sparse distribution of fission tracks at the scale of observation of granular palagonite (i.e., compare Figures 10(d) and 10(g), shown at similar scales). However, some previous reports of granular palagonite microtextures in submarine glasses from the Costa Rica Rift (*Plate 1 [3]* in Furnes et al. [50]), interpreted as evidence of microbial etching—but reinterpreted here as "abiotic" corrosion microtextures (Figure 20(c))—do provide compelling textural evidence to suggest that preferential palagonitization of *both alpha-recoil tracks and fission tracks* does take place during the alteration of submarine glasses. In particular, the bimodal distribution of a few large (ca. 5 μm) "fission track granules" surrounded by multitudes of smaller (ca. 0.5–1 μm) "alpha-recoil track granules" (Figure 20(c)) is consistent with the expected size and population distributions of fission tracks versus alpha-recoil tracks. Therefore, we suggest that in addition to the ca. 0.6 μm variety of granular palagonite (i.e., "granular palagonite ART alteration"; Figure 10), some larger (ca. 5 μm) varieties of granular palagonite (i.e., possibly representing "granular palagonite FT alteration"; Figure 20(c)) may also be considered to represent pseudo*microbial trace fossils*.

Similarly, it seems clear at this point that many previously documented examples of "tubular bioalteration" of basaltic glass (i.e., microscopic tunnels at the glass-palagonite interface in submarine glasses)—can now be reinterpreted as alpha-recoil track etch-tunnels. For instance, tubular textures in submarine basaltic glasses presented as "classic examples" of tubular bioalteration are essentially identical in size, form, and geological setting to the alpha-recoil track etch-tunnels documented at the glass-palagonite interface in DSDP-418A basaltic glass in the present study (e.g., compare at the same scale: Figures 1(a), 1(c), and 1(e) with Figures 1(b), 1(d), and 1(f), resp.). Therefore, we suggest that the biogenicity of most "tubular bioalteration" microtextures documented in submarine glasses worldwide (e.g., [11, 26], including the recently proposed *Tubulohyalichnus ichnogenus* and related ichnospecies, particularly the ichnospecies *Tubulohyalichnus simplus* of McLoughlin et al. [28]) can probably in many (if not most) cases be effectively refuted by our simple model of alpha-recoil track and fission track etch-tunnelling (possibly combined with etch-tunnel enhancement by pressure solution). For example, compare at the same scale, representative examples of *Tubulohyalichnus simplus* presented in Figures 2(a)–2(c) of McLoughlin et al. [28] with representative examples of alpha-recoil track etch-tunnels in Figures 1(b), 1(d), 1(f), and 7 in the present study.

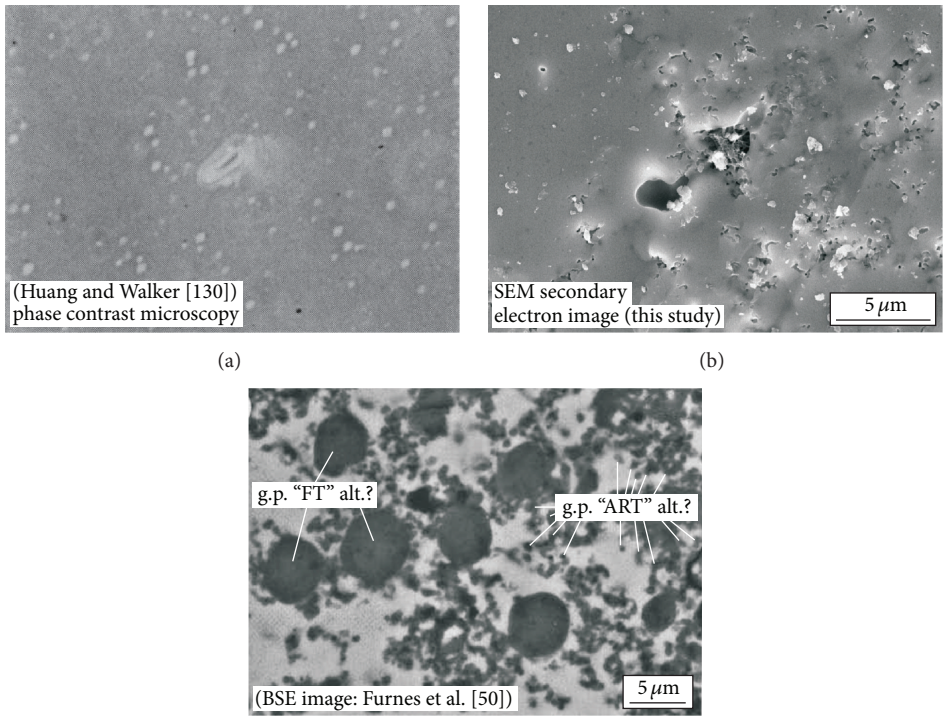

Figure 20: Three examples of "bimodal" distributions of microscopic corrosion features in geological samples—in each case, most likely related to the bimodal "size versus population (i.e., areal density)" distribution of fission tracks versus alpha-recoil tracks. (a) Phase contrast photomicrograph showing one large fission track etch-pit surrounded by a multitude of much smaller alpha-recoil track etch-pits on the experimentally etched cleavage surface of mica (from Huang and Walker [130]—no scale bar available). (b) SEM (secondary electron) image of one large fission track etch-tunnel surrounded by several much smaller alpha-recoil track etch-tunnels in *DSDP-418A-75-3-[120–123]* basaltic glass (close-up from Figure 11(a)). (c) SEM (BSE) image of several large palagonite granules surrounded by a multitude of much smaller palagonite granules (from Plate 1 in Furnes et al. [50] of sample *148–896A-11R-1*, 111–113 cm—from the Costa Rica Rift). The original interpretation is that both varieties of palagonite granules are biogenic in origin (i.e., "produced by the etching of microbes": Furnes et al. [50]). However, in light of our newly proposed "abiotic" paradigm for interpreting corrosion microtextures in submarine glasses (Figure 19), we reinterpret the bimodal distribution of palagonite granules in (c) to have more likely arisen due to the concomitant, preferential palagonitization of several large fission tracks (granular palagonite "FT" alteration—labelled as "g.p. 'FT' alt.?") and a multitude of tiny alpha-recoil tracks (granular palagonite "ART" alteration—labelled as "g.p. 'ART' alt.?"), during infiltration of seawater.

It then follows that "older" examples of titanite-mineralized tubular textures attributed to microbial activity that are preserved along healed fractures in the metamorphosed margins of pillow lavas in Archean greenstone belts [25, 35, 37, 91, 94] might also simply represent the preserved (titanite-mineralized) relicts of preferential corrosion of radiation damage and/or pressure solution etch-tunnelling (i.e., "abiotic" microtextures) that formed during the encroachment of seawater into these basaltic glass pillow margins in Archean times.

Consequently, we suggest that the observed worldwide distribution of "tubular" and "granular" microtextures in submarine glasses from >40 geological sites worldwide (e.g., [26, 27, 103]) might not necessarily be a reflection of a global lithoautotrophic microbial community causing the biocorrosion/bioalteration of volcanic glass, but instead it may simply be a reflection of the worldwide occurrence of U- and Th-bearing submarine glasses [146] and the associated "abiotic" corrosion/dissolution of radiation damage by encroaching seawater combined with the possible effects of pressure solution etch-tunnelling, as these glasses age under a deepening ocean (Figure 16).

At this point, it is important to highlight that there is also a much larger variety of other more peculiar morphological types of microscopic tunnels documented in submarine glasses around the globe (but not found in the present study), whose origin needs to be explained, whether "biotic" or "abiotic." This includes spiral/helical microtunnels, annulated microtunnels, and dendritic microtunnels (Figures 4–6 in McLoughlin et al. [28]), along with several other intricate microtunnel varieties documented more recently in submarine glasses such as flattened "petal shaped" tunnels exhibiting honey-comb or ribbed textures, crowned and palmate tunnel varieties, and tunnels exhibiting septae [103]. It has been suggested that some of these other intricate microtunnel varieties might be the product of microbial activity/microboring [28, 103] and some are currently designated as *bona fide* microbial trace fossils in basaltic glass (e.g., the recently erected ichnofossil species *Tubulohyalichnus spiralis*, *Tubulohyalichnus annularis*, and *Tubulohyalichnus*

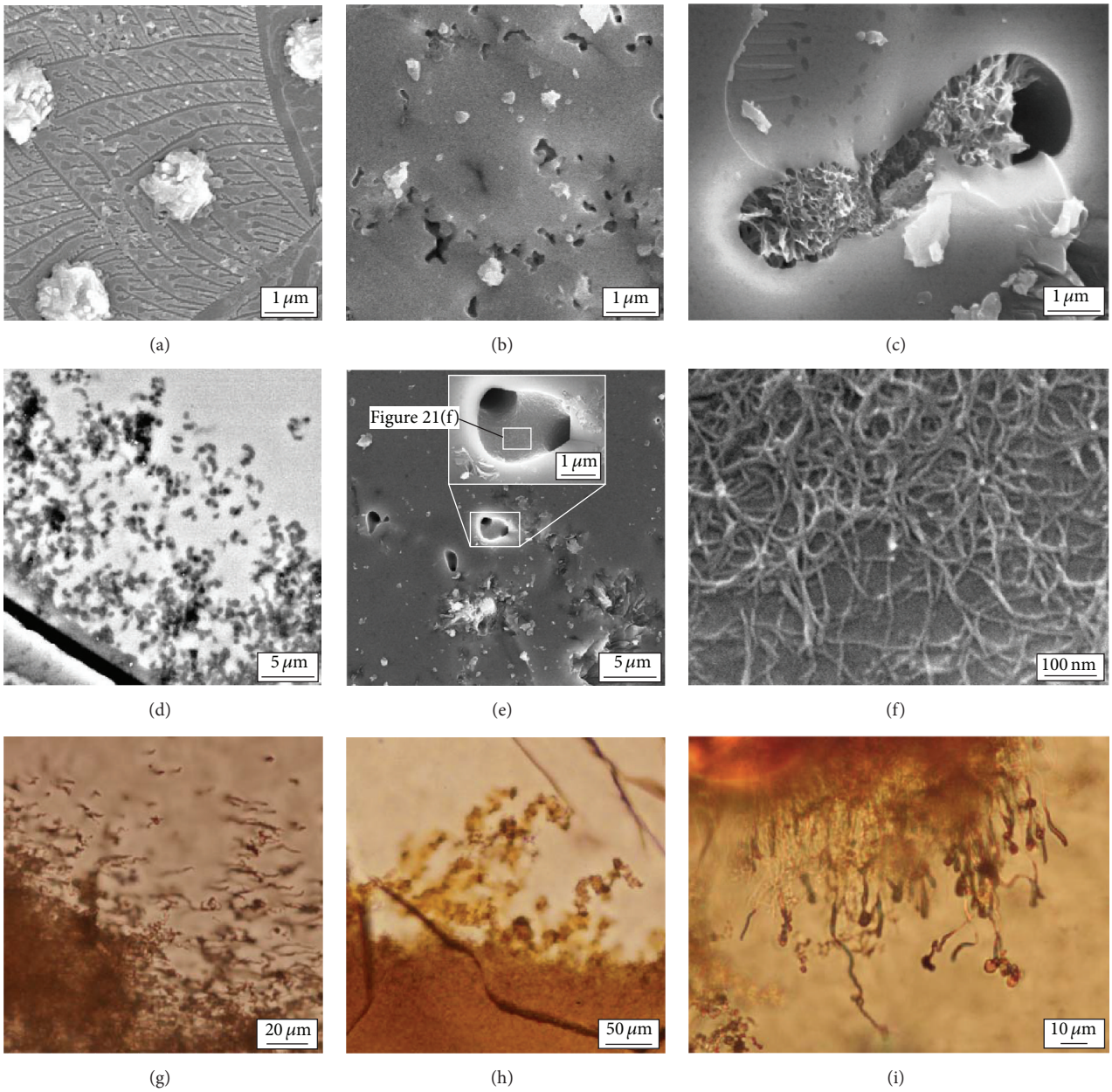

Figure 21: Summary of complex "abiotic" microtextures found in DSDP 418A basaltic glass that have the potential to be mistaken for signs of microbial activity (i.e., microbial etchings, groovings, borings, alteration, or remains). (a–c, e, f, h, and i) are from sample *DSDP-418A-75-3-[120–123]* and (d, g) are from sample *DSDP-418A-68-3[40–43]*. (a–f) are SEM (secondary electron) images ((a–c, e, and f) are from basaltic glass "chip samples" and (d) is from a polished petrographic section) and (g–i) are transmitted light photomicrographs of polished sections taken in plane polarized light (uncrossed polars). (a) Dendritic nanogrooves on a vesicle wall (close-up image from Figure 1(b) in French and Muehlenbachs [107]) that represent frozen viscous fingers of magmatic fluid injected into the vesicle wall upon quenching of the glass. (b) Alpha-recoil track etch-tunnels (ARTETs). (c) A fission track etch-tunnel. (d) Granular palagonite ART alteration (close-up from Figure 2(b)). (e) ARTETs at the glass-palagonite interface affected by prolonged overetching and/or are "pressure solution enhanced" (from Figure 17 in this study; Figure 1 in French [139])—akin to the tunnels shown in Figures 7(e) and 21(i)—also note that this region (e) occurs along the same glass-palagonite interface that is shown in Figure 11(a) (i.e., in the vicinity of dense concentrations of other *bona fide*/incipient ARTETs). (f) Authigenic imogolite filaments (close-up from (e); Figure 17; Figure 1 in French [139]). (g) ARTETs at the glass-palagonite interface. (h) Palagonite fingers that have overprinted previously existing ARTETs. (i) ARTETs—most of which have been affected by prolonged overetching and/or are "pressure solution enhanced," resulting in string-of-pearls texture and elongate wide tunnels (among other forms—see Figure 7(e)).

stipes of McLoughlin et al. [28]). Here, we suggest that these other morphological varieties of microtunnels in volcanic glass might also originate through some kind of pressure solution etch-tunnelling process (similar to that outlined in Section 5.3) as opposed to microbial activity, such that they could instead represent spiral/helical, annulated, and dendritic pressure solution etch-tunnels (e.g., that form in the absence of radiation damage?). Note that the idea of the "injection" of microscopic channels of geological fluids into basaltic glass is not that far-fetched, because dendritic patterns of nanoscopic grooves found on vesicle walls in submarine basaltic glass have recently been shown to form by the fluid mechanical process of viscous fingering, resulting essentially in the "injection" of narrow (~50–75 nm wide) fingers of magmatic vapour into hot basaltic glass upon quenching of the glass during pillow eruption (see companion study on nanogrooves within vesicles in DSDP-418A basaltic glass [107]). At any rate, the experimental etch-tunnelling of quartz using HF has also resulted in the formation of micron-scale spiral/helical microtunnels [116] that are similar in nature to those found in basaltic glass (e.g., those shown in Figure 5 of McLoughlin et al. [28]), and therefore nonbiological explanations such as microscopic etch-tunnelling, pressure solution etch-tunnelling, injection, and possibly even viscous fingering (cf. dendritic microchannels documented in French and Muehlenbachs [107]) should also be sought for the origin of these other (more peculiar) varieties of microtunnel in basaltic glass (i.e., spiral/helical, annulated, and dendritic, among other forms).

The discovery of naturally etched fission tracks and alpha-recoil tracks in submarine basaltic glass in this study has important implications for other fields of research as well, including geochronology (alpha-recoil track and fission track dating), the influence of radiation damage on weathering and corrosion processes in rocks, minerals, and glasses, and the astrobiological exploration of Mars (e.g., evaluating the origin and possible biogenicity/abiogenicity of corrosion microtextures found in Martian glasses), and provides an ideal natural laboratory for understanding the long-term breakdown and corrosion of nuclear waste glasses stored in deep geological repositories, all of which we address in the following four Sections 6.2–6.5.

6.2. Identification of Naturally Etched Fission Tracks in Submarine Basaltic Glass: Context within the Broader Field of Fission Track Dating

6.2.1. Background on Experimentally Etched Fission Tracks in Minerals and Glasses. The *experimental* etch-tunnelling of fission tracks is routinely carried out in fission track dating studies of a variety of geological materials that contain trace U (Figures 3(b) and 3(c)), and this includes minerals such as zircon [212], apatite [213], monazite [149], sphene [148], titanite [214], and muscovite [207], a variety of natural glasses including the glassy margins of midocean ridge pillow basalts [125, 147], glassy shards in marine sediments [140] and tephra beds [128], basaltic glass inclusions in volcanic quartz [215], tektites [216–219], and obsidian artefacts [220]—as well as in studies of borosilicate nuclear waste glasses [138, 144] and other synthetic materials used as fission track "detectors" such as diallyl phthalate resin [221] and CR-39 plastic [222]. Exposing a polished or cleavage surface to an etchant preferentially dissolves the damaged regions in the mineral or glass that result from the spontaneous fission of ^{238}U (Figure 3) or by the induced fission of ^{235}U caused by irradiating the sample with thermal neutrons from a nuclear reactor (Figure 3(b)—right) [202, 223, 224] (note: strong etchants such as HF, HNO_3, HCl, or NaOH solutions are typically used in fission track dating studies, although weak etchants—such as deionized water—have also been used to reveal fission tracks in silicate glasses (e.g., Figure 3(d)) [138]). Fission fragments cause linear damage tracks (Figure 3(a)) that range in etchable length depending on numerous factors including host mineralogy and composition [225, 226], fission fragment mass [225, 227], crystallographic orientation [228], etching time and efficiency [222], and the degree of thermal annealing which may have occurred [229]. For example, the mean etchable length of pristine fission tracks (e.g., unannealed or induced tracks) is ~8-9 μm in volcanic glass (Figure 3(b); Figure 1 in Sandhu et al. [198]; Figure 8(b) in Westgate and Naeser [199]; Arias et al. [126]; Sandhu and Westgate [128]) and tektites (Figures 1 and 2 in Storzer and Wagner [218], ~11 μm in zircon [212, 230], ~16 μm in apatite [213], and ~20 μm in micas [207, 229], although experimentally etched "fossil" (i.e., spontaneous) fission tracks may be substantially shorter in each case, especially due to annealing and track fading [126, 128, 207, 212, 213, 229, 230]. For natural (and synthetic) silicate glasses exhibiting a wide range of chemical compositions, the lengths of fully revealed (i.e., etched) fission tracks are consistently reported as being ~6–9 μm long (e.g., Figures 3(b), 3(d), and 3(e))—including those in hydrated silicic volcanic glass shards [128], tektites (including: australite [216, 231], bediasite [218], indochinite [216], and moldavite [128, 219]), obsidian archaeological artefacts [220], rhyolite glass [232], dredged and drilled samples of basaltic glass pillow margins [125, 127], and glasses from volcanic flows and glassy shards interlayered within sediments [126]—and they etch much faster in basaltic glass than in glasses with higher SiO_2 contents [144]. As highlighted above and in Section 3.4.2, the typical size of fully etched "pristine" fission tracks in volcanic glass (and tektites) is ~8-9 μm long (Figure 3(b) [126, 128]; Figure 1 in Sandhu et al. [198]; Figure 8(b) in Westgate and Naeser [199]; Figures 1 and 2 in Storzer and Wagner [218]).

During etch-tunnelling of fission tracks in the laboratory, the etched track widths grow linearly with time [212, 222], and when the full track length is revealed with minimal overetching they are on the order of ~1 μm wide [212, 221]. Thus, at ~1-2 μm wide and up to ~8 μm long, the naturally formed fission track etch-tunnels identified in DSDP-418A basaltic glass in this study (Figures 11, 13, and 15) are consistent with the expected dimensions of fully etched fission tracks in volcanic glass (and tektites) (see 1 : 1 scale comparison in Figure 3(e)), which adds support for our interpretation that these peanut-shaped cavities at the glass-palagonite interface (e.g., Figure 13) are in fact naturally etched fission tracks. Fission tracks in volcanic/impact glasses that are etched in the laboratory, typically exhibit a pointed "conical" shape during

etching of the track (at first), but once the etch-pit reaches the end of the track (i.e., when fully etched), the etch-pits then progressively take on a more rounded (prolate spheroidal to spherical) shape (Figure 2.6 in Wagner and Van den Haute [219]), such that fission tracks oriented perpendicular to the polished surface look like circles when fully etched, while those at oblique angles look like elongate ovals (Figure 3(b); Figures 2.7 and 6.7 in Wagner and Van den Haute [219]). Similarly, the fission track etch-tunnels identified here in DSDP-418A basaltic glass (Figure 13) have rounded tips and are considered to be "fully etched/revealed" fission tracks, which may also exhibit a circular appearance when they are intersected at a high angle (i.e., when viewed end-on: Figures 13(d) and 13(f)) and more elongate shapes when intersected at a shallow angle (e.g., Figures 13(a)–13(c), and 13(f)). However—instead of an oval shape—in this geological environment, the naturally etched fission tracks take on an overall "dumbbell" or "peanut" shape (Figures 3(e) and 13)—and this is interpreted to reflect syn- to postdissolutional necking (Figure 13(f)) that takes place in response to the conditions of high confining pressure that these glasses are subjected to during fission track etching (i.e., the elongate etch-tunnel has attempted—but failed—to pinch itself off as two smaller spheres that would ultimately have less surface energy and thus be more stable—a process that commonly takes place in tubular or planar fluid inclusions within minerals [122, 233]).

6.2.2. Adding to the Known Record of Naturally Etched Fission Tracks in Minerals and Glasses. It was noted early on that despite their possible widespread occurrence, reports of *naturally* etched fission tracks are rare [138, 234], prompting some to duly note that given the abundance of latent fission tracks in ancient U-bearing minerals and glasses "one can wonder why such a preferential etching of fission tracks in natural systems has never been reported." [138]. Some possible reasons put forth to explain this apparent lack of naturally etched fission tracks include the difficulty in recognizing naturally etched fission tracks due to the rough nature of mineral surfaces at the micron scale, the low concentrations of fissionable elements in many natural glasses, and the low dissolution rates of many ancient U-bearing minerals that contain abundant fission tracks (e.g., zircon and monazite). Nevertheless, at this point in time, there are actually a few documented cases of naturally etched fission tracks in geological samples, including the weathered outer surfaces of sphene grains from the ca. 450 Ma Coleraine granite, Western Australia [148], occurrences within apatite crystals of the Late Cretaceous Kunon pluton, Zhangzhou Igneous Complex, southeast China [150], and those formed by natural etching caused by fluids circulating along fractures within ~1 Ma monazite of unknown provenance [149] and possibly also within quartz grains picked on the borders of the natural fossil nuclear reactors at Oklo, Gabon [138, 234]. Therefore, the ~1-2 μm wide, up to ~8 μm long, fission track etch-tunnels identified in DSDP 418A basaltic glass in this study (Figures 11, 13, and 15) add to this relatively sparse record and represent the first documented occurrence of naturally etched fission tracks in basaltic glass (or for that matter, any other type of natural glass). This discovery provides new evidence that naturally etched fission tracks could be quite widespread on planet Earth (i.e., within a wide variety of possible U-bearing minerals and glasses that have been subjected to subaqueous weathering and dissolution); it is just that we have been relatively slow to recognize them thus far. Further evidence to support this idea comes from the bimodal distribution of "granular" palagonite alteration observed in some partially palagonitized submarine glasses (Figure 20(c) [50]), which may arise from the preferential palagonitization of relatively few large fission tracks along with multitudes of smaller alpha-recoil tracks (Figure 20(c)) during the infiltration of seawater.

6.3. Identification of Naturally Etched Alpha-Recoil Tracks in Submarine Basaltic Glass: Context within the Broader Field of Alpha-Recoil Track Dating

6.3.1. Adding to the Record of Naturally Etched Alpha-Recoil Tracks in Minerals and Glasses. Similarly, there is much direct (and indirect) evidence which suggests that the natural etching of alpha-recoil tracks in minerals is a widespread phenomenon on Earth [141], including, for example, irregular corrosion fronts associated with preferential alteration/weathering of high U- and Th-bearing metamict domains in zircon (e.g., Figure 7(a)—inset BSE image; Figure 9 in Lumpkin [193]; Appendix A in French [194]; Figure 1(d) in French [195]) or the leaching of certain radionuclides (e.g., ^{234}U and radiogenic Pb) from alpha-recoil track damaged sites within zircon (e.g., [141, 235]). Therefore, the discovery of alpha-recoil track etch-tunnels at the glass-palagonite interface in submarine basaltic glass in this study (readily observable by petrographic microscope: Figures 1(b), 1(d), 1(f), 7, 9(n), and 9(o); and by SEM: Figures 9, 11–13, and 15) provides new "microtextural evidence" for this likely globally widespread corrosion process and represents the first ever documented occurrence of naturally formed alpha-recoil track etch-tunnels (ARTETs) in any type of geological material. Furthermore, the observation that *granular palagonite ART alteration* at the glass-palagonite interface in DSDP 418A basaltic glass can be explained by the preferential palagonitization of multitudes of alpha-recoil tracks (Figure 10—also see Section 3.3.2) provides further evidence that alpha-recoil track etching/corrosion is an important process taking place within submarine basaltic glass—possibly at a global scale given the widespread distribution of U- and Th-bearing submarine glasses in the oceanic crust [146] and the widespread occurrence of microtunnels and granular alteration textures in submarine volcanic glasses (e.g., [26, 27, 103]).

6.3.2. Implications for Alpha-Recoil Track Dating of Natural Glasses. As with fission tracks, the areal density of alpha-recoil tracks in geological samples can be exploited as a geochronometer, when the tracks are revealed by chemical etching in the laboratory and then counted—although this geochronological technique has so far only been applied to

very young volcanic micas (i.e., <1 Ma phlogopites) due to the relatively rapid accumulation of alpha-recoil tracks and the simplicity of etching those which intersect the exposed cleavage surfaces of micas (Figure 4(b)) [129–134]. Therefore, the discovery of naturally etched alpha-recoil tracks in ~120.60 Ma basaltic glass in this study opens up for the first time, the possibility of carrying out geochronological studies of volcanic/impact glasses and obsidian archaeological artefacts using alpha-recoil tracks—originally suggested as being worthy of pursuit if alpha-recoil tracks were ever found in volcanic glass [130]. As mentioned above, the revelation of alpha-recoil tracks by experimental chemical etching has only ever been applied to micas [129], and this is in part because the perfectly flat cleavage surfaces of mica provide ideal surfaces for chemical etching of such faint and small (~120 nm diameter) nuclear tracks—avoiding the need for generating flat surfaces by means of polishing and mechanical abrasion—as is carried out in fission track dating studies of minerals such as apatite, zircon, or sphene, and notably volcanic/impact glasses. Therefore, if experimental chemical etching of latent alpha-recoil tracks in volcanic glass is ever attempted (it is beyond the scope of the present study), we suggest that it should be carried out on freshly broken fracture surfaces (i.e., generated in the laboratory) that are suitably flat and fresh, to avoid the possible destructive impact that polishing with fine abrasive powders would have on the revelation of such tiny damage tracks on an artificially "polished" surface (i.e., see polishing "scratches" in Figure 3(d)). It is also important to highlight that the naturally formed alpha-recoil track etch-tunnels identified in DSDP-418A basaltic glass in this study were "naturally etched" under conditions of considerably high hydrostatic pressure (~29–62 MPa), and so the "natural" revelation of alpha-recoil tracks in these volcanic glasses could in part have been facilitated by the immense weight of the overlying water column (Atlantic Ocean). This might also explain why, despite decades of fission track dating of natural glasses (e.g., [125, 126, 128, 140, 144, 147, 216, 219, 232]), no studies have ever hinted at the possible presence of etched alpha-recoil tracks in laboratory etching studies of polished samples of volcanic/impact glasses. Moreover, when comparing the etching acceleration (i.e., preferential etching ratio: $(V_T - V_G)/V_G$, where V_T is the "track" etch rate and V_G is the "general" etch rate) of alpha-recoil tracks (0.0015; i.e., V_T is 0.15% higher than V_G) versus fission tracks (3000; i.e., V_T is 3000 times higher than V_G!) in muscovite [145], it again becomes clear why alpha-recoil tracks may have been overlooked (or simply not revealed at all) in many previous fission track dating studies of natural glasses.

6.4. Implications for Long-Term Storage of Nuclear Waste Glass. The envisaged final steps in the nuclear fuel cycle are solidifying the high level radioactive waste, generally by vitrifying it and subsequently safe storage of this material in a deep dry geological repository such as salt domes, granite, or clay [227, 236]. Nuclear waste glasses are typically comprised of 40–50 wt.% SiO_2, 10–15 wt.% B_2O_3, 8–20 wt.% Na_2O, some MgO, Al_2O_3, Fe_2O_3, CaO, and TiO_2, and 10–15 wt.% high level radioactive waste [227]. Basaltic glass is considered to represent a suitable natural analog for the breakdown of borosilicate nuclear waste glasses, because both have similar SiO_2 contents and related corrosion rates and mechanisms [135, 191].

Most of the radiation damage in nuclear waste glasses comprises alpha-recoil tracks [227, 236–238]. As with alpha decay in rocks and minerals [132, 134], the kinetic energy of each recoiling daughter nucleus (~0.7 keV/nucleon) is lost through elastic collisions with the host glass, forming a ~30–50 nm long damage trail that comprises on the order of ~1000 atomic displacements [129, 237]. Some radiation damage in nuclear waste glasses also originates from other forms of self-radiation including alpha particles themselves, which cause ~200 atomic displacements over their travel range of ~10–20 μm, spontaneous fission tracks, which are very rare relative to alpha-recoil tracks but cause about ~40,000–60,000 atomic displacements per fission fragment, and beta particles which cause on average less than one atomic displacement per beta decay event [227, 236, 238].

Extrapolation of laboratory assessments of nuclear waste glass behaviour to longer time periods (i.e., 10,000 years or more) is currently one of the most important problems in nuclear waste disposal [193]. In the event that ground water breaches a repository sometime in the future, it is particularly important to understand the interactions of water with radiation damaged regions in old glass because leaching will occur preferentially in those regions [227]. Of special interest in this problem are the long-lived actinides (e.g., Np, Pu, Am, and Cm) in nuclear waste glasses that will cause abundant alpha-recoil damage during radioactive decay over the realistically long periods of storage time (i.e., some 10,000 years) in the repository [193, 236]. To some degree, this problem can be investigated by doping of synthetic nuclear waste glasses with short-lived actinides such as ^{238}Pu (half-life of 87.7 years) which leads to accelerated alpha-recoil damage during self-radiation and then assessing the stability of these glasses [238].

The natural system provided by DSDP 418A basaltic glass pillow margins described here represents an exceptional analog for this type of long-term investigation of nuclear waste glass stability, because the glass is ~120.6 million years old (for age constraints see Figures 5(c), 5(d) and Section 2.2), contains abundant alpha-recoil tracks (148,000,000 alpha-recoil tracks/cm^2) and fission tracks (1,310 fission tracks/cm^2), contains regions of fresh unaltered glass—as well as glass that has been affected by preferential corrosion of radiation damage (e.g., Figures 7 and 9–12), and has been exposed to seawater—possibly in a continual fashion since the Early Cretaceous. The antiquity of these basaltic glass pillow margins also compensates to some degree for the comparatively low concentrations of U and Th in the glass (e.g., 0.032–0.042 ppm U and 0.108–0.132 ppm Th: Table 1) when compared with the ~10–15 wt.% high level radioactive waste typically present in borosilicate nuclear waste glasses [227], and this is revealed by the observation that (in addition to the pattern of fracturing in the glass) the distributions of fission tracks and *especially* alpha-recoil tracks were primary factors in controlling the textural development of

the palagonite alteration/dissolution (i.e., corrosion) front (Figures 10 and 15). Fission tracks and alpha-recoil tracks (simulated by ion implantation) are known to drastically increase the etch rates of borosilicate nuclear waste glasses in water (e.g., Figure 3(d)) [137, 138]. Therefore, the discovery of naturally formed fission track etch-tunnels (Figure 13), alpha-recoil track etch-tunnels (Figure 12), and granular palagonite ART alteration (Figure 10) caused by the advancement of encroaching seawater into basaltic glass at DSDP 418A is particularly relevant to understanding the long-term behaviour of nuclear waste glass, especially given the relatively low (about a million times less) alpha-recoil dose of these natural submarine glasses (ca. 10^{18} alpha decay/m^3) when compared to that observed in accelerated long-term studies of synthetic nuclear waste glasses doped with short-lived actinides (e.g., ca. 10^{24} alpha decay/m^3 [238]).

Consequently, based on our observations of pronounced natural corrosion (i.e., etch-tunnelling and palagonitization) of radiation damaged sites in fresh basaltic glass at DSDP 418A, we highlight that deep burial of high level nuclear waste glasses in geological repositories should probably be avoided altogether to prevent dangerous radionuclides from leaking out into Earth's biosphere during the aging and associated physical breakdown of such nuclear waste glasses—should a repository be breached by subsurface groundwaters in the future.

6.5. Implications for the Astrobiological Exploration of Mars. Recent studies have suggested that the complex alteration microtextures commonly found within volcanic glass on Earth (i.e., granular and tubular bioalteration textures) should be sought as possible target biosignatures to look for in Martian glasses during future astrobiology missions to Mars, and possibly even other solar system bodies such as Europa [12]. Although it is true that "tubular" etch-tunnels and "granular" palagonite microtextures in submarine glasses do coincide with the sizes of typical microbes (which is cited as the main reason why they are thought to be biogenic in origin: e.g., [26]), here we highlight that these corrosion microtextures in basaltic glass are also, incidentally, the same size as fission tracks and alpha-recoil tracks (e.g., Figure 11(d)) and/or exhibit similar areal density and distribution (e.g.; Figures 10(e), 10(f), 10(h), 10(i), 15(c), and 15(d)). Therefore, the complex "abiotic" corrosion microtextures described from DSDP Hole 418A basaltic glass pillow margins in this study (i.e., alpha-recoil track etch-tunnels: Figures 7, 9, and 12; fission track etch-tunnels: Figure 13; and granular palagonite ART alteration: Figure 10) are important terrestrial analogs for Martian samples, because, if present, these abiotic corrosion microtextures might be readily mistaken for signs of biological activity (i.e., microbial borings/bioalteration) on Mars (as highlighted by French and Blake [111], French and Blake [112], and French [113]). Consequently, if such complex corrosion microtextures are found in samples of Martian glasses obtained during future sample return, robotic rover, or manned missions to Mars, by comparison with the present study, they would *not* constitute signs of past microbial life on Mars (i.e., microbial "trace fossils").

The possibility that alpha-recoil track etch-tunnels, fission track etch-tunnels, and granular palagonite ART alteration might occur in volcanic/impact glasses on the surface of Mars is considered to be very likely. This owes in part to the abundant remote sensing evidence for Hawaiian-style shield volcanism, flood volcanism, and giant dyke swarms in the Tharsis and Elysium regions [239, 240] and the evidence for widely distributed ground ice and past action of liquid water at the surface including development of valley systems, outflow channels, and possible oceans [158, 159]. Spectral measurements of Mars made by orbiting spacecraft and Earth based telescopes have long revealed a surface composition consistent with weathered mafic igneous rocks, and which are similar, for instance, to the corresponding spectra for Hawaiian palagonitic soils from Mauna Kea [151, 156, 241]. Impact cratering, which took place around the planet throughout much of the geological history of Mars [242], also provides a viable mechanism of forming abundant, widely distributed impact glasses through the formation and scattering of impact spherules. It has also been suggested that the interaction of basaltic magma with ground ice or glaciers could have resulted in the formation of abundant basaltic glass tuff deposits on Mars, ultimately supplying a large quantity of palagonite to the Martian soil through subsequent alteration and weathering [151, 243]. The surface of Mars has also been subdivided into two contrasting petrological domains along the planetary dichotomy on the basis of spectral data, including a basaltic composition dominated by plagioclase and clinopyroxene and an andesitic composition dominated by plagioclase and volcanic glass [153]. Remote sensing data also indicates that, in middle Mars history, the North Polar and Utopia basins in the northern hemisphere may have contained an ocean potentially as deep as ~ 1680 m [159]. Therefore, it is also possible that basaltic/impact glass may have existed within deep water on Mars and consequently been subjected to the effects of high hydrostatic pressure during preferential etch-tunnelling along radiation damaged sites, akin to the conditions of formation of abiotic corrosion microtextures in basaltic glass from DSDP 418A (Figure 16).

Consequently, in future astrobiology missions to Mars, evaluating the possible biogenicity of nano- to microscopic tunnels or nanoscopic filaments identified in Martian glasses should be carried out first by (a) assessing the possibility that the tunnels are alpha-recoil track etch-tunnels or fission track etch-tunnels; (b) whether or not pressure solution (or some other kind of abiotic etching process) may have played a role in forming them; and (c) whether or not the nanoscopic filaments are authigenic imogolite tubes, as we have suggested here for the nanofilaments observed within several etch-tunnels in DSDP 418A basaltic glass (Figures 12(g), 12(h), 17(c), and 17(f)).

It is also important to highlight at this point that a completely different variety of abiotically produced branching nanoscopic channel has also been described in a companion study on basaltic glass pillow margins from DSDP 418A (Figure 21(a) [107]). In that study, dendritic patterns of branching nanoscopic grooves are described from the interior surface of some vesicle walls of sample 418A-75-3-[120–123] (i.e.,

the same pillow margin sample as the present study), which appear to have formed by the nonbiological process of viscous fingering. These grooves are ~50 nm deep, 50–75 nm in width, and individual branches end as slightly larger terminal bulbs that measure 150–300 nm across, which makes them similar in size to alpha-recoil track etch-tunnels from this study (see a scale comparison in Figures 21(a) and 21(b)). In particular, these dendritic nanoscopic grooves represent frozen viscous fingers of magmatic fluid that were injected into the hot walls of some vesicles upon cooling through the glass transition during pillow eruption [107], and they represent another form of abiotic dendritic microchannel that might be found in Martian glasses, which could also potentially be mistaken as another form of microbial trace fossil on Mars. Therefore, during the astrobiological exploration of Mars, any branching nanoscopic channels found on vesicle walls in Martian glasses should also be compared with those nonbiological ones documented in our companion study on DSDP 418A basaltic glass (Figure 21(a) [107]).

A summary of all of these different varieties of complex "abiotic" microtextures found in DSDP 418A basaltic glass pillow margins—that look conspicuously biogenic but which are not—is shown in Figure 21, including dendritic nanogrooves on vesicle walls (Figure 21(a)), alpha-recoil track etch-tunnels (Figures 21(b) and 21(g)), fission track etch-tunnels (Figure 21(c)), granular palagonite ART alteration (Figure 21(d)), alpha-recoil track etch-tunnels affected by prolonged overetching (Figures 21(e) and 21(i)), authigenic imogolite filaments (Figure 21(f)), and palagonite fingers (overprinted ARTETs; Figure 21(h)). Note that authigenic imogolite filaments (Figure 21(f)) have good potential to be mistaken for certain biofilaments of similar size and form, such as the nanofilaments found within dessicated exopolysaccharide mucus produced by bacteria (see cover photo of Barker et al. [244]), or even filamentous strands of DNA (see Figure 1 in Anselmetti et al. [245]), which coincidentally have the same diameter (20 Å) and long, flexible, filamentous nature as imogolite [111, 139, 246]. Consequently, we highlight that all of these various "abiotic" microtextures found in submarine glasses at DSDP 418A (Figure 21) might also be found in volcanic/impact glasses on Mars, and so, in future astrobiology missions to Mars, special care should be taken to evaluate possible nonbiological origins for such features if analogous microtextures are eventually found on that planet.

Conflict of Interests

The authors declare that there is no conflict of interests regarding the publication of this paper.

Acknowledgments

Karlis Muehlenbachs (Department of Earth and Atmospheric Sciences, University of Alberta) is thanked for his comments and advice during collection of scientific data and for providing financial support for this project through the Natural Sciences and Engineering Research Council of Canada. The authors thank George Braybrook (Department of Earth and Atmospheric Sciences, University of Alberta) and Kathy Kato (NASA Ames Research Center) for assistance with SEM studies and Antonio Simonetti (University of Notre Dame) for the help with ICP-MS analyses carried out at the Radiogenic Isotope Facility (Department of Earth and Atmospheric Sciences, University of Alberta). Jason E. French would like to thank Thomas Chacko and Jeremy P. Richards (Department of Earth and Atmospheric Sciences, University of Alberta) for providing access to petrographic microscope and camera (photomicrographic) equipment during petrographic thin section work. In addition, Jason E. French would like to acknowledge the NASA Planetary Biology Internship Program for enabling SEM studies at the NASA Ames Research Center under the cosponsorship of David F. Blake and David J. Des Marais in July/August 1999.

References

[1] D. F. Blake, A. H. Treiman, H. E. F. Amundsen, S. J. Mojzsis, and T. Bunch, "Carbonate globules, analogous to those in ALH84001, from Spitsbergen, Norway: formation in a hydrothermal environment," in *Proceedings of the Abstracts: 30th Lunar and Planetary Science Conference*, Houston, Tex, USA, March 1999.

[2] J. P. Bradley, R. P. Harvey, H. Y. McSween Jr., E. Gibson Jr., K. Thomas-Keprta, and H. Vali, "No 'nanofossils' in martian meteorite," *Nature*, vol. 390, no. 6659, pp. 454–456, 1997.

[3] D. S. McKay, E. K. Gibson Jr., K. L. Thomas-Keprta et al., "Search for past life on Mars: possible relic biogenic activity in martian meteorite ALH84001," *Science*, vol. 273, no. 5277, pp. 924–930, 1996.

[4] D. S. McKay, E. Gibson Jr., K. Thomas-Keprta, and H. Vali, "Reply to: no 'nanofossils' in martian meteorite," *Nature*, vol. 390, pp. 455–456, 1997.

[5] K. L. Thomas-Keprta, D. S. McKay, S. J. Wentworth et al., "Bacterial mineralization patterns in basaltic aquifers: implications for possible life in martian meteorite ALH84001," *Geology*, vol. 26, no. 11, pp. 1031–1034, 1998.

[6] A. H. Treiman, H. E. F. Amundsen, D. F. Blake, and T. Bunch, "Hydrothermal origin for carbonate globules in Martian meteorite ALH84001: a terrestrial analogue from Spitsbergen (Norway)," *Earth and Planetary Science Letters*, vol. 204, no. 3-4, pp. 323–332, 2002.

[7] L. J. Rothschild, "Earth analogs for Martian life. Microbes in evaporites, a new model system for life on Mars," *Icarus*, vol. 88, no. 1, pp. 246–260, 1990.

[8] M. R. Walter and D. J. Des Marais, "Preservation of biological information in thermal spring deposits: developing a strategy for the search for fossil life on Mars," *Icarus*, vol. 101, no. 1, pp. 129–143, 1993.

[9] P. T. Doran, R. A. Wharton Jr., D. J. Des Marais, and C. P. McKay, "Antarctic paleolake sediments and the search for extinct life on Mars," *Journal of Geophysical Research E: Planets*, vol. 103, no. 12, pp. 28481–28493, 1998.

[10] P. J. Boston, M. V. Ivanov, and C. P. McKay, "On the possibility of chemosynthetic ecosystems in subsurface habitats on Mars," *Icarus*, vol. 95, no. 2, pp. 300–308, 1992.

[11] H. Furnes, N. R. Banerjee, H. Staudigel et al., "Comparing petrographic signatures of bioalteration in recent to Mesoarchean

pillow lavas: tracing subsurface life in oceanic igneous rocks," *Precambrian Research*, vol. 158, no. 3-4, pp. 156–176, 2007.

[12] M. R. M. Izawa, N. R. Banerjee, R. L. Flemming, N. J. Bridge, and C. Schultz, "Basaltic glass as a habitat for microbial life: implications for astrobiology and planetary exploration," *Planetary and Space Science*, vol. 58, no. 4, pp. 583–591, 2010.

[13] J. Farmer, D. Des Marais, R. Greeley, R. Landheim, and H. Klein, "Site selection for Mars exobiology," *Advances in Space Research*, vol. 15, no. 3, pp. 157–162, 1995.

[14] L. J. Rothschild and D. Des Marais, "Stable carbon isotope fractionation in the search for life on early Mars," *Advances in Space Research*, vol. 9, no. 6, pp. 159–165, 1989.

[15] D. E. Schwartz and R. L. Mancinelli, "Bio-markers and the search for extinct life on Mars," *Advances in Space Research*, vol. 9, no. 6, pp. 155–158, 1989.

[16] D. E. Schwartz, R. L. Mancinelli, and E. S. Kaneshiro, "The use of mineral crystals as bio-markers in the search for life on Mars," *Advances in Space Research*, vol. 12, no. 4, pp. 117–119, 1992.

[17] K. L. Thomas-Keprta, D. A. Bazylinski, J. L. Kirschvink et al., "Elongated prismatic magnetite crystals in ALH84001 carbonate globules: potential Martian magnetofossils," *Geochimica et Cosmochimica Acta*, vol. 64, no. 23, pp. 4049–4081, 2000.

[18] J. L. Bada and G. D. McDonald, "Amino acid racemization on Mars: implications for the preservation of biomolecules from an extinct Martian Biota," *Icarus*, vol. 114, no. 1, pp. 139–143, 1995.

[19] C. C. Allen, F. G. Albert, H. S. Chafetz et al., "Microscopic physical biomarkers in carbonate hot springs: implications in the search for life on Mars," *Icarus*, vol. 147, no. 1, pp. 49–67, 2000.

[20] B. L. Kirkland, F. L. Lynch, M. A. Rahnis, R. L. Folk, I. J. Molineux, and R. J. C. McLean, "Alternative origins for nannobacteria-like objects in calcite," *Geology*, vol. 27, no. 4, pp. 347–350, 1999.

[21] J. W. Schopf, "Microfossils of the early Archean apex chert: new evidence of the antiquity of life," *Science*, vol. 260, no. 5108, pp. 640–646, 1993.

[22] M. D. Brasier, O. R. Green, A. P. Jephcoat et al., "Questioning the evidence for Earth's oldest fossils," *Nature*, vol. 416, no. 6876, pp. 76–81, 2002.

[23] I. H. Thorseth, H. Furnes, and M. Heldal, "The importance of microbiological activity in the alteration of natural basaltic glass," *Geochimica et Cosmochimica Acta*, vol. 56, no. 2, pp. 845–850, 1992.

[24] M. R. Fisk, S. J. Giovannoni, and I. H. Thorseth, "Alteration of oceanic volcanic glass: textural evidence of microbial activity," *Science*, vol. 281, no. 5379, pp. 978–980, 1998.

[25] N. R. Banerjee, A. Simonetti, H. Furnes et al., "Direct dating of Archean microbial ichnofossils," *Geology*, vol. 35, no. 6, pp. 487–490, 2007.

[26] H. Furnes, N. McLoughlin, K. Muehlenbachs et al., "Oceanic pillow lavas and hyaloclastites as habitats for microbial life through time—a review," in *Links Between Geological Processes, Microbial Activities & Evolution of Life*, Y. Dilek, H. Furnes, and K. Muehlenbachs, Eds., vol. 4 of *Modern Approaches in Solid Earth Sciences*, pp. 1–68, Springer, Dordrecht, The Netherlands, 2008.

[27] H. Staudigel, H. Furnes, N. McLoughlin, N. R. Banerjee, L. B. Connell, and A. Templeton, "3.5 billion years of glass bioalteration: volcanic rocks as a basis for microbial life?" *Earth-Science Reviews*, vol. 89, no. 3-4, pp. 156–176, 2008.

[28] N. McLoughlin, H. Furnes, N. R. Banerjee, K. Muehlenbachs, and H. Staudigel, "Ichnotaxonomy of microbial trace fossils in volcanic glass," *Journal of the Geological Society*, vol. 166, no. 1, pp. 159–169, 2009.

[29] K. Muehlenbachs, H. Furnes, and M. de Wit, "Thermophile inhabitants of the Archean seafloor basalts," in *Proceedings of the Goldschmidt Conference Abstracts*, p. A911, Davos, Switzerland, June 2009.

[30] H. M. Sapers, G. R. Osinski, N. R. Banerjee, and L. J. Preston, "Enigmatic tubular features in impact glass," *Geology*, vol. 42, no. 6, pp. 471–474, 2014.

[31] N. McLoughlin, H. Furnes, N. Banerjee et al., "Microbioerosion in volcanic glass: extending the ichnofossil record to Archean basaltic crust," in *Current Developments in Bioerosion*, M. Wisshak and L. Tapanila, Eds., Erlangen Earth Conference Series, pp. 372–396, Springer, Berlin, Germany, 2008.

[32] C. Heberling, R. P. Lowell, L. Liu, and M. R. Fisk, "Extent of the microbial biosphere in the oceanic crust," *G-Cubed*, vol. 11, no. 8, pp. 1–15, 2010.

[33] H. Furnes and H. Staudigel, "Biological mediation in ocean crust alteration: how deep is the deep biosphere?" *Earth and Planetary Science Letters*, vol. 166, no. 3-4, pp. 97–103, 1999.

[34] H. Staudigel, B. Tebo, A. Yayanos et al., "The oceanic crust as a bioreactor," in *The Subseafloor Biosphere at Mid-Ocean Ridges*, W. S. Wilcock, E. F. DeLong, D. S. Kelley, J. A. Baross, and S. Craig Cary, Eds., vol. 144 of *AGU Geophysical Monograph Series*, pp. 325–341, AGU, 2004.

[35] H. Furnes, N. R. Banerjee, K. Muehlenbachs, H. Staudigel, and M. de Wit, "Early life recorded in archean pillow lavas," *Science*, vol. 304, no. 5670, pp. 578–581, 2004.

[36] R. A. Kerr, "New biomarker proposed for earliest life on Earth," *Science*, vol. 304, no. 5670, article 503, 2004.

[37] N. R. Banerjee, H. Furnes, K. Muehlenbachs, H. Staudigel, and M. De Wit, "Preservation of ~3.4–3.5 Ga microbial biomarkers in pillow lavas and hyaloclastites from the Barberton Greenstone Belt, South Africa," *Earth and Planetary Science Letters*, vol. 241, no. 3-4, pp. 707–722, 2006.

[38] D. Fliegel, J. Kosler, N. McLoughlin et al., "In-situ dating of the Earth's oldest trace fossil at 3.34 Ga," *Earth and Planetary Science Letters*, vol. 299, no. 3-4, pp. 290–298, 2010.

[39] W. G. Melson and G. Thompson, "Glassy abyssal basalts, Atlantic Sea floor near St. Paul's rocks: petrography and composition of secondary clay minerals," *Geological Society of America Bulletin*, vol. 84, no. 2, pp. 703–716, 1973.

[40] M. Morgenstein and T. J. Riley, "Hydration-rind dating of basaltic glass: a new method for archaeological chronologies," *Asian Perspectives*, vol. 17, no. 2, pp. 145–162, 1974.

[41] A. R. Geptner, "Palagonite and the process of palagonitization," *Litologiya i Poleznye Iskopaemye*, vol. 5, pp. 113–130, 1977.

[42] A. G. Kossowskaya, V. V. Petrova, and V. D. Shutov, "Mineral associations of palagonitization of oceanic basalts and aspects of extraction of mineral components," *Litologiya i Poleznye Iskopaemye*, vol. 4, pp. 10–31, 1982.

[43] H. Staudigel and S. R. Hart, "Alteration of basaltic glass: mechanisms and significance for the oceanic crust-seawater budget," *Geochimica et Cosmochimica Acta*, vol. 47, no. 3, pp. 337–350, 1983.

[44] Z. Zhou and W. S. Fyfe, "Palagonitization of basaltic glass from DSDP Site 335, Leg 37: textures, chemical composition, and mechanism of formation," *American Mineralogist*, vol. 74, no. 9-10, pp. 1045–1053, 1989.

[45] K. A. Ross and R. V. Fisher, "Biogenic grooving on glass shards," *Geology*, vol. 14, no. 7, pp. 571–573, 1986.

[46] K. Ross and R. V. Fisher, "Comment and reply on 'biogenic grooving on glass shards': reply," *Geology*, vol. 15, no. 5, p. 471, 1987.

[47] H. Staudigel, R. A. Chastain, A. Yayanos, and W. Bourcier, "Biologically mediated dissolution of glass," *Chemical Geology*, vol. 126, no. 2, pp. 147–154, 1995.

[48] I. H. Thorseth, H. Furnes, and O. Tumyr, "Textural and chemical effects of bacterial activity on basaltic glass: an experimental approach," *Chemical Geology*, vol. 119, no. 1–4, pp. 139–160, 1995.

[49] I. H. Thorseth, T. Torsvik, H. Furnes, and K. Muehlenbachs, "Microbes play an important role in the alteration of oceanic crust," *Chemical Geology*, vol. 126, no. 2, pp. 137–146, 1995.

[50] H. Furnes, I. H. Thorseth, O. Tumyr, T. Torsvik, and M. R. Fisk, "13. Microbial activity in the alteration of glass from pillow lavas from Hole 896A," in *Proceedings of the Ocean Drilling Program, Scientific Results*, J. C. Alt, H. Kinoshita, L. B. Stokking, and P. J. Michael, Eds., vol. 148, pp. 191–206, US Government Printing Office, 1996.

[51] S. J. Giovannoni, M. R. Fisk, T. D. Mullins, and H. Furnes, "14. Genetic evidence for endolithic microbial life colonizing basaltic glass/seawater interfaces," in *Proceedings of the Ocean Drilling Program, Scientific Results*, J. C. Alt, H. Kinoshita, L. B. Stokking, and P. J. Michael, Eds., vol. 148, pp. 207–214, Texas A&M University, College Station, Tex, USA, 1996.

[52] H. Staudigel, A. Yayanos, R. Chastain et al., "Biologically mediated dissolution of volcanic glass in seawater," *Earth and Planetary Science Letters*, vol. 164, no. 1-2, pp. 233–244, 1998.

[53] T. Torsvik, H. Furnes, K. Muehlenbachs, I. H. Thorseth, and O. Tumyr, "Evidence for microbial activity at the glass-alteration interface in oceanic basalts," *Earth and Planetary Science Letters*, vol. 162, no. 1–4, pp. 165–176, 1998.

[54] H. Furnes, K. Muehlenbachs, O. Tumyr, T. Torsvik, and I. H. Thorseth, "Depth of active bio-alteration in the ocean crust: Costa Rica Rift (Hole 504B)," *Terra Nova*, vol. 11, no. 5, pp. 228–233, 1999.

[55] J. C. Alt and P. Mata, "On the role of microbes in the alteration of submarine basaltic glass: a TEM study," *Earth and Planetary Science Letters*, vol. 181, no. 3, pp. 301–313, 2000.

[56] M. R. Fisk, I. H. Thorseth, U. Erbach, and S. J. Giovannoni, "14. Investigation of microorganisms and DNA from subsurface thermal water and rock from the east flank of Juan de Fuca Ridge," in *Proceedings of the Ocean Drilling Program, Scientific Results*, A. Fisher, E. E. Davis, and C. Escutia, Eds., vol. 168, pp. 167–174, Texas A&M University, College Station, Tex, USA, 2000.

[57] H. Furnes, K. Muehlenbachs, T. Torsvik, I. H. Thorseth, and O. Tumyr, "Microbial fractionation of carbon isotopes in altered basaltic glass from the Atlantic Ocean, Lau Basin and Costa Rica Rift," *Chemical Geology*, vol. 173, no. 4, pp. 313–330, 2001.

[58] H. Furnes, K. Muehlenbachs, O. Tumyr, T. Torsvik, and C. Xenophontos, "Biogenic alteration of volcanic glass from the Troodos ophiolite, Cyprus," *Journal of the Geological Society*, vol. 158, no. 1, pp. 75–84, 2001.

[59] H. Furnes, H. Staudigel, I. H. Thorseth, T. Torsvik, K. Muehlenbachs, and O. Tumyr, "Bioalteration of basaltic glass in the oceanic crust," *G-Cubed*, vol. 2, pp. 1–30, 2001.

[60] Shipboard Scientific Party, "Site 1184," in *Proceedings of the Ocean Drilling Program, Initial Reports*, J. J. Mahoney, J. G. Fitton, P. J. Wallace et al., Eds., vol. 192, pp. 1–131, Ocean Drilling Program, College Station, Tex, USA, 2001.

[61] H. Furnes, K. Muehlenbachs, T. Torsvik, O. Tumyr, and L. Shi, "Bio-signatures in metabasaltic glass of a Caledonian ophiolite, West Norway," *Geological Magazine*, vol. 139, no. 6, pp. 601–608, 2002.

[62] H. Furnes, I. H. Thorseth, T. Torsvik, K. Muehlenbachs, H. Staudigel, and O. Tumyr, "Identifying bio-interaction with basaltic glass in oceanic crust and implications for estimating the depth of the oceanic biosphere: a review," in *Volcano-Ice Interaction on Earth and Mars*, J. L. Smellie and M. G. Chapman, Eds., pp. 407–421, The Geological Society, London, UK, 2002.

[63] W. Bach and K. J. Edwards, "Iron and sulfide oxidation within the basaltic ocean crust: implications for chemolithoautotrophic microbial biomass production," *Geochimica et Cosmochimica Acta*, vol. 67, no. 20, pp. 3871–3887, 2003.

[64] N. R. Banerjee and K. Muehlenbachs, "Tuff life: bioalteration in volcaniclastic rocks from the Ontong Java Plateau," *G-Cubed*, vol. 4, no. 4, pp. 1–22, 2003.

[65] M. R. Fisk, M. C. Storrie-Lombardi, S. Douglas, R. Popa, G. McDonald, and C. Di Meo-Savoie, "Evidence of biological activity in Hawaiian subsurface basalts," *G-Cubed*, vol. 4, no. 12, pp. 1–24, 2003.

[66] H. Furnes and K. Muehlenbachs, "Bioalteration recorded in ophiolitic pillow lavas," in *Ophiolites in Earth's History*, Y. Dilek and P. T. Robinson, Eds., vol. 218 of *Geological Society of London Special Publications no. 218*, pp. 415–426, Geological Society of London, 2003.

[67] I. H. Thorseth, R. B. Pedersen, and D. M. Christie, "Microbial alteration of 0–30-Ma seafloor and sub-seafloor basaltic glasses from the Australian Antarctic Discordance," *Earth and Planetary Science Letters*, vol. 215, no. 1-2, pp. 237–247, 2003.

[68] A. W. Walton and P. Schiffman, "Alteration of hyaloclastites in the HSDP 2 phase 1 drill core 1. Description and paragenesis," *Geochemistry, Geophysics, Geosystems*, vol. 4, no. 5, pp. 1–31, 2003.

[69] H. Staudigel and H. Furnes, "Microbial mediation of oceanic crust alteration," in *Hydrogeology of the Oceanic Lithosphere*, E. Davis and H. Elderfield, Eds., pp. 606–626, Cambridge University Press, 2004.

[70] M. C. Storrie-Lombardi and M. R. Fisk, "Elemental abundance distributions in suboceanic basalt glass: evidence of biogenic alteration," *Geochemistry, Geophysics, Geosystems*, vol. 5, no. 10, Article ID Q10005, 15 pages, 2004.

[71] H. Furnes, N. R. Banerjee, K. Muehlenbachs, and A. Kontinen, "Preservation of biosignatures in metaglassy volcanic rocks from the Jormua ophiolite complex, Finland," *Precambrian Research*, vol. 136, no. 2, pp. 125–137, 2005.

[72] J. Einen, C. Kruber, L. Øvreås, I. H. Thorseth, and T. Torsvik, "Microbial colonization and alteration of basaltic glass," *Biogeosciences Discussions*, vol. 3, no. 2, pp. 273–307, 2006.

[73] M. R. Fisk, R. Popa, O. U. Mason, M. C. Storrie-Lombardie, and E. P. Vicenzi, "Iron-magnesium silicate bioweathering on Earth (and Mars?)," *Astrobiology*, vol. 6, no. 1, pp. 48–68, 2006.

[74] H. Furnes, Y. Dilek, K. Muehlenbachs, and N. R. Banerjee, "Tectonic control of bioalteration in modern and ancient oceanic crust as evidenced by carbon isotopes," *Island Arc*, vol. 15, no. 1, pp. 143–155, 2006.

[75] H. Staudigel, H. Furnes, N. R. Banerjee, Y. Dilek, and K. Muehlenbachs, "Microbes and volcanoes: a tale from the oceans, ophiolites, and greenstone belts," *GSA Today*, vol. 16, no. 10, pp. 4–10, 2006.

[76] K. Benzerara, N. Menguy, N. R. Banerjee, T. Tyliszczak, G. E. Brown Jr., and F. Guyot, "Alteration of submarine basaltic glass

from the Ontong Java Plateau: a STXM and TEM study," *Earth and Planetary Science Letters*, vol. 260, no. 1-2, pp. 187–200, 2007.

[77] H. Furnes, N. R. Banerjee, H. Staudigel, and K. Muehlenbachs, "Pillow lavas as a habitat for microbial life," *Geology Today*, vol. 23, no. 4, pp. 143–146, 2007.

[78] N. McLoughlin, M. D. Brasier, D. Wacey, O. R. Green, and R. S. Perry, "On biogenicity criteria for endolithic microborings on early Earth and beyond," *Astrobiology*, vol. 7, no. 1, pp. 10–26, 2007.

[79] C. S. Cockell and A. Herrera, "Why are some microorganisms boring?" *Trends in Microbiology*, vol. 16, no. 3, pp. 101–106, 2008.

[80] A. Herrera, C. S. Cockell, S. Self et al., "Bacterial colonization and weathering of terrestrial obsidian in Iceland," *Geomicrobiology Journal*, vol. 25, no. 1, pp. 25–37, 2008.

[81] M. Ivarsson, J. Lausmaa, S. Lindblom, C. Broman, and N. G. Holm, "Fossilized microorganisms from the emperor seamounts: implications for the search for a subsurface fossil record on earth and Mars," *Astrobiology*, vol. 8, no. 6, pp. 1139–1157, 2008.

[82] C. Kruber, I. H. Thorseth, and R. B. Pedersen, "Seafloor alteration of basaltic glass: textures, geochemistry, and endolithic microorganisms," *Geochemistry, Geophysics, Geosystems*, vol. 9, no. 12, 2008.

[83] A. W. Walton, "Microtubules in basalt glass from Hawaii Scientific Driling Project #2 phase 1 core and Hilina slope, Hawaii: evidence of the occurrence and behavior of endolithic microorganisms," *Geobiology*, vol. 6, no. 4, pp. 351–364, 2008.

[84] C. S. Cockell, K. Olsson-Francis, A. Herrera, and A. Meunier, "Alteration textures in terrestrial volcanic glass and the associated bacterial community," *Geobiology*, vol. 7, no. 1, pp. 50–65, 2009.

[85] C. S. Cockell, K. Olsson, F. Knowles et al., "Bacteria in weathered basaltic glass, Iceland," *Geomicrobiology Journal*, vol. 26, no. 7, pp. 491–507, 2009.

[86] C. R. Cousins, J. L. Smellie, A. P. Jones, and I. A. Crawford, "A comparative study of endolithic microborings in basaltic lavas from a transitional subglacial—marine environment," *International Journal of Astrobiology*, vol. 8, no. 1, pp. 37–49, 2009.

[87] E. G. Grosch, N. McLoughlin, M. de Wit, and H. Furnes, "Drilling for the archean roots of life and tectonic earth in the barberton mountains," *Scientific Drilling*, no. 8, pp. 24–28, 2009.

[88] G. F. Slater, "International year of planet earth 6. Biosignatures, interpreting evidence of the origins and diversity of life," *Geoscience Canada*, vol. 36, no. 4, pp. 170–178, 2009.

[89] N. R. Banerjee, M. R. M. Izawa, H. M. Sapers, and M. J. Whitehouse, "Geochemical biosignatures preserved in microbially altered basaltic glass," *Surface and Interface Analysis*, vol. 43, no. 1-2, pp. 452–457, 2011.

[90] N. J. Bridge, N. R. Banerjee, W. Mueller, K. Muehlenbachs, and T. Chacko, "A volcanic habitat for early life preserved in the Abitibi Greenstone belt, Canada," *Precambrian Research*, vol. 179, no. 1–4, pp. 88–98, 2010.

[91] D. Fliegel, R. Wirth, A. Simonetti et al., "Septate-tubular textures in 2.0-Ga pillow lavas from the Pechenga Greenstone Belt: a nano-spectroscopic approach to investigate their biogenicity," *Geobiology*, vol. 8, no. 5, pp. 372–390, 2010.

[92] M. R. M. Izawa, N. R. Banerjee, R. L. Flemming, and N. J. Bridge, "Preservation of microbial ichnofossils in basaltic glass by titanite mineralization," *Canadian Mineralogist*, vol. 48, no. 5, pp. 1255–1265, 2010.

[93] N. Mcloughlin, H. Staudigel, H. Furnes, B. Eickmann, and M. Ivarsson, "Mechanisms of microtunneling in rock substrates: distinguishing endolithic biosignatures from abiotic microtunnels," *Geobiology*, vol. 8, no. 4, pp. 245–255, 2010.

[94] N. McLoughlin, D. J. Fliegel, H. Furnes et al., "Assessing the biogenicity and syngenicity of candidate bioalteration textures in pillow lavas of the ~2.52 Ga Wutai greenstone terrane of China," *Chinese Science Bulletin*, vol. 55, no. 2, pp. 188–199, 2010.

[95] H. Staudigel and D. A. Clague, "The geological history of deep-sea volcanoes: biosphere, hydrosphere, and lithosphere interactions," *Oceanography*, vol. 23, no. 1, pp. 58–71, 2010.

[96] D. Fliegel, R. Wirth, A. Simonetti, A. Schreiber, H. Furnes, and K. Muehlenbachs, "Tubular textures in pillow lavas from a Caledonian west Norwegian ophiolite: a combined TEM, LA–ICP–MS, and STXM study," *Geochemistry, Geophysics, Geosystems*, vol. 12, no. 2, Article ID Q02010, 21 pages, 2011.

[97] N. McLoughlin, "Archean traces of life," in *Encyclopedia of Astrobiology*, M. Gargaud, R. Amils, J. Cernicharo Quintanilla et al., Eds., pp. 74–84, Springer, Berlin, Germany, 2011.

[98] N. McLoughlin, D. Wacey, C. Kruber, M. R. Kilburn, I. H. Thorseth, and R. B. Pedersen, "A combined TEM and NanoSIMS study of endolithic microfossils in altered seafloor basalt," *Chemical Geology*, vol. 289, no. 1-2, pp. 154–162, 2011.

[99] L. J. Preston, M. R. M. Izawa, and N. R. Banerjee, "Infrared spectroscopic characterization of organic matter associated with microbial bioalteration textures in basaltic glass," *Astrobiology*, vol. 11, no. 7, pp. 585–599, 2011.

[100] D. Fliegel, E. Knowles, R. Wirth et al., "Characterization of alteration textures in Cretaceous oceanic crust (pillow lava) from the N-Atlantic (DSDP Hole 418A) by spatially-resolved spectroscopy," *Geochimica et Cosmochimica Acta*, vol. 96, pp. 80–93, 2012.

[101] E. Knowles, R. Wirth, and A. Templeton, "A comparative analysis of potential biosignatures in basalt glass by FIB-TEM," *Chemical Geology*, vol. 330-331, pp. 165–175, 2012.

[102] N. McLoughlin, E. G. Grosch, M. R. Kilburn, and D. Wacey, "Sulfur isotope evidence for a Paleoarchean subseafloor biosphere, Barberton, South Africa," *Geology*, vol. 40, no. 11, pp. 1031–1034, 2012.

[103] M. Fisk and N. McLoughlin, "Atlas of alteration textures in volcanic glass from the ocean basins," *Geosphere*, vol. 9, no. 2, pp. 317–341, 2013.

[104] N. McLoughlin, H. Furnes, H. Staudigel, and E. Hanski, "7.8.4. Seeking textural evidence of a Palaeoproterozoic sub-seafloor biosphere in pillow lavas of the pechenga greenstone belt," in *Reading the Archive of Earth Oxygenation, Vol. 1: The Palaeoproterozoic of Fennoscandia as a Context for the Fennoscandian Arctic Russia—Drilling Early Earth Project*, V. A. Melezhik, A. R. Prave, A. E. Fallick et al., Eds., pp. 1371–1394, Springer, 2013.

[105] H. Staudigel, H. Furnes, and M. Smits, "Deep biosphere record of in situ oceanic lithosphere and ophiolites," *Elements*, vol. 10, no. 2, pp. 121–126, 2014.

[106] B. P. Glass, "Comment and reply on 'Biogenic grooving on glass shards': comment," *Geology*, vol. 15, no. 5, pp. 470–471, 1987.

[107] J. E. French and K. Muehlenbachs, "The origin of nanoscopic grooving on vesicle walls in submarine basaltic glass: implications for nanotechnology," *Journal of Nanomaterials*, vol. 2009, Article ID 309208, 14 pages, 2009.

[108] K. Lepot, K. Benzerara, and P. Philippot, "Biogenic versus metamorphic origins of diverse microtubes in 2.7 Gyr old volcanic ashes: Multi-scale investigations," *Earth and Planetary Science Letters*, vol. 312, no. 1-2, pp. 37–47, 2011.

[109] E. G. Grosch and N. McLoughlin, "Reassessing the biogenicity of Earth's oldest trace fossil with implications for biosignatures in the search for early life," *Proceedings of the National Academy of Sciences of the United States of America*, vol. 111, no. 23, pp. 8380–8385, 2014.

[110] A. Drief and P. Schiffman, "Very low-temperature alteration of sideromelane in hyaloclastites and hyalotuffs from Kilauea and Mauna Kea volcanoes: implications for the mechanism of palagonite formation," *Clays and Clay Minerals*, vol. 52, no. 5, pp. 622–634, 2004.

[111] J. E. French and D. F. Blake, "Abiotic corrosion microtextures in volcanic glass: reevaluation of a putative biosignature for Earth and Mars," in *2012 Conference on Life Detection in Extraterrestrial Samples, San Diego, California. Program and Abstract Volume*, LPI Contribution no. 1650, pp. 34–35, LPI, 2012.

[112] J. E. French and D. F. Blake, "Role of self-incurred radiation damage in development of tubular and granular microtextures in submarine volcanic glass: implications for Mars exploration," in *Proceedings of the Geological Association of Canada/Mineralogical Association of Canada Annual Meeting*, vol. 35 of *Abstracts*, p. 45, St. John's, Canada, May 2012.

[113] J. E. French, "Questioning the textural evidence for microbial bioalteration of volcanic glass and its robustness as a terrestrial analog biosignature for Mars astrobiology," in *Proceedings of the Geological Association of Canada/Mineralogical Association of Canada Annual Meeting*, vol. 36, p. Abstracts, Winnipeg, Canada, May 2013.

[114] L. R. Pedersen, N. McLoughlin, P. E. Vullum, and I. H. Thorseth, "Abiotic and candidate biotic micro-alteration textures in subseafloor basaltic glass: a high-resolution in-situ textural and geochemical investigation," *Chemical Geology*, vol. 410, pp. 124–137, 2015.

[115] J. W. Nielson and F. G. Foster, "Unusual etch pits in quartz crystals," *American Mineralogist*, vol. 45, pp. 299–310, 1960.

[116] T. Hanyu, "Dislocation etch tunnels in quartz crystals," *Journal of the Physical Society of Japan*, vol. 19, no. 8, p. 1489, 1964.

[117] H. Carstens, "The lineage structure of quartz crystals," *Contributions to Mineralogy and Petrology*, vol. 18, no. 4, pp. 295–304, 1968.

[118] S. Takasu and S. Shimanuki, "Tunnel-like defects of flux grown magnetic garnets," *Journal of Crystal Growth*, vol. 24-25, pp. 641–645, 1974.

[119] F. Iwasaki, "Line defects and etch tunnels in synthetic quartz," *Journal of Crystal Growth*, vol. 39, no. 2, pp. 291–298, 1977.

[120] S. L. Brantley, S. R. Crane, D. A. Crerar, R. Hellmann, and R. Stallard, "Dissolution at dislocation etch pits in quartz," *Geochimica et Cosmochimica Acta*, vol. 50, no. 10, pp. 2349–2361, 1986.

[121] A. C. Lasaga and A. E. Blum, "Surface chemistry, etch pits and mineral-water reactions," *Geochimica et Cosmochimica Acta*, vol. 50, no. 10, pp. 2363–2379, 1986.

[122] T. N. Tingle, E. Roedder, and H. W. Green II, "Formation of fluid inclusions and etch tunnels in olivine at high pressure," *American Mineralogist*, vol. 77, no. 3-4, pp. 296–302, 1992.

[123] T. Lu, J. E. Shigley, J. I. Koivula, and I. M. Reinitz, "Observation of etch channels in several natural diamonds," *Diamond and Related Materials*, vol. 10, no. 1, pp. 68–75, 2001.

[124] K. Lepot, P. Philippot, K. Benzerara, and G.-Y. Wang, "Garnet-filled trails associated with carbonaceous matter mimicking microbial filaments in Archean basalt," *Geobiology*, vol. 7, no. 4, pp. 393–402, 2009.

[125] D. Storzer and M. Sélo, "Fission track age of magnetic anomaly *M*-zero and some aspects of sea-water weathering," in *Initial Reports of the Deep Sea Drilling Project*, LI, LII, LIII, Part 2, pp. 1129–1133, US Government Publishing Office, Washington, DC, USA, 1980.

[126] C. Arias, G. Bigazzi, and F. P. Bonadonna, "Size corrections and plateau age in glass shards," *Nuclear Tracks*, vol. 5, no. 1-2, pp. 129–136, 1981.

[127] M. Sélo and D. Storzer, "Uranium distribution and age pattern of some deep-sea basalts from the Entrecasteaux area, southwestern pacific: a fission-track analysis," *Nuclear Tracks*, vol. 5, no. 1-2, pp. 137–145, 1981.

[128] A. S. Sandhu and J. A. Westgate, "The correlation between reduction in fission-track diameter and areal track density in volcanic glass shards and its application in dating tephra beds," *Earth and Planetary Science Letters*, vol. 131, no. 3-4, pp. 289–299, 1995.

[129] K. Gögen and G. A. Wagner, "Alpha-recoil track dating of Quaternary volcanics," *Chemical Geology*, vol. 166, no. 1-2, pp. 127–137, 2000.

[130] W. H. Huang and R. M. Walker, "Fossil alpha-particle recoil tracks: a new method of age determination," *Science*, vol. 155, no. 3766, pp. 1103–1106, 1967.

[131] R. Jonckheere and K. Gögen, "A Monte-Carlo calculation of the size distribution of latent alpha-recoil tracks," *Nuclear Instruments and Methods in Physics Research B*, vol. 183, no. 3-4, pp. 347–357, 2001.

[132] K. Stübner and R. C. Jonckheere, "A Monte-Carlo calculation of the size distribution of latent alpha-recoil tracks in phlogopite: implications for the recoil-track dating method," *Radiation Measurements*, vol. 41, no. 1, pp. 55–64, 2006.

[133] K. Stübner, R. C. Jonckheere, and L. Ratschbacher, "Alpha-recoil track densities in mica and radiometric age determination," *Radiation Measurements*, vol. 40, no. 2–6, pp. 503–508, 2005.

[134] M. Lang, U. A. Glasmacher, B. Moine, C. Müller, R. Neumann, and G. A. Wagner, "Artificial ion tracks in volcanic dark mica simulating natural radiation damage: a scanning force microscopy study," *Nuclear Instruments and Methods in Physics Research B*, vol. 191, no. 1–4, pp. 346–351, 2002.

[135] G. Malow, W. Lutze, and R. C. Ewing, "Alteration effects and leach rates of basaltic glasses: implications for the long-term stability of nuclear waste form borosilicate glasses," *Journal of Non-Crystalline Solids*, vol. 67, no. 1–3, pp. 305–321, 1984.

[136] J.-L. Crovisier, T. Advocat, and J.-L. Dussossoy, "Nature and role of natural alteration gels formed on the surface of ancient volcanic glasses (Natural analogs of waste containment glasses)," *Journal of Nuclear Materials*, vol. 321, no. 1, pp. 91–109, 2003.

[137] J. C. Dran, M. Maurette, and J. C. Petit, "Radioactive waste storage materials: their α-recoil aging," *Science*, vol. 209, no. 4464, pp. 1518–1520, 1980.

[138] J.-C. Dran and J.-C. Petit, "Etching of fission tracks in silicate glasses by means of deionized water," *International Journal of Radiation Applications and Instrumentation. Part D: Nuclear Tracks and Radiation Measurements*, vol. 12, no. 1–6, pp. 851–854, 1986.

[139] J. E. French, "Imogolite: an ideal mineralogical substrate for the prebiotic assembly of long polynucleotides," *Mineralogical Magazine*, vol. 77, no. 5, p. 1109, 2013, F—Goldschmidt Abstracts 2013.

[140] D. Macdougall, "Fission track dating of volcanic glass shards in marine sediments," *Earth and Planetary Science Letters*, vol. 10, no. 4, pp. 403–406, 1971.

[141] R. L. Fleischer, "Alpha-recoil damage: relation to isotopic disequilibrium and leaching of radionuclides," *Geochimica et Cosmochimica Acta*, vol. 52, no. 6, pp. 1459–1466, 1988.

[142] J.-C. Petit, C. Brousse, J.-C. Dran, and G. D. Mea, "Use of fission tracks for deciphering the dissolution mechanism of silicate glasses," *Nuclear Tracks*, vol. 12, no. 1–6, pp. 847–850, 1985.

[143] A. S. Sandhu, J. A. Westgate, and S. J. Preece, "Thermal stability of fission tracks in natural and synthetic glasses: an assessment of compositional effects," *Radiation Measurements*, vol. 31, no. 1, pp. 665–668, 1999.

[144] A. S. Sandhu and K. Singh, "Etching and annealing studies of nuclear tracks in glasses," *Radiation Physics and Chemistry*, vol. 61, no. 3–6, pp. 579–581, 2001.

[145] R. L. Fleischer, "Etching of recoil tracks in solids," *Geochimica et Cosmochimica Acta*, vol. 67, no. 24, pp. 4769–4774, 2003.

[146] K. P. Jochum, A. W. Hofmann, E. Ito, H. M. Seufert, and W. M. White, "K, U and Th in mid-ocean ridge basalt glasses and heat production, K/U and K/Rb in the mantle," *Nature*, vol. 306, no. 5942, pp. 431–436, 1983.

[147] F. Aumento, "The Mid-Atlantic Ridge near 45° N.V. Fission track and ferromanganese chronology," *Canadian Journal of Earth Science*, vol. 6, pp. 1431–1440, 1969.

[148] A. J. W. Gleadow and J. F. Lovering, "The effect of weathering on fission track dating," *Earth and Planetary Science Letters*, vol. 22, no. 2, pp. 163–168, 1974.

[149] C. Weise, K. G. van den Boogaart, R. Jonckheere, and L. Ratschbacher, "Annealing kinetics of Kr-tracks in monazite: implications for fission-track modelling," *Chemical Geology*, vol. 260, no. 1-2, pp. 129–137, 2009.

[150] J.-L. Tien and C.-H. Chen, "Naturally etched tracks in apatites and the correction of fission track dating," *Radiation Measurements*, vol. 31, no. 1, pp. 669–672, 1999.

[151] C. C. Allen, J. L. Gooding, M. Jercinovic, and K. Keil, "Altered basaltic glass: a terrestrial analog to the soil of Mars," *Icarus*, vol. 45, no. 2, pp. 347–369, 1981.

[152] S. Erard and W. Calvin, "New composite spectra of Mars, 0.4–5.7 μm," *Icarus*, vol. 130, no. 2, pp. 449–460, 1997.

[153] J. L. Bandfield, V. E. Hamilton, and P. R. Christensen, "A global view of martian surface compositions from MGS-TES," *Science*, vol. 287, no. 5458, pp. 1626–1630, 2000.

[154] R. Rieder, R. Gellert, R. C. Anderson et al., "Chemistry of rocks and soils at Meridiani Planum from the Alpha Particle X-ray Spectrometer," *Science*, vol. 306, no. 5702, pp. 1746–1749, 2004.

[155] S. W. Squyres, R. E. Arvidson, J. F. Bell III et al., "Ancient impact and aqueous processes at Endeavour crater, Mars," *Science*, vol. 336, no. 6081, pp. 570–576, 2012.

[156] J. Orenberg and J. Handy, "Reflectance spectroscopy of palagonite and iron-rich montmorillonite clay mixtures: implications for the surface composition of Mars," *Icarus*, vol. 96, no. 2, pp. 219–225, 1992.

[157] B. Horgan and J. F. Bell III, "Widespread weathered glass on the surface of Mars," *Geology*, vol. 40, no. 5, pp. 391–394, 2012.

[158] S. W. Squyres, "Urey prize lecture: water on Mars," *Icarus*, vol. 79, no. 2, pp. 229–288, 1989.

[159] J. W. Head III, H. Hiesinger, M. A. Ivanov, M. A. Kreslavsky, S. Pratt, and B. J. Thomson, "Possible ancient oceans on Mars: evidence from Mars orbiter laser altimeter data," *Science*, vol. 286, no. 5447, pp. 2134–2137, 1999.

[160] Shipboard Scientific Parties, "Site 418," in *Initial Reports of the Deep Sea Drilling Project*, LI, LII, LIII, (Part 1), pp. 351–626, US Government Printing Office, Washington, DC, USA, 1980.

[161] M. F. J. Flower, W. Ohnmacht, P. T. Robinson, G. Marriner, and H.-U. Schmincke, "Lithologic and chemical stratigraphy at deep sea drilling sites 417 and 418," in *Initial Reports of the Deep Sea Drilling Project*, LI, LII, LIII, (Part 2), pp. 939–956, US Government Printing Office, Washington, DC, USA, 1980.

[162] G. R. Byerly and J. M. Sinton, "Compositional trends in natural basaltic glasses from deep sea drilling project holes 417D and 418A," in *Initial Reports of the Deep Sea Drilling Project*, LI, LII, LIII, (Part 2), pp. 957–971, US Government Printing Office, Washington, DC, USA, 1980.

[163] S. H. Richardson, S. R. Hart, and H. Staudigel, "Vein mineral ages of old oceanic crust," *Journal of Geophysical Research*, vol. 85, no. 12, pp. 7195–7200, 1980.

[164] J. C. Alt, "Subseafloor processes in mid-ocean ridge hydrothermal systems," in *Seafloor Hydrothermal Systems: Physical, Chemical, Biological, and Geological Interactions*, vol. 91 of *Geophysical Monograph*, pp. 85–114, American Geophysical Union, 1995.

[165] M. Ozima, I. Kaneoka, and M. Yanagisawa, "^{40}Ar–^{39}Ar geochronological studies of drilled basalts from Leg 51 and Leg 52," in *Initial Reports of the Deep Sea Drilling Project*, LI, LII, LIII, (Part 2), pp. 1127–1128, US Government Printing Office, Washington, DC, USA, 1980.

[166] S. Gartner, "Calcareous nannofossils, deep sea drilling project holes 417A, 417D, and 418A," in *Initial Reports of the Deep Sea Drilling Project*, LI, LII, LIII, Part 2, pp. 815–821, US Government Publishing Office, Washington, DC, USA, 1980.

[167] R. D. Müller, M. Sdrolias, C. Gaina, and W. R. Roest, "Age, spreading rates, and spreading asymmetry of the world's ocean crust," *Geochemistry, Geophysics, Geosystems*, vol. 9, no. 4, Article ID Q04006, 19 pages, 2008.

[168] F. J. Vine and D. H. Matthews, "Magnetic anomalies over oceanic ridges," *Nature*, vol. 199, no. 4897, pp. 947–949, 1963.

[169] F. J. Vine, "Spreading of the ocean floor: new evidence," *Science*, vol. 154, no. 3755, pp. 1405–1415, 1966.

[170] C. G. A. Harrison, "Marine magnetic anomalies—the origin of the stripes," *Annual Review of Earth And Planetary Sciences*, vol. 15, pp. 505–543, 1987.

[171] P. D. Rabinowitz, H. Hoskins, and S. M. Asquith, "Geophysical site survey results near deep sea drilling project sites 417 and 418 in the central Atlantic Ocean," in *Initial Reports of the Deep Sea Drilling Project*, LI, LII, LIII, (Part 1), pp. 629–669, US Government Printing Office, Washington, DC, USA, 1980.

[172] Shipboard Scientific Parties, "Introduction and explanatory notes," in *Initial Reports of the Deep Sea Drilling Project*, LI, LII, LIII, (Part 1), pp. 5–22, US Government Printing Office, Washington, DC, USA, 1980.

[173] R. D. Müller, W. R. Roest, J.-Y. Royer, L. M. Gahagan, and J. G. Sclater, "Digital isochrons of the world's ocean floor," *Journal of Geophysical Research B: Solid Earth*, vol. 102, no. 2, Article ID 96JB01781, pp. 3211–3214, 1997.

[174] P. Keary and F. J. Vine, *Global Tectonics*, Blackwell Science, London, UK; Cambridge University Press, 2nd edition, 1996.

[175] D. E. Bird, S. A. Hall, K. Burke, J. F. Casey, and D. S. Sawyer, "Early Central Atlantic Ocean seafloor spreading history," *Geosphere*, vol. 3, no. 5, pp. 282–298, 2007.

[176] J. E. T. Channell, E. Erba, M. Nakanishi, and K. Tamaki, "Late Jurassic–Early Cretaceous timescales and ocean magnetic anomaly block models," in *Geochronology Timescales and Global Stratigraphic Correlation*, W. A. Berggren, Ed., vol. 54, pp. 51–63, SEPM (Society for Sedimentary Geology) Special Publication, 1995.

[177] K. D. Klitgord and H. Schouten, "Plate kinematics of the central Atlantic," in *The Geology of North America, Volume M. The Western North Atlantic Region*, P. R. Vogt and B. E. Tucholke, Eds., pp. 351–378, Geological Society of America, Boulder, Colo, USA, 1986.

[178] W. Roest, "Seafloor spreading pattern of the North Atlantic between 10° and 40° N," *Geologica Ultraiectina*, vol. 48, pp. 1–121, 1987.

[179] A. Schettino and E. Turco, "Breakup of Pangaea and plate kinematics of the central Atlantic and Atlas regions," *Geophysical Journal International*, vol. 178, no. 2, pp. 1078–1097, 2009.

[180] A. J. Biggin, D. J. J. van Hinsbergen, C. G. Langereis, G. B. Straathof, and M. H. L. Deenen, "Geomagnetic secular variation in the Cretaceous Normal Superchron and in the Jurassic," *Physics of the Earth and Planetary Interiors*, vol. 169, no. 1–4, pp. 3–19, 2008.

[181] E. J. W. Jones, S. C. Cande, and F. Spathopoulos, "Evolution of a major oceanographic pathway: the equatorial Atlantic," in *The Tectonics, Sedimentation and Palaeoceanography of the North Atlantic Region*, R. A. Scrutton, M. S. Stoker, G. B. Shimmield, and A. W. Tudhope, Eds., Geological Society Special Publication no. 90, pp. 199–213, The Geological Society, London, UK, 1995.

[182] N. A. Stroncik and H.-U. Schmincke, "Palagonite—a review," *International Journal of Earth Sciences*, vol. 91, no. 4, pp. 680–697, 2002.

[183] I. H. Thorseth, H. Furnes, and O. Tumyr, "A textural and chemical study of Icelandic palagonite of varied composition and its bearing on the mechanism of the glass-palagonite transformation," *Geochimica et Cosmochimica Acta*, vol. 55, no. 3, pp. 731–749, 1991.

[184] R. A. F. Cas and J. V. Wright, *Volcanic Successions: Modern and Ancient*, Allen and Unwin Publishers Ltd, London, UK, 1987.

[185] A. Allaby and M. Allaby, "Axiolitic structure," in *A Dictionary of Earth Sciences*, M. Allaby, Ed., Oxford University Press, 3rd edition, 2008.

[186] C. M. Scarfe, "Secondary minerals in some basaltic rocks from Deep Sea Drilling Project Legs 52 and 53, hole 418A," in *Initial Reports of the Deep Sea Drilling Project*, LI, LII, LIII, (Part 2), pp. 1243–1251, US Government Printing Office, Washington, DC, USA, 1980.

[187] Shipboard Scientific Party, "3. Site 1188," in *Proceedings of the Ocean Drilling Program, Initial Reports*, R. A. Binns, F. J. A. S. Barriga, D. J. Miller et al., Eds., vol. 193, pp. 1–305, Ocean Drilling Program, College Station, Tex, USA, 2002.

[188] S. Umino, "5. Data report: textural variation of units 1256C-18 and 1256D-1 lava pond, with special reference to recrystallization of the base of unit 1256C-18," in *Proceedings of the Ocean Drilling Program, Scientific Results*, D. A. H. Teagle, D. S. Wilson, G. D. Acton, and D. A. Vanko, Eds., vol. 206, pp. 1–32, College Station, Tex, USA, 2007.

[189] J. Gottsmann, A. J. L. Harris, and D. B. Dingwell, "Thermal history of Hawaiian pāhoehoe lava crusts at the glass transition: implications for flow rheology and emplacement," *Earth and Planetary Science Letters*, vol. 228, no. 3-4, pp. 343–353, 2004.

[190] A. Steiner, "Clay minerals in hydrothermally altered rocks at Wairakei, New Zealand," *Clays and Clay Minerals*, vol. 16, no. 3, pp. 193–213, 1968.

[191] I. Techer, T. Advocat, J. Lancelot, and J.-M. Liotard, "Dissolution kinetics of basaltic glasses: control by solution chemistry and protective effect of the alteration film," *Chemical Geology*, vol. 176, no. 1–4, pp. 235–263, 2001.

[192] D. K. Smith and J. R. Cann, "Mid-Atlantic ridge volcanic processes: how erupting lava forms Earth's anatomy," *Oceanus Magazine*, vol. 41, no. 1, pp. 11–14, 1998.

[193] G. R. Lumpkin, "Alpha-decay damage and aqueous durability of actinide host phases in natural systems," *Journal of Nuclear Materials*, vol. 289, no. 1-2, pp. 136–166, 2001.

[194] J. E. French, *U-Pb dating of Paleoproterozoic mafic dyke swarms of the South Indian shield: implications for paleocontinental reconstructions and identifying ancient mantle plume events [Ph.D. thesis]*, University of Alberta, Alberta, Canada, 2007.

[195] J. E. French, "Dendritic zircon formation by deterministic volume-filling fractal growth: implications for the mechanisms of branch formation in dendrites," *American Mineralogist*, vol. 95, no. 5-6, pp. 706–716, 2010.

[196] J. P. Gustafsson, "The surface chemistry of imogolite," *Clays and Clay Minerals*, vol. 49, no. 1, pp. 73–80, 2001.

[197] J. M. Guilbert and C. F. Park Jr., *The Geology of Ore Deposits*, W.H. Freeman and Company, New York, NY, USA, 1986.

[198] A. S. Sandhu, J. A. Westgate, and B. V. Alloway, "Optimizing the isothermal plateau fission-track dating method for volcanic glass shards," *Nuclear Tracks and Radiation Measurements*, vol. 21, no. 4, pp. 479–488, 1993.

[199] J. A. Westgate and N. D. Naeser, "Tephrochronology and fission-track dating," in *Dating Methods for Quaternary Deposits*, N. W. Rutter and N. R. Catto, Eds., pp. 15–28, Geological Association of Canada, St. John's, Canada, 1995.

[200] A. H. Jaffey, K. F. Flynn, L. E. Glendenin, W. C. Bentley, and A. M. Essling, "Precision measurement of half-lives and specific activities of ^{235}U and ^{238}U," *Physical Review C*, vol. 4, no. 5, pp. 1889–1906, 1971.

[201] N. E. Holden and D. C. Hoffman, "Spontaneous fission half-lives for ground-state nuclides," *Pure and Applied Chemistry*, vol. 72, pp. 1525–1562, 2000.

[202] G. Faure, *Principles of Isotope Geology*, John Wiley & Sons, New York, NY, USA, 2nd edition, 1986.

[203] A. Simonetti, M. R. Buzon, and R. A. Creaser, "In-situ elemental and Sr isotope investigation of human tooth enamel by laser ablation-(MC)-ICP-MS: successes and pitfalls," *Archaeometry*, vol. 50, no. 2, pp. 371–385, 2008.

[204] R. H. Steiger and E. Jäger, "Subcommission on geochronology: convention on the use of decay constants in geo- and cosmochronology," *Earth and Planetary Science Letters*, vol. 36, no. 3, pp. 359–362, 1977.

[205] M. Trieloff, M. Falter, and E. K. Jessberger, "The distribution of mantle and atmospheric argon in oceanic basalt glasses," *Geochimica et Cosmochimica Acta*, vol. 67, no. 6, pp. 1229–1245, 2003.

[206] H. Cheng, R. L. Edwards, J. Hoff, C. D. Gallup, D. A. Richards, and Y. Asmerom, "The half-lives of uranium-234 and thorium-230," *Chemical Geology*, vol. 169, no. 1-2, pp. 17–33, 2000.

[207] G. Bigazzi, "Length of fission tracks and age of muscovite samples," *Earth and Planetary Science Letters*, vol. 3, pp. 434–438, 1967.

[208] R. F. Galbraith and G. M. Laslett, "Some calculations relevant to thermal annealing of fission tracks in apatite," *Proceedings of the Royal Society A: Mathematical, Physical and Engineering Sciences*, vol. 419, no. 1857, pp. 305–321, 1988.

[209] J. G. Sclater and L. Wixon, "The relationship between depth and age and heat flow and age in the Western North Atlantic," in *The Geology of North America, Vol. M, The Western North Atlantic Region*, P. R. Vogt and B. E. Tucholke, Eds., pp. 257–270, Geological Society of America, New York, NY, USA, 1986.

[210] R. Tada and R. Siever, "Pressure solution during diagenesis," *Annual Review of Earth and Planetary Sciences*, vol. 17, pp. 89–118, 1989.

[211] H. L. Lescinsky and L. Benninger, "Pseudo-borings and predator traces: artifacts of pressure—dissolution in fossiliferous shales," *Palaios*, vol. 9, no. 6, pp. 599–604, 1994.

[212] R. Yamada, T. Tagami, and S. Nishimura, "Assessment of overetching factor for confined fission-track length measurement in zircon," *Chemical Geology*, vol. 104, no. 1–4, pp. 251–259, 1993.

[213] A. J. W. Gleadow, I. R. Duddy, P. F. Green, and J. F. Lovering, "Confined fission track lengths in apatite: a diagnostic tool for thermal history analysis," *Contributions to Mineralogy and Petrology*, vol. 94, no. 4, pp. 405–415, 1986.

[214] R. C. Jonckheere and G. A. Wagner, "On the occurrence of anomalous fission tracks in apatite and titanite," *American Mineralogist*, vol. 85, no. 11-12, pp. 1744–1753, 2000.

[215] D. Vincent, R. Clocchiatti, and Y. Langevin, "Fission-track dating of glass inclusions in volcanic quartz," *Earth and Planetary Science Letters*, vol. 71, no. 2, pp. 340–348, 1984.

[216] R. L. Fleischer and P. B. Price, "Fission track evidence for the simultaneous origin of tektites and other natural glasses," *Geochimica et Cosmochimica Acta*, vol. 28, no. 6, pp. 755–IN5, 1964.

[217] W. Gentner, B. P. Glass, D. Storzer, and G. A. Wagner, "Fission track ages and ages of deposition of deep-sea microtektites," *Science*, vol. 168, no. 3929, pp. 359–361, 1970.

[218] D. Storzer and G. A. Wagner, "Fission track ages of North American tektites," *Earth and Planetary Science Letters*, vol. 10, no. 4, pp. 435–440, 1971.

[219] G. Wagner and P. Van den Haute, *Fission-Track Dating*, Kluwer Academic Publishers, Dodrecht, The Netherlands, 1992.

[220] D. S. Miller and G. A. Wagner, "Fission-track ages applied to obsidian artifacts from South America using the plateau-annealing and the track-size age-correction techniques," *Nuclear Tracks*, vol. 5, no. 1-2, pp. 147–155, 1981.

[221] T. Tsuruta, "Reduction in etching time for fission tracks in diallyl phthalate resin," *Radiation Measurements*, vol. 34, no. 1–6, pp. 167–170, 2001.

[222] N. Yasuda, M. Yamamoto, N. Miyahara, N. Ishigure, T. Kanai, and K. Ogura, "Measurement of bulk etch rate of CR-39 with atomic force microscopy," *Nuclear Instruments and Methods in Physics Research B*, vol. 142, no. 1-2, pp. 111–116, 1998.

[223] P. B. Price and R. M. Walker, "Observation of fossil particle tracks in natural micas," *Nature*, vol. 196, no. 4856, pp. 732–734, 1962.

[224] P. B. Price and R. M. Walker, "Fossil tracks of charged particles in mica and the age of minerals," *Journal of Geophysical Research*, vol. 68, no. 16, pp. 4847–4862, 1963.

[225] R. Jonckheere and P. Van den Haute, "On the frequency distributions per unit area of the projected and etchable lengths of surface-intersecting fission tracks: influences of track revelation, observation and measurement," *Radiation Measurements*, vol. 30, no. 2, pp. 155–179, 1999.

[226] J. Barbarand, A. Carter, I. Wood, and T. Hurford, "Compositional and structural control of fission-track annealing in apatite," *Chemical Geology*, vol. 198, no. 1-2, pp. 107–137, 2003.

[227] H. Matzke, "Radiation damage in nuclear materials," *Nuclear Instruments and Methods in Physics Research B*, vol. 65, no. 1–4, pp. 30–39, 1992.

[228] R. F. Galbraith, "Some remarks on fission-track observational biases and crystallographic orientation effects," *American Mineralogist*, vol. 87, no. 7, pp. 991–995, 2002.

[229] P. P. Metha and Rama, "Annealing effects in muscovite and their influence on dating by fission track method," *Earth and Planetary Science Letters*, vol. 7, no. 1, pp. 82–86, 1969.

[230] S. Krishnaswami, D. Lal, N. Prabhu, and D. Macdougall, "Characteristics of fission tracks in zircon: applications to geochronology and cosmology," *Earth and Planetary Science Letters*, vol. 22, no. 1, pp. 51–59, 1974.

[231] D. Storzer and G. A. Wagner, "Correction of thermally lowered fission track ages of tektites," *Earth and Planetary Science Letters*, vol. 5, pp. 463–468, 1968.

[232] G. Bigazzi, F. P. Bonadonna, M. A. Laurenzi, and S. Tonarini, "A test sample for fission-track dating of glass shards," *Nuclear Tracks and Radiation Measurements*, vol. 21, no. 4, pp. 489–497, 1993.

[233] F. Renard, D. K. Dysthe, J. G. Feder, P. Meakin, S. J. S. Morris, and B. Jamtveit, "Pattern formation during healing of fluid-filled cracks: an analog experiment," *Geofluids*, vol. 9, no. 4, pp. 365–372, 2009.

[234] J. C. Dran, J. P. Duraud, Y. Langevin, M. Maurette, and J. C. Petit, "Contribution of radiation damage studies to the understanding of the Oklo phenomenon," Natural Fission Reactors IAEA-TC-119/12, 1978.

[235] D. W. Davis and T. E. Krogh, "Preferential dissolution of ^{234}U and radiogenic Pb from α-recoil-damaged lattice sites in zircon: implications for thermal histories and Pb isotopic fractionation in the near surface environment," *Chemical Geology*, vol. 172, no. 1-2, pp. 41–58, 2001.

[236] H. Matzke, "Actinide behavior and radiation damage produced by α-decay in materials to solidify nuclear waste," *Inorganica Chimica Acta*, vol. 94, no. 1–3, pp. 142–143, 1984.

[237] W. Primak, "Radiation effects in silicate glasses pertinent to their application as a radioactive waste storage medium," *Nuclear Technology*, vol. 60, no. 2, pp. 199–205, 1983.

[238] W. J. Weber and F. P. Roberts, "A review of radiation effects in solid nuclear waste forms," *Nuclear Technology*, vol. 60, no. 2, pp. 178–198, 1983.

[239] P. Cattermole, "Volcanic flow development at Alba Patera, Mars," *Icarus*, vol. 83, no. 2, pp. 453–493, 1990.

[240] R. E. Ernst, E. B. Grosfils, and D. Mège, "Giant dike swarms: Earth, Venus, and Mars," *Annual Review of Earth and Planetary Sciences*, vol. 29, pp. 489–534, 2001.

[241] R. V. Morris, J. L. Gooding, H. V. Lauer Jr., and R. B. Singer, "Iron mineralogy of a Hawaiian palagonitic soil with Mars-like spectral and magnetic properties," in *Proceedings of the Abstracts: 21st Lunar and Planetary Science Conference*, pp. 811–812, Houston, Tex, USA, March 1990.

[242] N. G. Barlow, "Crater size-frequency distributions and a revised Martian relative chronology," *Icarus*, vol. 75, no. 2, pp. 285–305, 1988.

[243] P. Toulmin III, A. K. Baird, B. C. Clark et al., "Geochemical and mineralogical interpretation of the Viking inorganic chemical results," *Journal of Geophysical Research*, vol. 82, no. 28, pp. 4625–4634, 1977.

[244] W. W. Barker, S. A. Welch, and J. F. Banfield, "Biogeochemical weathering of silicate minerals," *Reviews in Mineralogy and Geochemistry*, vol. 35, no. 1, pp. 391–428, 1997.

[245] D. Anselmetti, J. Fritz, B. Smith, and X. Fernandez-Busquets, "Single molecule DNA biophysics with atomic force microscopy," *Single Molecules*, vol. 1, no. 1, pp. 53–58, 2000.

[246] N. Jiravanichanun, K. Yamamoto, K. Kato et al., "Preparation and characterization of imogolite/DNA hybrid hydrogels," *Biomacromolecules*, vol. 13, no. 1, pp. 276–281, 2012.